EFFECT OF MODIFIED MOISTURE BARRIER IN MITIGATING PAVEMENT DISTRESSES DUE TO EXPANSIVE SUBGRADE

by

PRATIBHA PANDEY

Presented to the Faculty of the Graduate School of

The University of Texas at Arlington in Partial Fulfilment

of the Requirements

for the Degree of

DOCTOR OF PHILOSOPHY IN CIVIL ENGINEERING

THE UNIVERSITY OF TEXAS AT ARLINGTON

May 2021

ACKNOWLEDGEMENT

I would like to express my sincere gratitude to my supervising professor, Dr. MD. Sahadat Hossain for his continuous support, encouragement, and guidance throughout my graduate studies. His knowledge, experience, and excellent mentorship helped me a lot for the successful completion of my dissertation. This research would not have been possible without his support and belief in me, and I feel very lucky to have the opportunity to be the part of his research team.

I would like to thank my committee members, Dr. Xinbao Yu, Dr. Seyed Mohsen Shahandashti, and Dr. Muhammad N Huda for spending their valuable time serving on my dissertation committee, and for their valuable insights. I would also like to thank the Texas Department of Transportation for providing fund for the research and to Navarro County for their great help during field activities.

Special thanks to all the SWIS members for their support and assistance. I am very thankful to Niloy Gupta Shuvro, Shopnil Shams, Prabesh Bhandari, Sachini Madanayake, Muhasina Manjur Dola, Asif Akhtar and Tanvir Imtiaz for their continuous help during all the field activities and extended thanks to Dr. Anuja Sapkota, Dr. Asif Ahmed and Dr. Jobair Bin Alam for their invaluable suggestion and guidance during the study.

Finally, I would like to express my deep and sincere gratitude to my family (my parents, sisters and to my brother) for their unconditional love and encouragement. I would not have been able to achieve this milestone without their support. Last but not the least, I would like to thank my husband Sandesh Gautam for his endless love, care, and support throughout my academic journey.

March 26, 2021

ABSTRACT

EFFECT OF MODIFIED MOISTURE BARRIER IN MITIGATING PAVEMENT DISTRESSES DUE TO EXPANSIVE SUBGRADE

Pratibha Pandey, PhD

The University of Texas at Arlington, 2021

Supervising Professor: MD Sahadat Hossain

Surficial distresses in roadways of Texas are very common due to presence of high plastic clayey soil in the subgrade. Increased sensitivity of high plastic clay towards seasonal moisture change results in repeated swelling and shrinkage, and ultimately the development of pavement cracks. Annual expenses of such distresses impose huge financial liability to maintenance authorities. Studies have indicated rainwater intrusion into underlying expansive subgrade soil coupled with inadequate drainage as the main cause of pavement damage in semi-arid regions. The inability of drainage layer to laterally drain the excess moisture may lead to moisture accumulation within the base layer which can also be a source of water for the subgrade soil which tends to swell and shrink periodically. This indicates the need for a cost effective and reliable method to prevent the moisture intrusion into the pavement system using appropriate mechanism.

Among several types of moisture barrier system, Modified Moisture Barrier (MMB) placed at base-subgrade interface offers a promising potential in isolating the subgrade soil from changing climatic conditions. Additionally, the geocomposite component of MMB can enhance the pavement drainage thereby reducing the detrimental effect of moisture on pavements. The previous usage of modified moisture barrier is limited to the edge of pavement with the main aim of controlling moisture intrusion from the edge. However, the

study does not take into account the moisture infiltration that may occur from pavement surface along fine cracks formed by ageing and wearing of asphalt. Therefore, the main objective of this study is to evaluate the effectiveness of modified moisture barrier when placed throughout the width of an actual compromised pavement section. For this, a compromised pavement section in Frost, Texas was selected. Two sections were considered- one with the barrier and other without barrier to compare the performance of pavement system. The field performance of pavement sections was regularly monitored using integrated moisture/temperature sensors and horizontal inclinometer.

The performance monitoring results indicated seasonal moisture variation as well as temporary response to rainfall events in control section. In contrast, equilibrium moisture content was recorded by the sensors in barrier section. The results from the moisture sensors were reflected on the deformation results from inclinometer. The use of modified moisture barrier was able to reduce the swelling and shrinkage by 89%. Field data-based prediction models were developed for the control section by analyzing the moisture and deformation trend observed in the field. The model was further validated with other field studies from North Texas for its wide applicability. The effects of both the rainfall and temperature were incorporated in the model. The performance of the subgrade was further evaluated through numerical study where the model was first calibrated and analysis on the swell potential at different dry and wet initial condition was performed. In addition, flow evaluation along the geocomposite component of MMB in response to several rainfall intensities was studied in SEEP/W. Parametric study was conducted to evaluate the effect of different transmissivity of geocomposite in laterally draining infiltrated rainwater out of the system.

Table of Contents

LIST OF FIGURES

LIST OF TABLES

Chapter 1

INTRODUCTION

1.1 Background

Expansive soils pose significant threat to the overlying structures and are well known as a problematic soil all over the world (Chen, 1988; Manosuthkij, 2008). These soils exhibit moderate to high plasticity, low to moderate strength, and high swell and shrink behavior with the changing moisture content (Holtz and Gibbs, 1956). In United States, expansive soil covers one-fourth of the area (Buhler and Cerato, 2007) and has been reported to cause damage ranging in between 9 to 15 billion USD annually (Nelson and Miller, 1997; Jones and Jefferson, 2012). Due to their low stiffness, light loaded nature, pavements are usually more vulnerable to the effects of expansive soils. Steinberg (1989) states more than 50% of damages due to expansive soil occurring in pavements and highways. Particularly in Texas, TxDOT spends nearly $180 million annually maintaining 197,500 lane miles of roadway (Lee, 2017) of which majority are low volume roads. This imposes huge economic liability to the concerned authorities and highlights the cruciality of the issue.

The pavements supported by highly plastic expansive clay exhibits distresses due to non-uniform and cyclic swelling and shrinkage behavior of subgrade in response to seasonal moisture fluctuation. Previous studies have identified climatic loading as the main cause of moisture variation within the pavement subgrade. The seasonal change in moisture takes place within the active zone of the subgrade soil mainly due to rainfall, moisture intrusion from cracks, freeze- thaw cycles, leakage, evapotranspiration etc. (Hedayati, 2014). The resulting moisture variation causes cycling swelling and shrinkage inducing huge volumetric strain during the process. As a result, cracks initiate and propagates to the surface over time and are reflected in various forms such as longitudinal cracking, rutting,

edge drop, heaving, differential settlement, etc. (Zornberg and Gupta, 2009; Dessouky et al., 2015). Of these, longitudinal cracks are more prevalent. The cracks formed on the surface further accelerates the rainwater intrusion and results in the formation of more severe desiccation cracks over time, thereby forming a vicious circle. Therefore, it is imperative to identify cost effective and reliable method to prevent seasonal moisture fluctuation in highly plastic expansive clayey soil and mitigate associated pavement distresses that can ultimately compromise the serviceability of the pavement.

Several remedies have been proposed to mitigate the detrimental effect of expansive subgrade soil. For instance, replacing the expansive soil with inert materials, prewetting, chemical stabilization using lime and cement, moisture control measures etc., (Snethen, 1979). Prewetting and replacement of expansive soil through active zone is not always economically and practically feasible because of the amount of soil involved. Chemical treatment is another stabilization method which uses various stabilizer like lime and cement to improve the strength of soil and reduce swell potential that may occur due to damaging effects of moisture. Although common in practice, stabilization using lime and cement are not suitable for all types of soil and are especially detrimental to high sulfate soils (Sherwood, 1962; Mitchell and Dermatas, 1992; Petry and Little, 1992). In addition, such chemical treatment requires several days to gain strength which makes it less feasible for roads with heavy traffic due to necessity of reopening traffic (Sebesta, 2002; Harris, 2008; Dessouky et al., 2015).

With the moisture having direct relation to volumetric deformation of expansive soil, using barriers for controlling moisture fluctuation in the pavement subgrade soil can be an effective solution. Various kinds of moisture barriers have been introduced and utilized to regulate the moisture within the soil mass, such as vertical moisture barriers, horizontal

moisture barriers, geocomposite capillary barrier drain (GCBD), modified moisture barrier etc., (Steinberg, 1989; Elseifi et al., 2001; Henry et al., 2002; Ahmed et al., 2018). These barriers have been found to enhance the performance of the roadways by maintaining the equilibrium moisture content in the subgrade soil. The studies in the past utilizing the vertical moisture barrier displayed significant increase in the life of pavement (Holden, 1992; Evans and McManus, 1999). However, no measures were taken to prevent the rainwater intrusion from pavement surface and surface cracks. Also, the associated time and construction difficulty make this approach less feasible.

On the other hand, GCBD that is designed to limit the percolation of rainwater into the pavement subgrade due to capillary barrier effect offers a great potential in limiting the downward movement of water. It is placed horizontally and consists of a layer of geonet sandwiched in between geotextile. The upper geotextile layer in the system acts as a transport layer, geonet as a capillary barrier and the bottom geotextile layer as a separator to prevent the clogging of geonet (Elseifi et al., 2001). Although the difference in the permeability of layers offers a great potential in limiting the downward movement of water, the system allows some percolation during the period of extended rainfall events (where the system reaches a breakthrough point) and thus may not be effective at all times (Rahardjo et al., 2012). To overcome this limitation, an additional layer of geomembrane was added underneath the system and is referred to as Modified Moisture Barrier (Ahmed et al., 2018) which is used in the current study. Modified moisture barrier can be considered an economical and sustainable solution to control the pavement distress by reducing moisture infiltration.

The modified moisture barrier consists of a layer of geo-composite (interconnected geotextile-geo net-geotextile layer) underlain by a geomembrane layer (Ahmed et al.,

2018). This method has the potential to address various issues in pavement system such as excess moisture in the structure, insufficient drainage, migration of fine contents from subgrade soil to base layer that can impede the function of drainage layer (Bhandari et al., 2019; Timsina et al., 2019), and moisture variation due to periodic wetting and drying cycles. The main purpose of modified moisture barrier in the current study is to isolate the pavement from climate changes as the impermeable geomembrane layer prevents moisture to infiltrate into the pavement layers and the geocomposite layer (geotextile-geonet-geotextile layer) drains the excess moisture away from the system (Ahmed et al., 2018; Sapkota et al., 2019).

1.2 Problem Statement

Modified moisture barrier has been used in the past to prevent moisture intrusion into the pavement system (Ahmed et al., 2018; Sapkota et al., 2019). However, the studies conducted so far have utilized the barrier only at the edge of the pavement assuming asphalt layer to be impermeable and moisture intrusion taking place only from the edge. Although, in reality, asphalt pavements are not completely impermeable and considerable amount of moisture can infiltrate through pavement's surface along fine cracks formed by the wearing and ageing of asphalt layer (Cedergren, 1974). Past studies have also shown that vertical moisture barrier installed at the edge of the pavement to be less efficient over time with gradual decrease in serviceability index as they only prevent moisture infiltration and exfiltration through the edges and not through the pavement surface itself (Steinberg, 1989). As such, modified moisture barrier at the edge may not be effective in preventing the moisture intrusion taking place from the surface which can be as much as 33 to 50 percent as per the research conducted by FHWA (Cedergren, 1974). This might lead to the occurrence of much more severe cracks, which will eventually require more extensive

repair works. Therefore, an approach with the modified moisture barrier installed across the whole pavement needs to be studied and its performance should be evaluated.

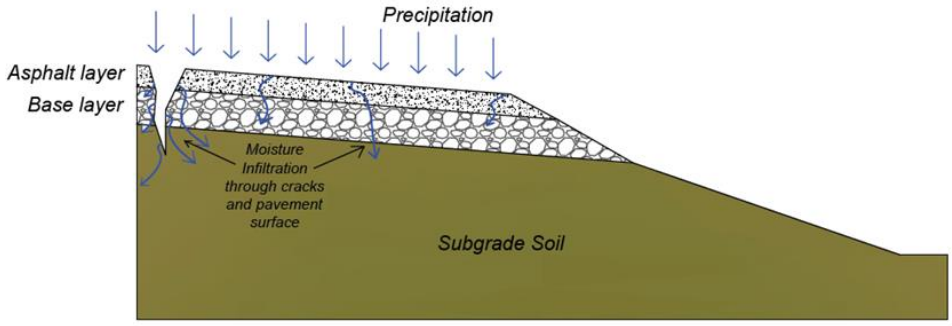

Figure 1–1 Schematic Illustration of Rainwater Intrusion into the Pavement Layers

1.3 Research Objectives

The objective of the current study is to evaluate the effectiveness of modified moisture barrier in mitigating swelling-shrinkage associated pavement distresses. The barrier can prevent rainwater infiltration and drain infiltrated water laterally towards the drainage ditch. The specific tasks performed to fulfill the objective of the study were:

- Site investigation and selection of full-scale study area;
- Development of installation layout for modified moisture barrier;
- Field installation of modified moisture barrier;
- Field Instrumentations at the barrier and control sections to evaluate the performance;
- Performance monitoring of the study area and analysis of field monitoring results;
- Evaluation of modified moisture barrier in controlling potential pavement distresses due to moisture intrusion;
- Development of moisture and deformation model for expansive subgrade soil;

- Numerical study of behavior of expansive subgrade soil in response to climatic loading.
- Evaluation of flow along drainage layer of modified moisture barrier through numerical analysis.

1.4 Dissertation Organization

The dissertation is organized into the following chapters:

Chapter 1 provides the general information about the topic, problem statement, research objectives along with a brief summary of dissertation organization.

Chapter 2 presents complete literature review on the subject including behavior of expansive clay in response to seasonal climatic loading, its impact on the stability of overlying flexible pavement system along with their remedial measures. Details on the existing remedial measures for expansive soils have been provided along with the need to develop novel and cost-effective solution. Several case studies with the implementation of moisture barrier system to limit the effect of moisture has also been discussed. Finally, the limitations of previous studies are highlighted and the research objective for the current study was formulated.

Chapter 3 focuses on the detailed site investigation of a pavement site which experienced significant deformation and demonstrated the need of extensive repair work. The site investigation program including initial visual survey, soil boring along with advanced site investigation using GPR survey and pavement coring has been discussed. The site investigation results were evaluated and stabilization technique with the incorporation of drainage and impermeable geosynthetic layers at the base-subgrade interface was proposed.

Chapter 4 focuses on the field implementation of modified moisture barrier and instrumentation in the pavement sections for performance monitoring. The selection of geosynthetic materials, the details on the monitoring instruments as well as the adopted field installation procedure have been discussed in this chapter.

Chapter 5 presents the performance monitoring results from the field. The barrier and control sections were regularly monitored and compared to evaluate the effectiveness of modified moisture barrier in controlling sensitivity of highly expansive subgrade to climatic loading. The detailed discussion on the field observations is presented in this chapter along with the comparison to previous studies.

Chapter 6 presents the details on moisture and deformation prediction model development. The seasonal trend along with temporary fluctuations due to rainfall and temperature were quantified. Statistical analyses were conducted to generate subgrade moisture and deformation prediction equations for expansive clayey soil. Validation of the models to check their respective accuracies are also presented.

Chapter 7 includes the results and analyses of a numerical study conducted using 2D finite element software SIGMA/W and SEEP/W in GeoStudio. The analysis in SIGMA/W was performed to evaluate the hydro-mechanical behavior of expansive subgrade soil in response to climatic loading with and without moisture barrier system. In addition, flow evaluation along the drainage layer of modified moisture barrier system using SEEP/W has been explained in this chapter. A parametric evaluation on the transmissivity of geocomposite and rainfall intensity was performed, and the results are presented.

Chapter 8 summarizes the main conclusion from the current research and provides recommendation for future work.

Chapter 2

LITERATURE REVIEW

2.1 Introduction

American Society of Civil Engineers (ASCE) have assigned a C- grade to the infrastructures system of the United States (ASCE, 2021). Critical infrastructures under ASCE's Report Card include roads, bridges, energy systems, solid waste, and water network systems among others, which are all key in determining the quality of life and economy of the country (ASCE, 2021). Although this is the highest grade in 20 years, the need of research on infrastructures still remains prevalent. An increasing number of studies exploring the restoration of electrical grids (Shahidehpour et al., 2016), water pipe networks (Pudasaini et al., 2017; Pudasaini and Shahandashti, 2018; Shahandashti and Pudasaini, 2019; Pudasaini and Shahandashti, 2020), and roads (Ahmed and Islam, 2020; Ahmed et al., 2020) substantiate the significance of such studies. Research on rehabilitation of highway systems and pavements have their equal share owing to their criticality. However, due to involvement of several vulnerabilities, a set of challenges remain to be addressed. One such vulnerability is the negative impact of expansive soils.

2.2 Expansive Soil

Expansive soils are the soils which respond to change in moisture with swelling and shrinkage. Moisture fluctuation in expansive soil results in expansion from all directions inducing volumetric deformation and causing severe damage to the overlying infrastructures (Chen, 1988). These types of soil are found worldwide with many countries reporting the problems caused by them (Chen, 1988; Manosuthikij, 2008). In United States, expansive soil covers one-fourth of the area (Buhler and Cerato, 2007) with the damage

ranging in between 9 to 15 billion USD annually (Nelson and Miller, 1997; Jones and Jefferson, 2012).

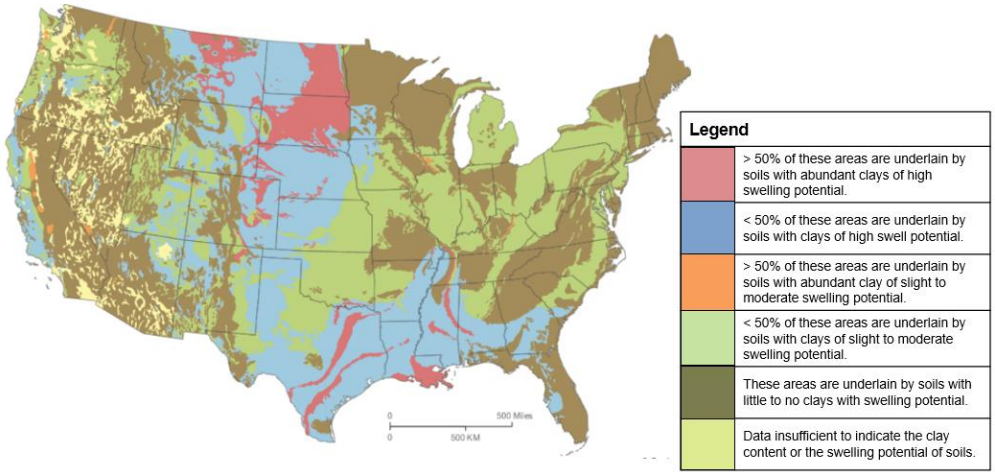

Figure 2–1 Map of United States Showing Expansive Clay (Source: www.geology.com)

The swelling and shrinkage property of expansive soils can be attributed to the presence of montmorillonite mineral which is extremely sensitive to moisture change (Young, 2012). They are usually found in the regions where the annual evapotranspiration is higher than the precipitation (Chen, 1988). In these areas, the wetting and drying climatic conditions exist throughout the year. As explained by Jones and Jefferson (2012), the soil experiences water deficit to a deeper depth during long dry period and subsequent rainfall events result in swelling phenomenon. The effect is more pronounced within upper few feet of unsaturated soil mass where the soil is in close proximity to seasonal rainfall and evapotranspiration. The periodic effect of wetting and drying cycle induces distress in the soil that results in permanent deformation as swelling and shrinkage are not fully reversible (Holtz and Kovacs, 1981). Swelling can cause the upward movement of structure while shrinkage can induce differential settlement.

2.2.1 Swell-Shrink Mechanism of Expansive Soil

Figure 2–2 illustrates the mechanism of swelling and shrinkage of expansive soil with the water infiltration and exfiltration in micro scale. As the soil comes in contact to moisture, water molecules interact with the clay mineral via hydrogen bonding and increases the interlayer distance between clay sheets. This is reflected as a swelling in macro scale (Hensen and Smit, 2002). Exfiltration of water molecules on the other hand reduces the distance between the clay sheets and results in overall shrinkage of the soil. Kalz et al., (2001) states that the soil containing montmorillonite can undergo 30% volume change during wetting and drying cycle.

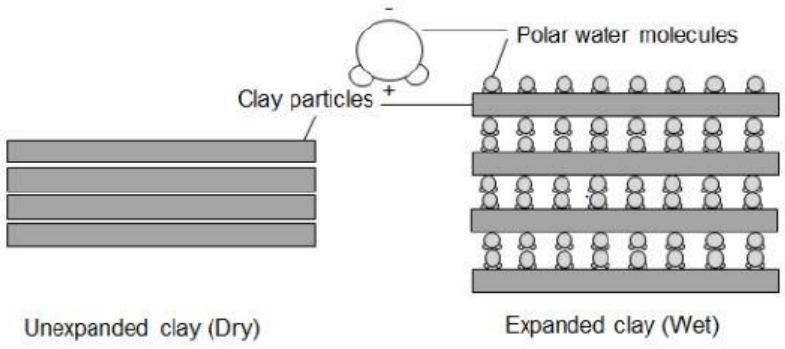

Figure 2–2 Infiltration of Water Molecules between Clay Sheets (Hensen and Smit, 2002)

2.2.2 Volume Change Behavior of Expansive Soil

Volume change in expansive soil occurs with a change in stress state of soil in response to varying moisture condition. Net normal stress and matric suction are the parameters that can be used to explain the stress state of soil. The accurate analysis of soil deformation can be achieved through coupled stress/ pore water pressure analysis (Hedayati, 2014). The response of soil mass to the change in stress state can be explained using constitutive relationships. The volume mass characterization of the soil can be done using void ratio

and moisture content or degree of saturation (Fredlund et al., 2012) as a function of matric suction and normal stress which is given by:

$$de = \alpha_t \, d(\sigma_m - u_a) + \alpha_m \, d\,(u_a - u_w)$$

$$dw = b_t \, d(\sigma_m - u_a) + b_m \, d(u_a - u_w)$$

where, $\sigma_m - u_a$= Mean net stress

$u_a - u_w$= Matric Suction

α_t= Coefficient of compressibility with respect to net normal stress =$\frac{\partial e}{\partial(\sigma_m - \sigma_a)}$

α_m= Coefficient of compressibility with respect to matric suction =$\frac{\partial e}{\partial(u_m - u_a)}$

b_t= Coefficient of moisture variation with respect to net normal stress =$\frac{\partial w}{\partial(\sigma_m - \sigma_a)}$

b_m= Coefficient of moisture variation with respect to matric suction =$\frac{\partial w}{\partial(u_m - u_a)}$

Figure 2–3 illustrates constitutive surface where volume mass properties i.e., void ratio and water content are represented as a function of stress state variables- matric suction and normal stress.

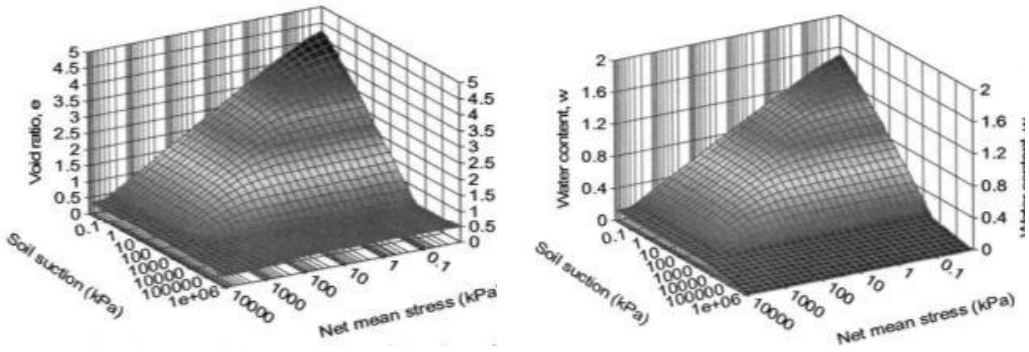

(a) (b)

Figure 2–3 Volume Mass Constitutive Surface of Regina Clay (Pham, 2005)

Volume change behavior of expansive soil can be evaluated by observing the individual effect of stress state variables. This can be achieved by considering different cases that includes e-σ relationship with varying suction, e-ψ relationship with varying normal stress and w- ψ relationship with varying normal stress (Fredlund et al., 2006).

2.2.3 Problems Due to Expansive Soil

The shrink swell potential of expansive soil makes it unsuitable for construction. However, increasing population and urbanization have led to extensive construction over expansive soil (Williams, 2003), thus posing great deal of challenge to the geotechnical engineers all over the world. Chen (1988) states that the expansive soil can induce a pressure of about 273 metric tons/m^2 upon swelling which can damage the infrastructures over them. Hudak (1998) states that the frequency of damage in the foundation to be three times more when constructed over soil with high swell-shrink potential than on sandy loam soils with moderate shrink swell potential. Expansive soil affects highway system infrastructures such as pavements (Hedayati, 2014; Ahmed, 2017), highway embankments (Ahmed et al., 2020; Bhandari et al., 2020), and bridge abutments. The non-uniform heaving during wet period and the shrinkage following the dry period initiates crack in the subgrade soil which gradually reflects on the surface compromising the serviceability of pavements.

2.3 Impact of Expansive Soil on Flexible Pavement System

Failure of pavement constructed over expansive subgrade is a very common phenomenon in many US roads. In North Texas, low volume roads which form the significant part of transportation system exhibits frequent pavement failure and require routine repair and maintenance. There are different factors that might cause damage to the pavements, of which expansive subgrade soil plays the vital role. It has been reported by Wanyan et al. (2010) that 18 out of 25 Texas Department of Transportation Districts exhibit pavement

failure due to expansive subgrade soil. The cyclic swelling and shrinkage that exist throughout the year induces stress in the subgrade soil compromising its strength which is reflected on the surface in the form of pavement distresses. As a result, the useful life of the pavement becomes significantly less than the design life. Some of commonly observed pavement distresses due to expansive subgrade soil are rutting, fatigue, longitudinal cracking, heaving, and differential settlement.

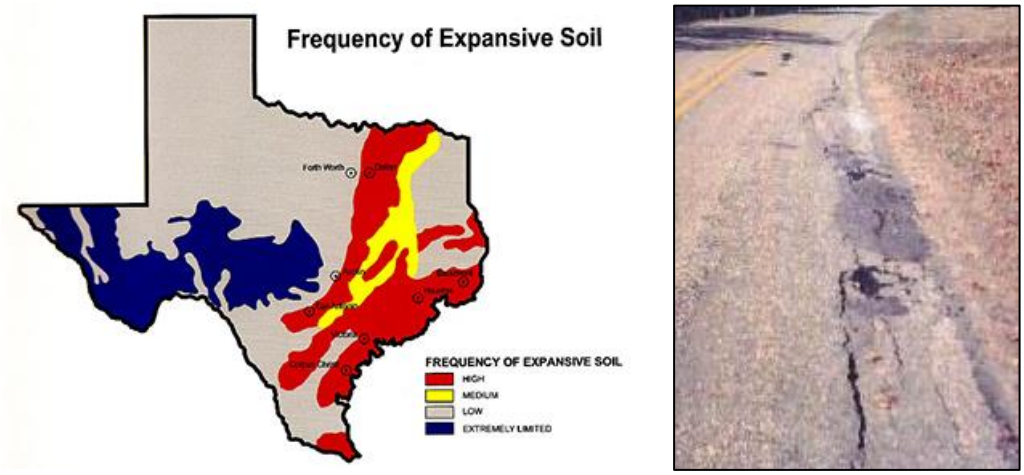

Figure 2–4 Frequency of Expansive Soil in Texas (Tella Firma, 2017) and Observed Pavement Failure due to Expansive Subgrade Soil (Sebesta, 2002)

It is reported that the TxDOT spends more than 50% of their annual budget on the repair and maintenance of these pavement distresses. The repair and maintenance generally focus on the surficial treatment of pavement without addressing problematic subgrade soil. Consequently, the cracks reappear after certain time requiring more extensive repair work.

Most of the surficial distresses are localized at the pavement shoulder due to lateral moisture intrusion from the edge. However, fissures and cracks on the pavement surface might as well act as a conduit for moisture infiltration saturating the underlying soil layers (Hedayati, 2014). Since the soil is highly heterogenous in the field with varying response

to the moisture changes, differential movement might occur within the subgrade soil. For instance, pavement surface towards the edge might lift due to high variation in moisture while at the center depression may occur. Conversely, center lift might occur when the soil at the center gets moist because of capillary action or moisture intrusion through surficial fissures and cracks. The differential movement increases stress concentration in the soil developing cracks (Luo and Prozzi, 2010).

Fredlund et al. (2006) categorizes the pavement distresses into two groups: Differential movement due to volumetric changes and inadequate support. Shrinkage of soil tends to separate the contact of slab and the supporting soil. Edge cracks/ drop off, longitudinal or transverse cracking, reflection cracking and upheaval and swelling etc. are observed due to combined effect of differential movement and inadequate support. Two most common types of cracks frequently observed in pavement are shown in Figure 2–5.

(a) (b)

Figure 2–5 (a) Edge Drop and (b) Longitudinal Cracks due to Expansive Subgrade Soil

2.4 Moisture Distribution in Subgrade Soil

As discussed earlier, deformation in expansive soil is triggered by change in moisture content and therefore is important to understand. Moisture redistribution may occur in the soil whenever water infiltrates or exfiltrates from the soil mass by various means and disturbs the equilibrium condition in the soil. Equilibrium condition refers to a condition when the soil neither lose nor gain moisture. Several means leading to transient moisture variation in pavement subgrade has been discussed in the following section.

2.4.1 Moisture Intrusion into Subgrade Soil

Moisture intrusion may take place from cracks in pavement surface, through shoulder and side ditches, free water from pavement base, capillary rise from ground water table etc. (Cedergren et al., 1972; Ridgeway, 1982) The effect of climatic loading has been identified as the primary cause of moisture fluctuation in semi-arid regions where water table is usually at deeper depth.

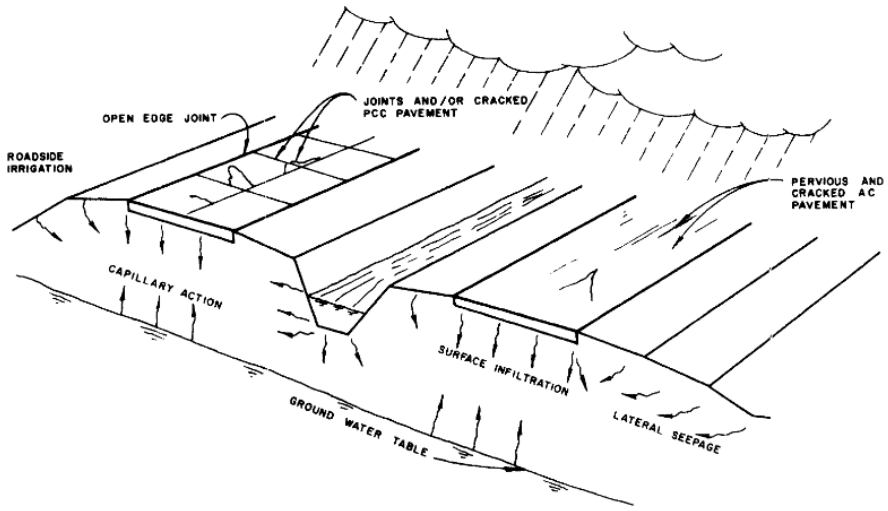

Figure 2–6 Sources of Water in Pavement (Cedergren et al., 1972)

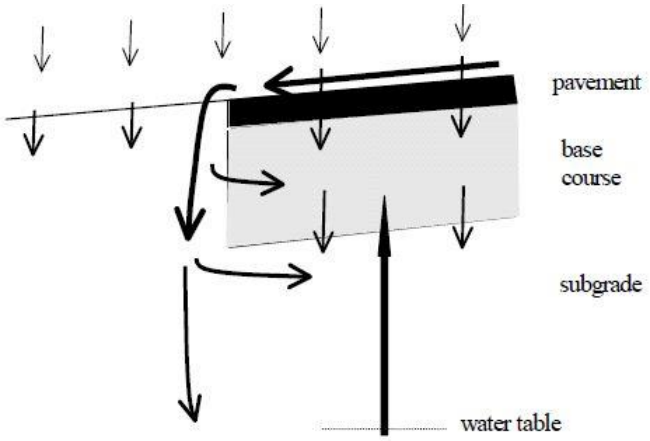

Figure 2–7 Schematic Illustration of Sources of Water in Pavement Layers (Stormont et al., 2009)

2.4.2 Effect of Cracks

Desiccation cracks are widely observed in semi-arid regions during dry period when soil loses its moisture and shrinks. The crack initiates when maximum stress in the subgrade soil is more than its tensile strength. These cracks propagate to the surface due to low tensile strength and weak bond between the pavement layers (Uzan et al., 1972). The presence of cracks can vary the rate of moisture infiltration in the soil. Moisture can penetrate much more rapidly from cracks than in intact soil mass, hence play vital role in the extreme moisture variation in the field (Aubeny and Long, 2007).

The effects of soil cracking on soil volume change and on unsaturated flow properties was studied by Abbaszadeh (2011) through modeling. The cracked soils were reported to have bimodal SWCC through laboratory testing which plays significant role in the moisture infiltration from the soil mass. The infiltration rate for the non-cracked soil was found to be distinctly lower than the cracked area initially. However, the cracks tend to close as the water fills up the crack and caused the soil to swell. Figure 2–8 show the infiltration rates

for cracked and intact soils measured using infiltrometer on a slope constructed over expansive clay as reported by Zhan et al. (2007).

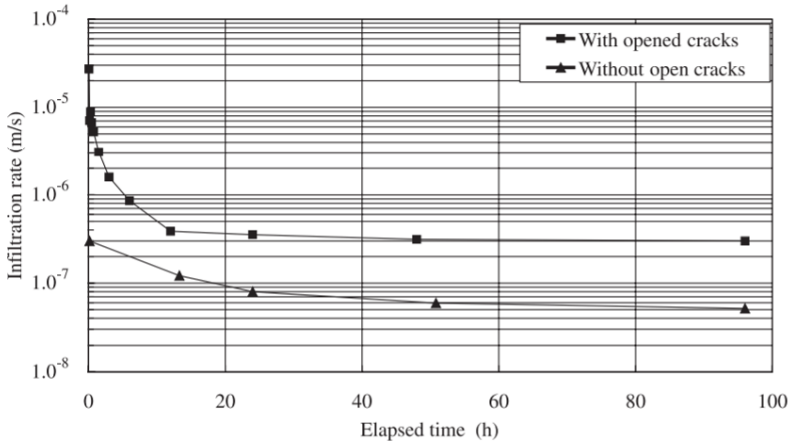

Figure 2–8 Infiltration Rates for Cracked and Intact Soils (Zhan et al., 2007)

Qi and Vanapalli (2015) also states that the desiccation cracks can significantly affect the hydraulic properties and have considerable influence on the hydraulic response of expansive soil under infiltration.

2.4.3 Effect of Vegetation

Studies have shown that the moisture distribution in the soil is largely affected by vegetation in the vicinity. Various factors including the type of vegetation, soil and ground water conditions, climate, foundation type and distance from the vegetation (Fredlund and Hung, 2001) governs the effect of vegetation in the soil moisture condition. The presence of vegetation can increase the depth of suction variation (Mitchell, 2013). As a result, maximum settlement can be anticipated in the region. Fredlund and Hung (2001) performed a study on the influence of trees in the movement of soil. A settlement of 85 mm was observed where the tree was located while the value decreased to 40 mm at a distance of 8 m from the tree at ground surface.

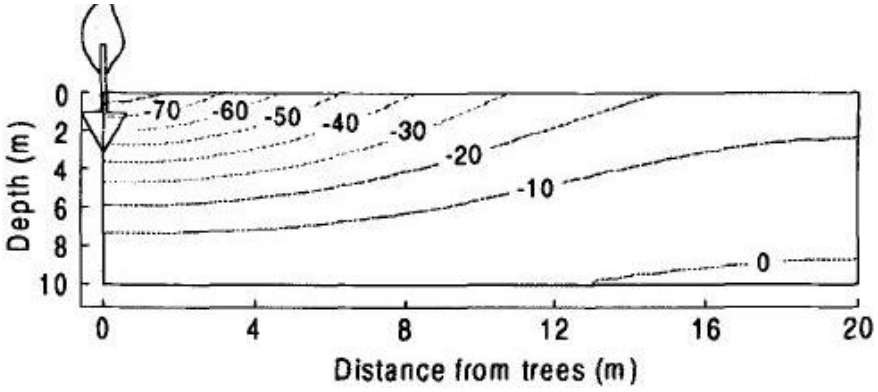

Figure 2–9 Contours of Vertical Displacement (Fredlund and Hung, 2001)

Williams and Pidgeon (1983) analyzed the effect of vegetation and its removal in the movement of expansive soils from different case studies. It was found that the significant change in stress state of the soil might occur with the removal of vegetation as suction profile is primarily governed by evapotranspiration from the vegetation. The removal of vegetation result in the accumulation of rainwater in the shallow layer near the surface and can result in excessive swelling in the potentially expansive soils. As a result, the swelling movement was recorded to be about 150 mm and to the most 374 mm after the removal of vegetation from the field study in various sites of South Africa. Also, in the case where the soil surface was shaded with the grasses or the surface cover, the effect of evaporation was insignificant.

2.5 Previous Studies on Expansive Subgrade Soil

2.5.1 Field Based Studies

Several field-based studies can be found in the literature with the focus on evaluating the moisture fluctuation and deformation of expansive subgrade soil due to climatic loading. Bayomy and Salem (2004) instrumented and monitored five different sites with expansive soil in Idaho for five years starting from 1999 to 2003. The monitoring results indicated

seasonal change in average soil moisture content at all sites. Since the data collection was performed at large time interval, instant change in moisture could not be captured and the results were reported in terms of average moisture content over time. It is to be noted that the average soil moisture values were found to be different depending on specific site conditions. For instance, Lewiston site recorded about 20% of average soil moisture content while Pack river site showed average value of 40%. The author also reported temperature variations over time which exhibited sinusoidal pattern.

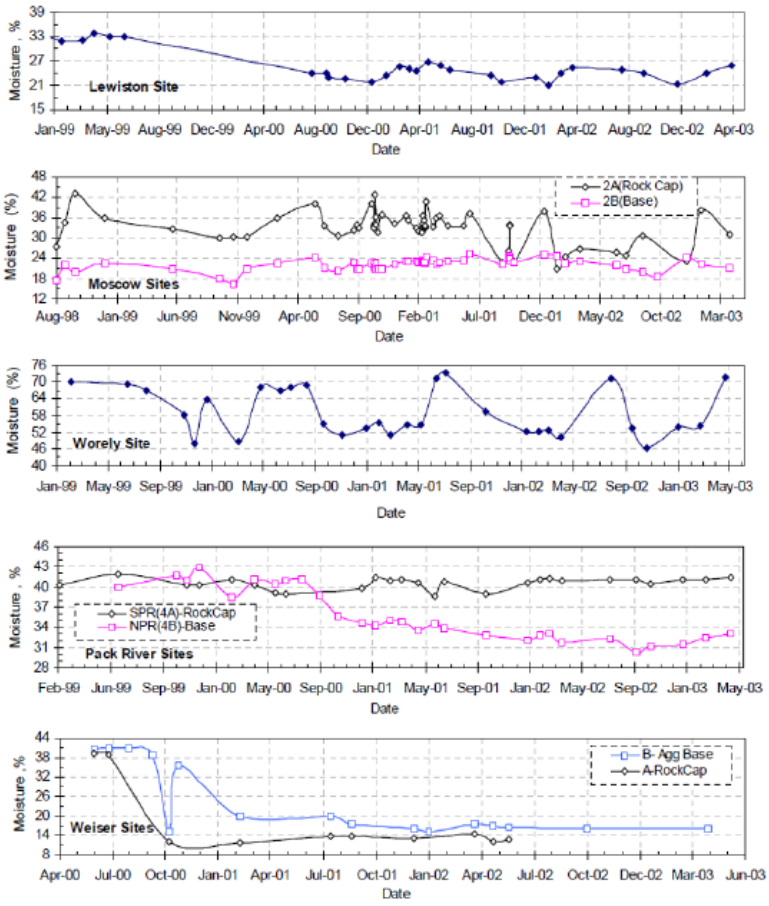

Figure 2–10 Average Subgrade Volumetric Moisture Content at different sites of Idaho, USA (Baymoy and Salem, 2004)

Manosuthkij (2008) instrumented sensors at four different sites in Texas which consisted of highly plastic expansive clay as a subgrade soil. The continuous monitoring of the site found the edge cracking taking place when the mean moisture content, defined as a difference between monthly highest and lowest moisture values was greater than 20%. The cracks were reported after summer when the difference is usually maximum. The suction value at the time of crack initiation was found to be 1635 kPa and 1098 kPa owing to dry condition. All these observations indicated the impact of climatic conditions in initiating cracks in the pavement system.

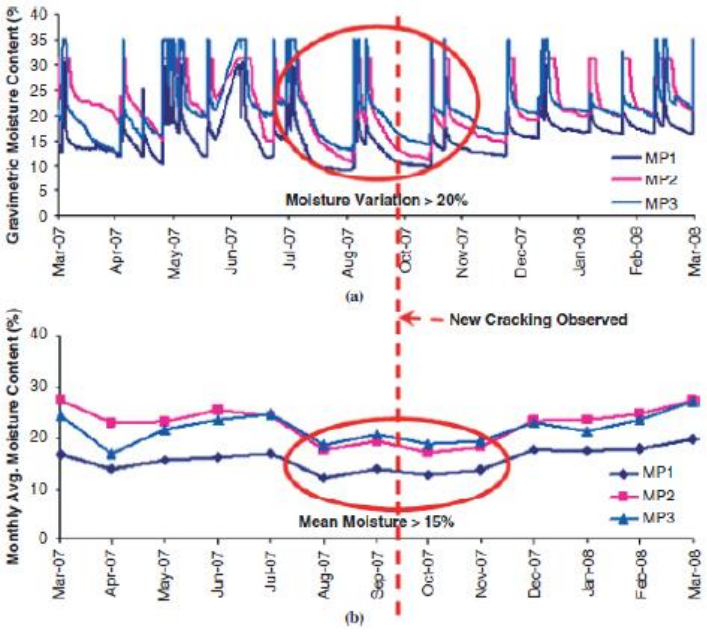

Figure 2–11 In-situ Instrumentation Results in Texas, USA (Manosuthikij, 2008)

Another study by Nguyen et al. (2010) evaluated the suction variation under both driving lane and side slope up to a depth of 2.2 m through field instrumentations. The suction variation within the instrumented region was found to be dependent on the climatic conditions i.e., precipitation and freezing temperature. The impact was more at the shallow

regions and side slopes where the soil was in relatively close contact to the environment. The highest suction of 150 kPa was observed under driving lane while suction as high as 800 kPa was recorded at the side slope. The author utilized the field result to define the zone with suction variation that could potentially result in pavement distresses. However, no surveying or any other deformation results were reported by the author. It should be noted that the soil suction at shallow depth and side slope was observed to be more sensitive to precipitation with temporary variations. The author concluded pavement distresses to be more at the shoulder than in the centerline of the pavement.

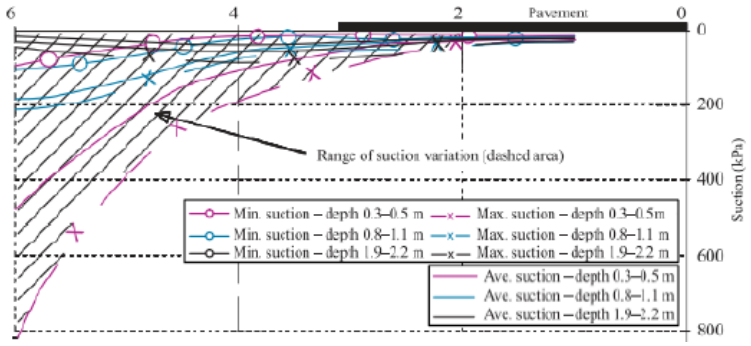

Figure 2–12 Suction Variation in the Subgrade Soil of Highway due to Climatic Loading (Nguyen et al., 2010)

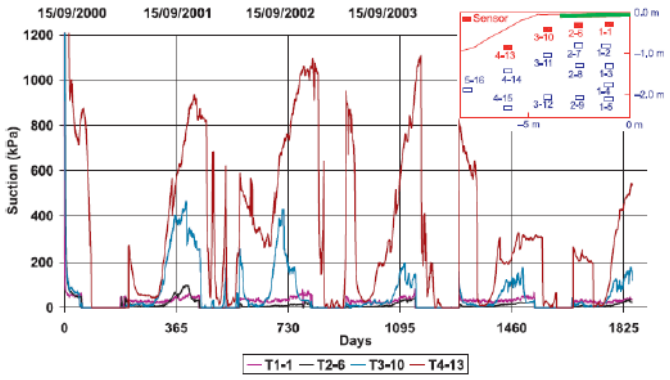

Figure 2–13 Temporal Variation of Suction at Shallow Depths underneath the Pavement and Side Slope (Nguyen et al., 2010)

Heydinger (2003) evaluated moisture and temperature variation at two different sites in Ohio. Similar to a study by Bayomy and Salem (2004), the study reported average moisture values collected at different time of year showing seasonal pattern. The shallow sensor installed at 2 inches from the surface had the most variation due to rainwater seepage and was able to capture transient change in moisture due to rainfall events. However, a sinusoidal moisture model was developed without the effect of precipitation. The study also presents the impact of change in moisture on resilient modulus of soil.

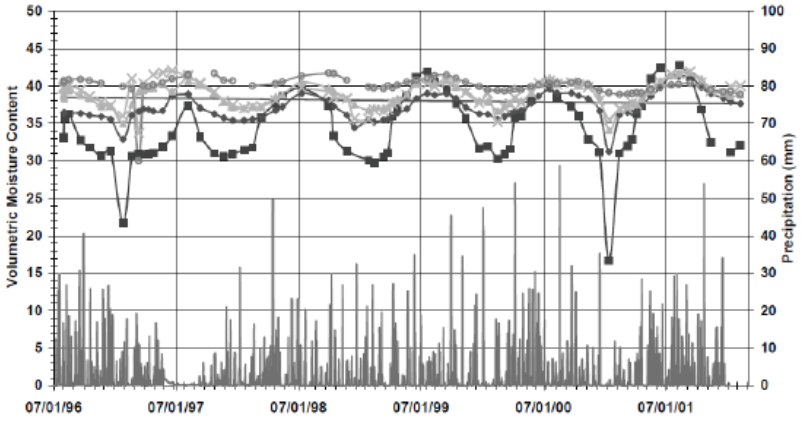

Figure 2–14 In-situ Moisture Measurement in Ohio, USA (Heydinger, 2003)

Kodikara et al. (2014) monitored several sites in Melbourne, Australia for more than 2 years. The maximum depth of investigation was 1500 mm. The study showed that the effect of precipitation was found to be prominent up to a depth of 550 mm while the rest of the moisture probe at deeper depths depicted periodic variation. The change in soil moisture at deeper depths was reported to be dependent on the evaporation rate at the ground surface causing the lag period of three to four months. Field based real time moisture model using 12 months data was developed by fitting the cyclic moisture variation with first degree Fourier series trend. However, no effect of precipitation was incorporated

in the model. The prediction accuracy was observed to be improving with the increasing depth where the effect of rainfall was minimal. The accuracy was even observed to drop below 60% at shallow depths at times. Figure 2–15 show the predicted and measured moisture graph from the study.

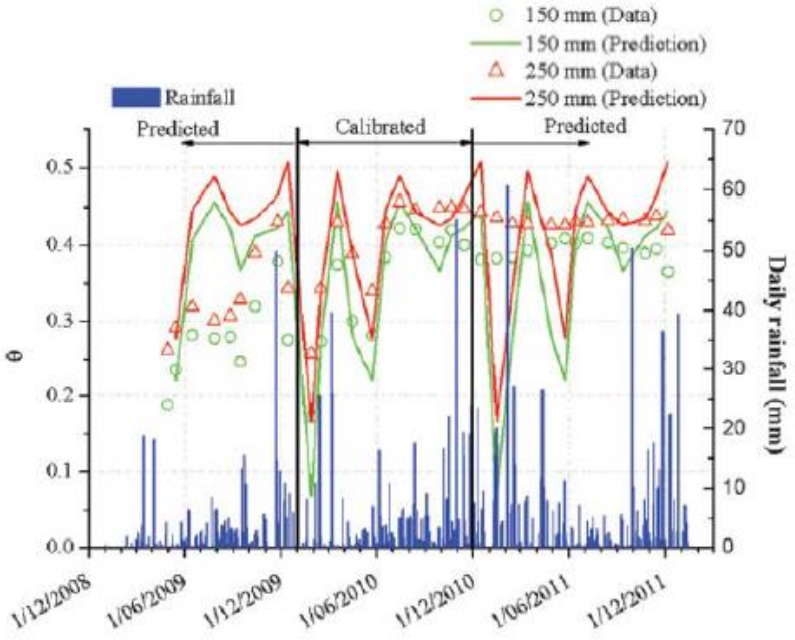

Figure 2–15 Measured vs. Predicted Moisture Profile at Shallow Depths (Kodikara et al., 2014)

Hedayati (2014) instrumented Farm to Market road in North, Texas to evaluate the effect of seasonal climatic loading on the behavior of highly expansive subgrade soil and its impact on the pavement's serviceability. An array of sensors was installed at the edge, outer wheel path, inner wheel path and centerline of the pavement subgrade at varying depths. The study reported the seasonal and transient change in soil moisture content which was found to diminish with the increasing depth. The effect of edge crack was observed with more variation at the edge sensors than the sensors at the center. The effect of moisture variation was also captured in the form of swelling and shrinkage measured

using horizontal inclinometer installed across the roadway. Similar observations were made by Ahmed (2017) who instrumented expansive subgrade soil of State Highway 342 with sensors and inclinometer casings and investigated the effect of climatic loading on the performance of flexible pavement. Both the studies developed a field-based model to quantify the effect of climatic loading on the moisture and deformation of expansive subgrade soil.

Armstrong and Zornberg (2018) investigated the moisture fluctuation along with the surface profile in a Farm to Market Road located 25 miles northeast of Austin. The monitoring was carried out in two phases; one when only the flexible base was laid over the surface and second after laying the asphalt over the base layer. With only the base layer, the subgrade soil wetted and dried quickly. There was not much difference in the matric suction fluctuations between two time periods. However, there was difference in the pavement profile before and after the placement of asphalt layer. In absence of asphalt layer that can possibly act as hydraulic barrier, the wetting of subsoil occurred at the same rate, thus not causing differential movement between the centerline and the edges.

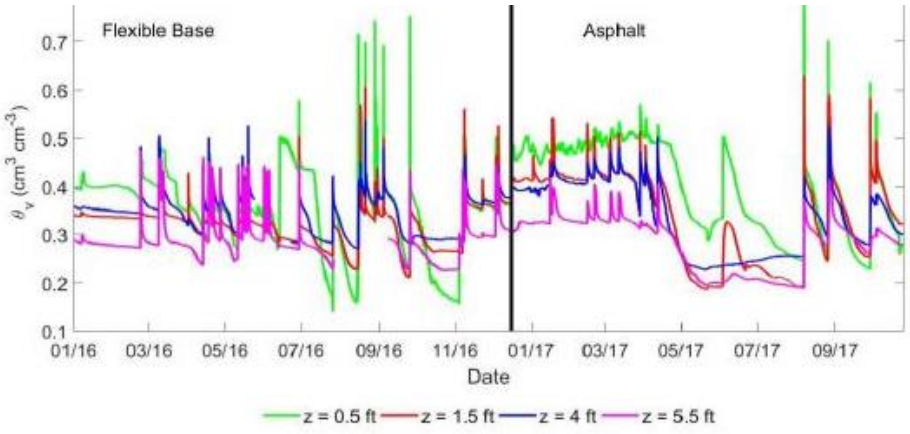

Figure 2–16 Subgrade Volumetric Moisture Content Fluctuations (Armstrong and Zornberg, 2018)

Teltayev and Suppes (2019) studied moisture distribution and temperature variation in pavement layers and highway subgrade of Kazakistan through long term monitoring. The effect of climatic loading was studied with the emphasis on evaluating the impact of temperature on moisture distribution in subgrade at different times. The monitoring results revealed a random daily temperature variation. The sharp increase and decrease in the recorded moisture values was attributed to moisture phase transitions from liquid aggregate condition (water) into solid aggregate condition (ice) and vice versa.

The effect of climatic loading is more at the shallow soil regions and less at the deeper soils. The maximum depth to which the effect of climatic loading can be observed in terms of moisture variation and deformation is referred to as active zone. Clarke (2006) determined active zone, edge moisture variation distance, and long- term equilibrium moisture beneath the covered area by measuring subgrade resistivity. Figure 2–17 show the resistivity profile measured at 3- months interval in a pavement slope of Oklahoma. The author concluded the depth of active zone for the investigated site in Oklahoma to be 1.6 m. The measurement was taken over nine months which indicated seasonal moisture fluctuation at the edge. The change was extreme at the surface which decreased with increasing depth.

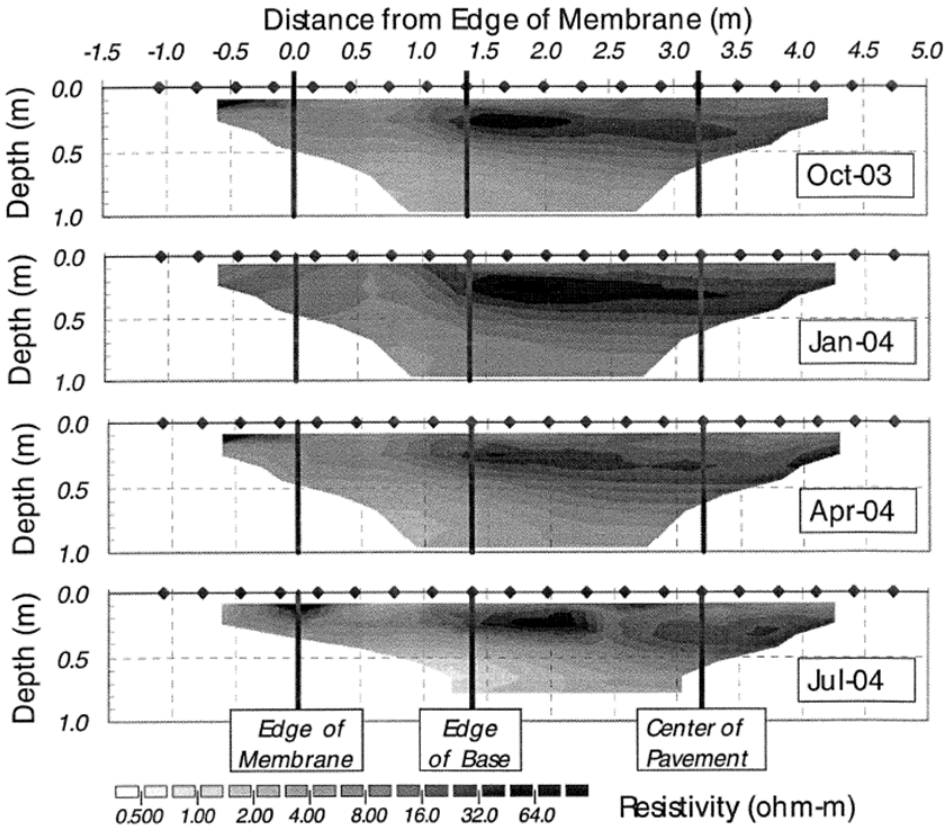

Figure 2–17 Observed Resistivity Profile in a Pavement Slope of Oklahoma (Clarke, 2006)

Moisture variation results in swelling and shrinkage of expansive clay. Nelson et al. (2011) proposed a method to predict heave in terms of moisture infiltration by conducting the study on for residential homes. The author reported unrealistic estimation of heave when the active zone was considered to be too large. Similar statement was made by Talluri et al (2011) and reported that volumetric deformation can be realistically estimated when the active zone is confined to a depth 2 to 3 ft for suction-based methods else over prediction of heave may occur.

Hossain (2013) investigated moisture and suction variation at different depths of a slope built on expansive clay through extensive field instrumentation and concluded the active zone to be 3.2 m in Texas based on the collected data. The dielectric sensors were installed at 4 ft., 8 ft., 12 ft., and 20 ft., at the crest and middle of the slope. The moisture variation was observed to be more to a depth of 8 ft which was found to be diminishing with the increasing depth. The study also incorporated the effect of rainfall duration and intensity on the rainwater infiltration. The long duration low intensity rainfall was found to delay the rainwater intrusion compared to high intensity rainfall. The suction was found to vary in between 0 to 800 kPa during the monitoring period.

Matric suction exceeding 1500 kPa in summer has been reported to initiate shrinkage cracking in pavements (Puppala et al., 2014). The authors evaluated pavement cracking due to shrinkage and concluded linear relationship between shrinkage and gravimetric moisture content as shown in following equations. It should be noted that the study did not consider the effect of excessive tensile strain in the pavement section. Here, the change in moisture content is the difference in soil moisture values prior to and after the completion of shrinkage test.

$$\varepsilon_{sh,vert} = 0.23\,\Delta w$$

$$\varepsilon_{sh,vol} = 0.66\,\Delta w$$

where, $\varepsilon_{sh,vert}$ = Vertical Shrinkage Strain

$\varepsilon_{sh,vol}$= Volumetric Shrinkage Strain

Δw = Variation of Gravimetric Moisture Content

Bruyn and C (1974) analyzed the soil moisture variations and the associated movements under different climatic and soil conditions. In addition, the effect of surface cover in the moisture distribution was analyzed. The study provided some major findings such as the surface layer with fissured highly expansive soil showed much greater seasonal movement. The depth of moisture redistribution is governed by the amplitude of seasonal variation and the varying permeabilities in the shallow depth due to type of soil and climate. Moreover, same amount of heave was observed in both fiber glass covered area and the fallow area due to absence of grassy vegetation which plays a major part in evapotranspiration.

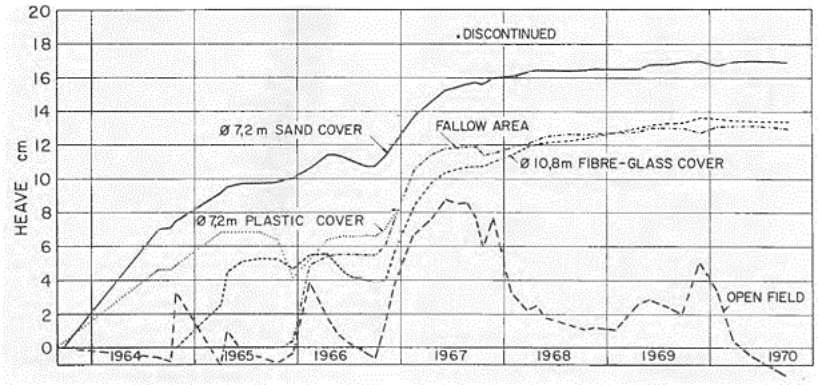

Figure 2–18 Heave against Time in Ondersteport with Different Surface Covers (Bryun and C, 1974)

2.5.2 Analytical Studies

This field of study has also witnessed several research and development of analytical frameworks along with prediction model for better inclusion of several parameters in the design. Change in soil moisture content can be explained as a function of seasonal change in climate and temporary change due to rainfall events. Seasonal change in moisture content demonstrates the periodic variation which can be described using Fourier series.

Seasonal variation is more prominent at deeper depths where the effect of climate is minimal. In the other hand, the moisture variation at shallow depths exhibits temporary rise in moisture in addition to the seasonal variation.

Kodikara et al. (2014) developed a moisture model which captured the periodic fluctuation. The authors utilized the following equation simplified from one dimensional nonlinear diffusion equation to describe moisture fluctuation considering some assumptions.

$$\frac{\partial \theta}{\partial t} = \frac{\partial}{\partial z}\left(D(\theta)\,\frac{\partial \theta}{\partial z}\right)$$

where, θ = Volumetric Soil Moisture Content at depth z at time t

$D(\theta)$ = Soil Moisture Diffusivity

The analytical solution of above equation was developed considering following assumptions:

i) the soil surface experiences harmonic sinusoidal moisture variation considering no transient change due to precipitation

ii) soil moisture is constant and is equal to average soil moisture at infinite depth.

iii) moisture diffusivity is constant throughout the soil profile and over the year. This assumption can be backed by other studies conducted by various research which stated that the change in moisture does not result in higher change in soil moisture diffusivity (Kutilek, 1984; Clothier and White, 1981).

Based on the above assumptions, the solution for the simplified equation can be given by

$$\theta(z,t) = \theta_o + \theta_s e^{-\frac{z}{d}} \sin(\omega t - \frac{z}{d} + C_o)$$

where, $\theta(z,t)$ = soil moisture at any depth z at time t

θ_o= average soil moisture at z over a single period

θ_s= surface soil moisture amplitude

C_o= phase angle correction

ω= angular frequency of the periodic soil moisture fluctuation (2π/T, T = time period)

d = damping depth $\sqrt{\left(\frac{2D}{\omega}\right)}$ (D = diffusivity)

The weather boundary conditions, which are not true harmonic functions as represented by the sinusoidal boundary condition, can be modeled using Fourier analysis. The authors presented the following Fourier solution for the variable weather boundary condition:

$$\theta(z,t) = \theta_o + \sum_{L=1}^{\infty} R_L(z) \sin[L\omega t + \phi_L(z)]$$

Figure 2–19 shows the comparison between the predicted moisture contents from the developed model and the measured moisture from the field. As the model considered only the seasonal variation and omitted the effect of transient moisture change due to rainfall events, the model predictions were more consistent at deeper depths with the measured data. In the other hand, the differences were more at the shallower depths. The incorporation of transient change in moisture at shallow depth due to rainfall would have improved the accuracy of the model.

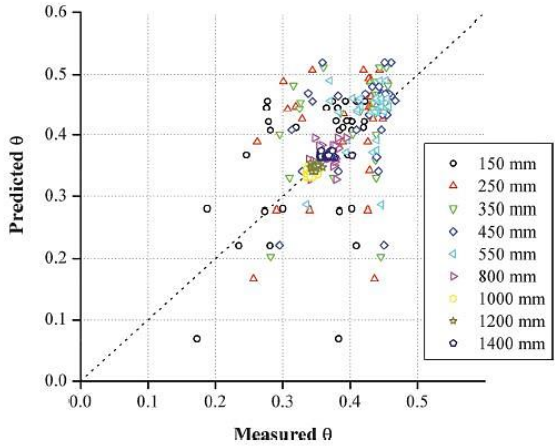

Figure 2–19 Comparison Between Measured and Predicted Moisture Values (Kodikara et al., 2014)

Hedayati (2014) also developed a model incorporating the temporary rise in moisture at shallow depth due to rainfall in addition to the seasonal variation. The author performed a non-parametric analysis in MATLAB with the field obtained time series of moisture. The analysis identified two trends: a main seasonal trend defined using Fourier series with 95% confidence band, and additional peak values due to environmental loading which was analyzed as additional water content and determined by subtracting the peak value from the main seasonal value.

The main seasonal trend was determined by temporarily removing any data outside the periodic fluctuation of moisture explained as

$$\theta = \theta_o + \theta_a \sin(\omega t + C_o)$$

where, θ = volumetric moisture content (m^3/m^3)

θ_o= average moisture content (m^3/m^3)

θ_a= domain of variation(m^3/m^3)

ω= frequency (day^{-1})

C_o= phase correction angle

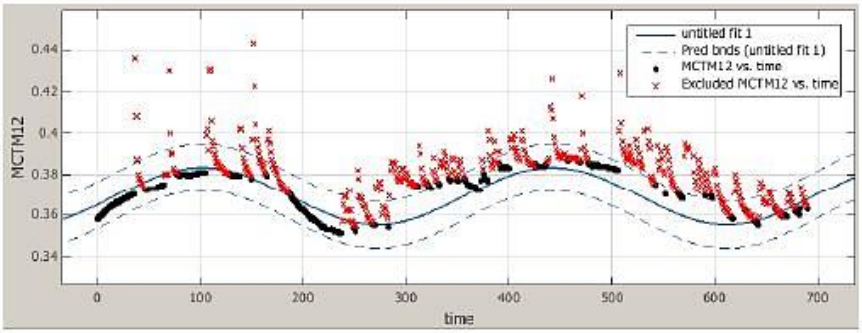

Figure 2–20 Trending Analysis of Moisture (Hedayati, 2014)

The analysis was performed for all sensors and the series parameters were obtained. The effect of sensor's location on the series parameters i.e., domain of variation, frequency and average moisture content of sensors were also studied. Among these, domain of average moisture variation was found to vary the most with depth following the trend that was best explained by an exponential function with R^2= 0.82 as shown in Figure 2–21. The trend showed that the shallower depths exhibited the most variation which reduced rapidly with deeper depths.

$$\theta_a = 0.053\, e^{-0.639\, z}$$

However, no particular trend was observed along the horizontally arranged array of sensors.

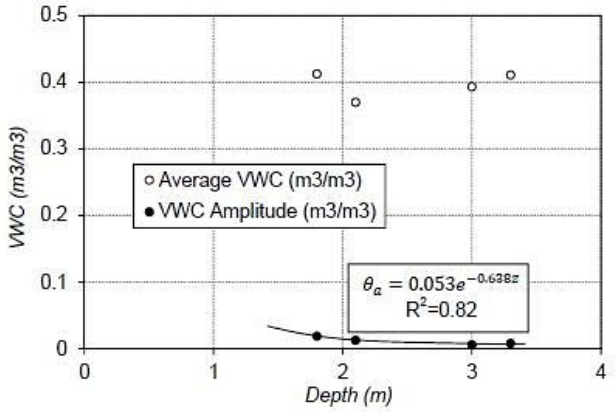

Figure 2–21 Dependency of Moisture Variation Parameters on Sensor Location (Hedayati, 2014)

The temporary increase in moisture from the seasonal trend due to rainfall was analyzed statistically plotting the values against the observed rainfall. A possible trend between rainfall (independent variable), and net and percentage increase of moisture (dependent variable) was studied. The trend was best explained by a linear function. The author concluded that the ability of soil to absorb the moisture and attain saturation level is highly dependent on the existing soil moisture content rather than the amount of rainfall.

The final developed modeled was presented as follows:

$$\theta = f(t,z) + f(t,rainfall)$$

$$= 0.4104 + 0.053\, e^{-0.639\, z} \sin(0.0172t) + 0.0058 Rain_t$$

Figure 2–22 shows the accuracy of the model. The incorporation of moisture increase due to rainfall was found to improve the model accuracy.

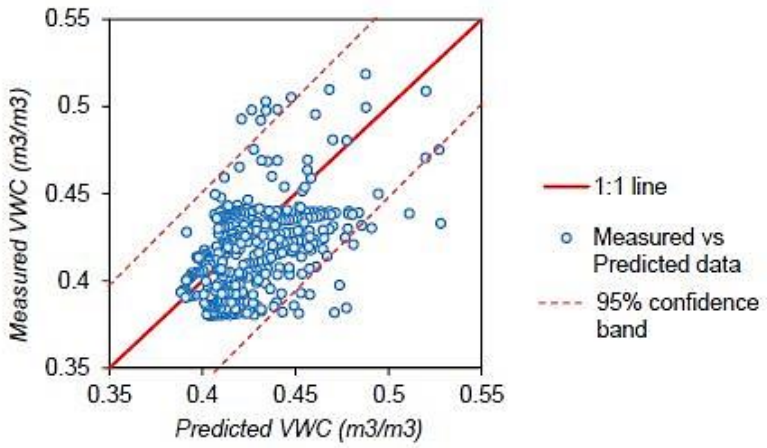

Figure 2–22 Accuracy of the predicted model (Hedayati, 2014)

Similar study was conducted by Ahmed (2017) who developed a moisture model including seasonal and temporary variation. A similar approach as presented by Kodikara et al. (2014) and Hedayati (2014) was followed. The author used the equation given below by Sastry (2012) to obtain the variables of the Fourier series.

$$f\,(t) = a_o + \sum_{n=1}^{\infty}\left(a_n cos\frac{2n\pi x}{T} + b_n sin\frac{2n\pi x}{T}\right)$$

From the overall analysis, the developed moisture model was as follows:

M.C. = [Seasonal Variation] + [Variation due to Rainfall]

= [a_0 + a_1 * cos (x * ω) + b_1 * sin (x * ω)] + [f (rainfall)]

= [17.2825 – 0.46828 * cos (x * 0.01864) + 0.5417 * sin (x * 0.01864)] + [(1.39 + 2.2085 * Rainfall)]

The developed model was validated using data from a randomly selected sensor which is shown in Figure 2–23.

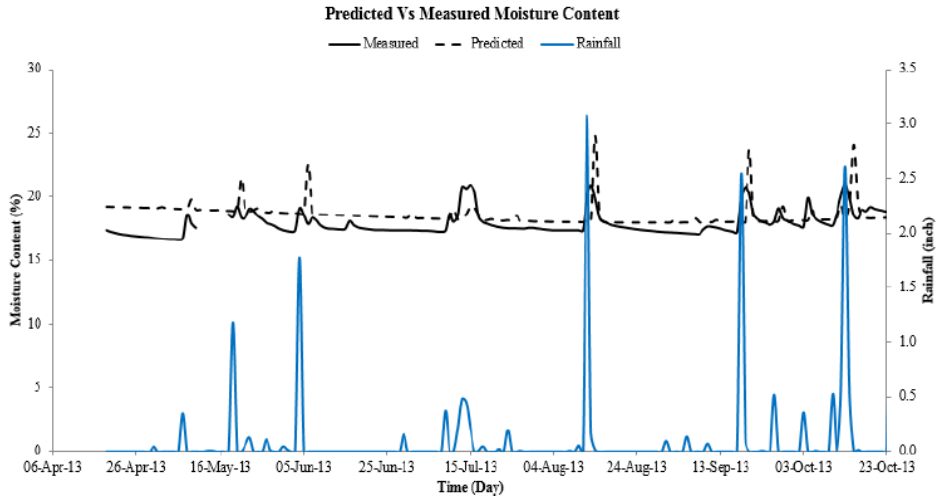

Figure 2–23 Validation of developed moisture model (Ahmed, 2017)

Figure 2–24 shows the comparison of two models developed by Kodikara et al. (2014) and Ahmed (2017). It can be depicted that the model prediction improved significantly after including the temporary variation.

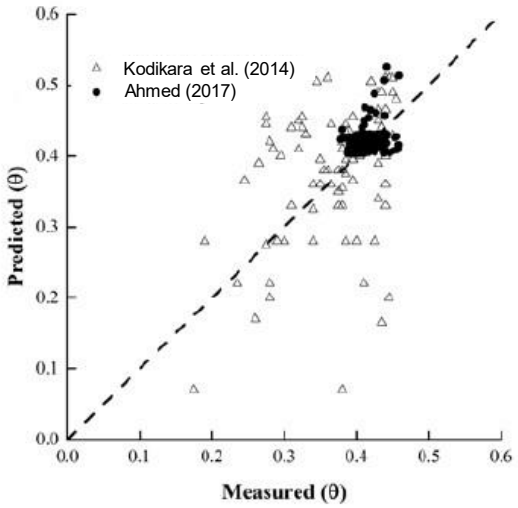

Figure 2–24 Comparison between Kodikara et al. (2014) and Ahmed (2017)

The depth of moisture variation due to rainfall depends on how deep the moisture can penetrate into the soil mass. This is governed by a very important parameter which is referred to as soil moisture diffusion coefficient α. Moisture moves within the soil mass due to change in suction. Following equation can be used to explain the moisture movement in unsaturated soil mass.

$$\frac{\partial^2 u}{\partial x^2} + \frac{\partial^2 u}{\partial y^2} + \frac{\partial^2 u}{\partial z^2} = \frac{1}{\alpha}\frac{\partial u}{\partial t}$$

where α = moisture diffusion coefficient

t= time

u= total suction expressed on logarithmic scale

The change in suction over time at the ground surface can be defined in terms of sinusoidal function as stated by Mitchell (1979) which can be given by

$$u\,(0,t) \;=\; U_e \;+\; U_o\, cos\,(2\pi t n)$$

where U_e= Invariant component of suction

U_o = amplitude of suction variation at the ground surface

n=frequency of suction cycles

Here U_o is estimated from the observed seasonal variation in surface suction. As the surface suction decays with depth exponentially, Mitchell (1979) showed the suction varying with depth symmetric about the equilibrium suction U_e as shown.

$$u\,(y,t) \;=\; U_e \;+\; U_o\, exp\,(-\sqrt{\pi y^2 n/\alpha})\, cos\,(2\pi t n \;-\; \sqrt{\pi y^2 n/\alpha})$$

However, McKeen and Johnson (1990) reported a non-sinusoidal variation in suction from the field measurement. The suction was measured at a depth of 0.15 m in Dallas Fortworth area which is shown in the Figure 2–25. Therefore, surface suction approximated as a sinusoidal function results in the uncertainty in the analysis (Aubeny and Long, 2007).

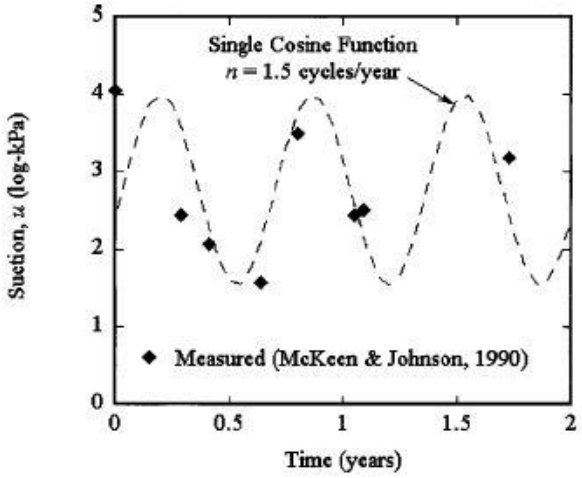

Figure 2–25 Measured Surface Suction History at Dallas- Fort Worth Site (McKeen and Johnson, 1990)

To address this uncertainty in analysis, Aubeny and Long (2007) developed a simple model for defining a suction envelope in terms of maximum suction observed in dry climate U_{dry}, and minimum suction observed in wet climate U_{wet}. In humid climate, equilibrium suction U_e is much closer to the wet season and vice versa in arid climate. Moreover, the depth of penetration of moisture is less in predominantly humid and arid climates than in climates where wet and dry season occurs for equal duration (Mitchell 1979). The unequal duration of wet and dry period creates an asymmetric suction envelope which was modeled using step functions of surface suction.

The developed generalized solution for suction within the soil mass corresponding to non-harmonic surface suction conditions is given by:

$$u(y,t) = U_e + (U_{dry} - U_{wet}) \sum_{k=1}^{\infty} \alpha_k \, exp\,(-\sqrt{\lambda k}) \, cos\,(\tau k - \sqrt{\lambda k})$$

Aubeny and Long (2007) further compared the moisture diffusion coefficient value estimated from field measured suction values and laboratory tests. Soil samples collected from Texas sites were utilized to measure the moisture diffusion coefficient in lab. The samples were collected from relatively shallow depths ranging from 0.3 to 4.3m. The laboratory obtained moisture diffusivity value indicate a range of α = 0.1 – 0.3 m^2/year.

In the other hand, various approaches can be adopted to measure the diffusion coefficient in the field. McKeen and Johnson (1990) back calculated α from the decay of seasonal variation of surface suction with depth using following equation.

$$u\,(y,t) = U_e + U_o \, exp\,(-\sqrt{\pi y^2 n/\alpha}) \, cos\,(2\pi t n - \sqrt{\pi y^2 n/\alpha})$$

The estimated diffusion coefficient was in the range of 3.2 to 13 m^2/year. The alternative approach to estimate α from the change in suction within the soil mass due to permanent change in suction on the boundary was followed by Mitchell (1979) and the parameter was determined to be 0.33 m^2/year. McKeen and Johnson (1990) when applied this method, α was estimated to be 4.5 m^2/year which was within the range of diffusion coefficient estimated from suction decay measurements. The third approach was the time lag approach which is not very common, and the estimated value was 1.9 m^2/year (Mitchell 1979). Besides the discussed approach, the depth of moisture active zone can provide rough estimate of diffusion coefficient.

The comparison of the field and lab obtained diffusion coefficient indicated that the field value can vary up to nearly two orders of magnitude greater than laboratory range. The author suggested the desiccation crack within the soil mass to be the main reason for the

differences. The moisture diffuses much more rapidly in cracked soil than in intact soil. The suction on the surface of cracks equals the suction at the free surface. This deepens the moisture variation within the soil mass.

Saha et al. (2019) develop an improved prediction model of equilibrium suction taking into account various factors such as precipitation, evapotranspiration, field capacity etc. to overcome the limitation of EICM which use depth to ground water table to compute the moisture content and the corresponding suction in subgrade. A GIS based TMI contour map of the continental United States was developed by the authors using temperature and precipitation data which showed good agreement with the original TMI map. A model was developed for equilibrium suction based on Mitchell's steady state diffusivity equation (given below) and a functional relationship between TMI and mean annual moisture depth.

$$u\,(z) = u_e \pm u_o * e^{-\sqrt{\frac{\pi n}{\alpha}}z}$$

where, $u\,(z)$ is the suction at depth z (cm) from the ground surface

u_e is the equilibrium value of suction

u_o is the suction profile amplitude

n is the number of suction cycles per second (1 year = 365 x 24 x 60 x 60s)

α is the unsaturated soil diffusion coefficient (cm^2/sec)

A GIS based equilibrium suction contour map was generated which can be used to extract equilibrium suction at any geographic coordinate. Then, a simplified regression model was developed to predict the equilibrium suction from readily available and influential parameters such as TMI, plasticity index and dry suction value. The developed model when

used in an analysis approach can accurately estimate critical parameters such as subgrade resilient modulus and vertical movement due to swelling and shrinking of expansive clays.

A study conducted by Heydinger (2003) showed the seasonal variation of moisture at a pavement site in Ohio. Waveform data from time domain reflectometry (TDR) probes were analyzed to obtain volumetric moisture content (VMC) for more than 5 years. The soil moisture data were analyzed using sinusoidal equations as shown below:

$$VMC\ (t) = 37.1 + 1.66\sin\left[\frac{2\pi}{365.25(t-130)}\right]$$

2.5.3 Numerical Studies

Numerical modeling is widely adopted to deal with complex real field problems by computational simulation. It utilizes mathematical models to describe the physical conditions and solves them to get interpretable results. Among various geotechnical scenarios, researchers have been frequently using numerical modeling to estimate the behavior of expansive subgrade soil primarily in terms of transient moisture flow and deformation analysis. Figure 2–26 below represents the widely followed modeling process to study the transient seepage analysis due to climatic condition and subsequent deformation.

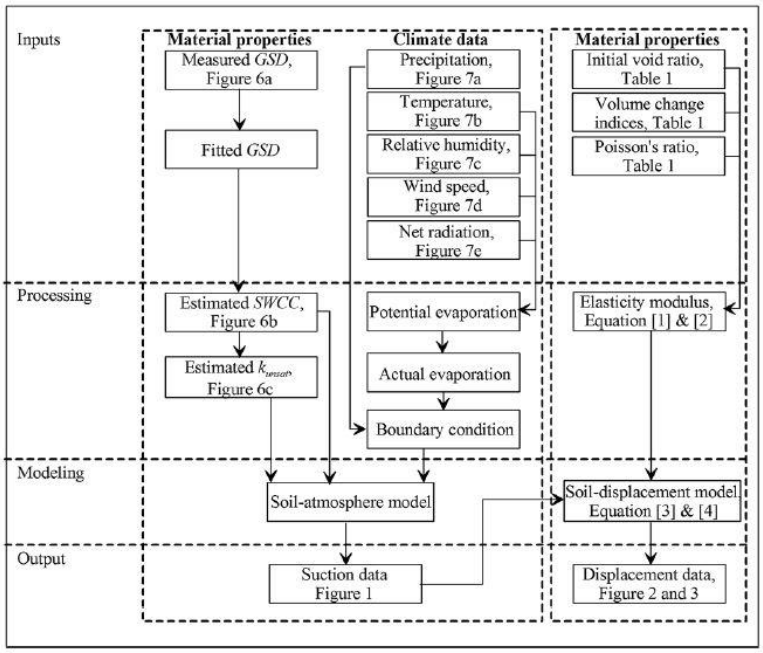

Figure 2–26 Modeling Process (Ito et al., 2014)

Ikra and Wang (2017) predicted the moisture content in the expansive subgrade soil beneath flexible pavement in response to weather conditions using VADOSE/W. The climate data applied on the model as a boundary flux after establishing initial conditions simulated the moisture condition in the subgrade soil which corresponded well with the field measured values.

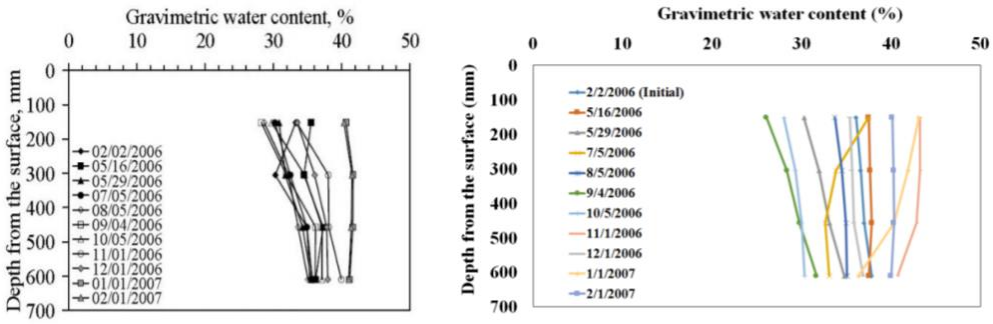

Figure 2–27 Measured and Simulated Water Content Data (Ikra and Wang, 2017)

Pufahl and Lytton (1991) computed the temperature and suction profiles beneath highway pavements for the specified time using computer model. The temperature and suction profile were computed for three instrumented sites in the US with variable climatic conditions. Some discrepancies in the model computed suction values with the field values was associated to cracks in the real field which could not be simulated in the numerical model.

Hansson et al. (2005) studied the water flow patterns in the flexible pavement due to variations in precipitation and fracture conductivity by modifying the numerical code, Hydrus- 2D. It was observed that the larger precipitation amount expanded the infiltration zone laterally as the infiltration capacity of soil adjacent to asphalt was exceeded. The study concluded that water flow patterns altered with the precipitation statistics and surface fractures.

Rajeev et al. (2012) predicted the long-term moisture and temperature variations using numerical modeling. The study showed that the effect of rainfall was maximum at the shallow depth exhibiting peaks immediately after the rainfall while a lag period of 4 weeks to several months was seen for deeper depths. In the study, initial suction values were assigned such that corresponding moisture values from SWCC corresponded to the field moisture content at the start date of analysis. Also, field soil temperature measured on the same day was used as initial temperature profile. After calibrating the model with the field results, the long-term modeling of soil moisture and temperature was performed. Numerical models can be simulated with higher precision if SWCCs reconstructed from field data are incorporated (Ahmed et al., 2021).

Liu (2015) investigated the influence of rainfall characteristics in the distribution of subgrade moisture fields from physical model and numerical modeling. The study showed

that the moisture zone expanded in logarithmic manner with the increase in rainfall intensity.

Ito et al. (2014) developed a two-staged deformation model by simultaneously calculating soil suction and stress state. The soil atmosphere model was utilized to obtain suction profile in a soil mass with appropriate material properties and boundary flux provided in terms of precipitation, temperature, relative humidity, wind speed and net radiation. The study showed that the volume changes were more at the surface which decreased gradually with the increasing depth due to isolation from meteorological conditions.

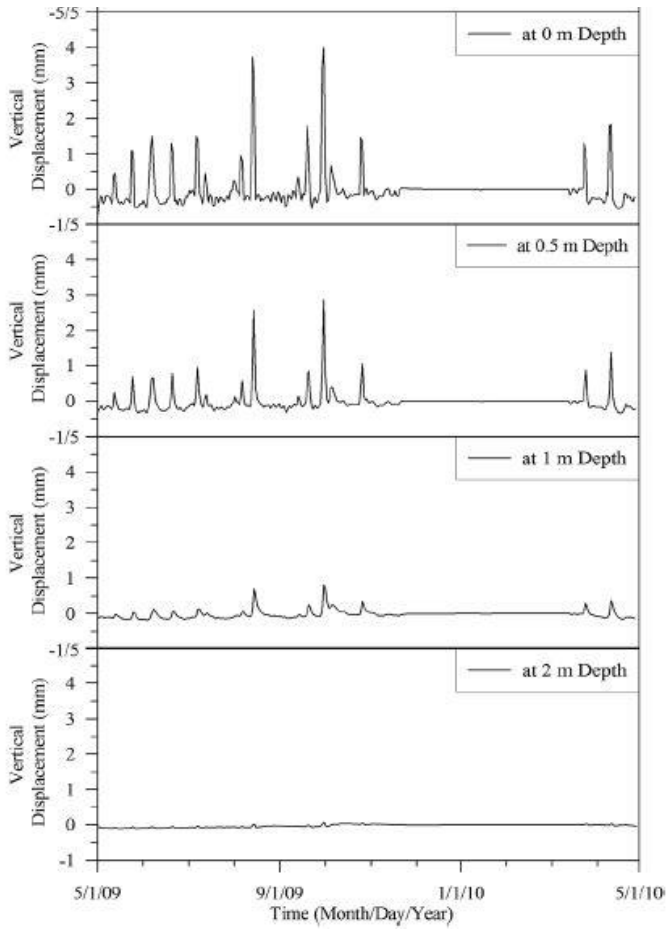

Figure 2–28 Predicted Soil Deformation under Exposed Surface (Ito et al., 2014)

Luo and Prozzi (2010) investigated the mechanism of longitudinal cracks development in the pavement due to expansive soils. The author utilized ABAQUS to determine the developed shrinkage stress that can initiate the crack in the pavement structure. The modeling revealed that the crack initiates in the subgrade soil which propagates to the surface over time. Linear elastic fracture mechanics theory was utilized to analyze the crack propagation to the surface.

Wanyan et al. (2014) studied crack propagation through the base and HMA layers using finite element program. Moisture content based longitudinal shrinkage crack model developed by Sabnis (2008) was used in the program. The study showed higher tensile stresses developing within top 5 inches of subgrade initiating the longitudinal cracks at the base-subgrade interface most of the times. Moreover, the weak bond of materials at the shoulder interface caused cracks to appear near the shoulder surface.

The effect of climatic loading on concrete pavements over expansive clay was also studied by Zhang and Liu (2008) in numerical environment. Coupled hydro mechanical stress analysis in ABAQUS was utilized for the purpose. The initial condition was set with the constant suction of 100 kPa at the bottom increasing linearly up to the surface and weather condition for two-year period was applied. The impact of changing climatic conditions was very much evident at the edge of the pavement than the center.

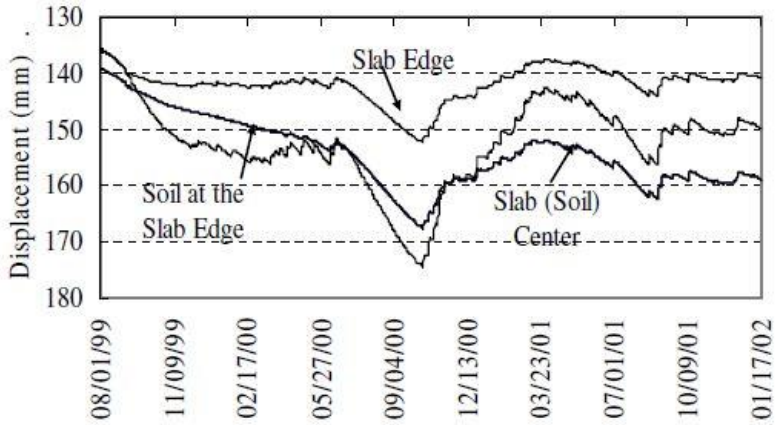

Figure 2–29 Vertical Displacement for Different Locations at Different Times (Zhang and Liu 2008)

Fredlund and Hung (2001) predicted the volume change in an expansive soil as a result of vegetation and environmental changes. The authors performed both seepage and stress-deformation analyses using a Partial Differential Equation Solver, PDEase2D for the unsaturated soil. The study showed that the magnitude of deformation of structures and soils close to the trees decreases with the vertical and horizontal distance from trees and with decreasing of water uptake rates.

Fredlund et al (2003) simulated the swelling and shrinking around slabs on ground constructed on expansive soils. Three scenarios of edge drop due to evaporation, edge lift due to infiltration and edge lift due to constant thickness of concrete slab was considered for the study. Similar study was carried out by Zhang et al (2009) where residential building built on expansive soils influenced by the local daily weather conditions and a tree over a period of two years was analyzed using ABAQUS. The analysis showed shrinkage of soils at the edge resulting in no contact between the slab and soil after a prolonged period drought. In the other hand rainy season was characterized with the heaving of soil outside the building resulting in uniform distribution of contact pressure.

Abbaszadeh, M (2011) studied the effect of cracks on unsaturated flow and volume change properties of expansive clays and on performance of the foundation. The study was carried out in finite element program SVFlux. Two soil layers were considered in the simulation: the top layer as cracked surface and bottom layer as intact surface. Same SWCC and different K-function were used for two layers. The author concluded to have significant influence of cracks in unsaturated hydraulic conductivity of soil. However, there lacks the study on crack healing and its effect on saturated and unsaturated hydraulic conductivities across wider range of clay types.

2.6 Remedy for Expansive Soil

The overall performance of pavement depends greatly on the properties of the supporting soil. However, these properties are governed by various factors. The selection of appropriate remedial measures and its proper implementation can mitigate the potential damage to the pavement structure and enhances the serviceability of pavement. Different methods have been proposed to control the swell-shrink potential of expansive soil which are as follows:

a) Soil removal and replacement: The weak soil can be removed to a certain depth and replaced with stronger and stiff soil. However, this is not possible if the expansive soil is extended to greater depth.

b) Prewetting of soil: In this method, the expansive clay subgrade soil is inundated with moisture and allowed to attain full swelling.

c) Re compaction and strengthening of subgrade and pavement section: The compaction of subgrade soil at a moisture content slightly drier than optimum has been successfully used to control subgrade volume change (Petry and Little, 2002).

d) Chemical treatment for base and subgrade: Chemical stabilization has been found to enhance the properties of subgrade soil. Lime stabilization is most frequently used for alteration in the subgrade soil. It has also been reported 2 to 3 percent Type I cement can reduce swelling of the soil significantly. In some instances, liquid ionic soil stabilizers have also been used to enhance engineering properties of expansive clay (Gautam et al., 2020). These stabilizers increase the strength and stiffness of the soil, reduce swelling, decrease permeability etc. It may be noted that stabilization using lime and cement are not suitable for all types of soil and are especially detrimental to high sulfate soils (Sherwood, 1962; Mitchell and Dermatas, 1992; Petry and Little, 1992). In addition, such chemical treatments require several days to gain strength which makes them less feasible for roads with heavy traffic due to necessity of reopening traffic (Sebesta, 2002; Harris, 2008; Dessouky et al., 2015).

e) Moisture control using barrier: Maintaining a constant moisture content in the subgrade soil can reduce the potential swell shrink behavior. Various moisture barrier has been discovered to be effective in minimizing the moisture variation in the subgrade soil and controlling the possible volumetric deformation.

2.7 Controlling Rainwater Intrusion in Pavement Subgrade

An engineering solution becomes sustainable when its life cycle cost is less. Even though the upfront resources might be intensive, a sustainable solution exhibits low investments in terms of cost and labor over a period of time. This is due to the decrease in repair and maintenance requirements on a long run. Numerous engineering solutions, for instance, the use of recycled plastic pins in geotechnical applications (Bhandari et al., 2020; Badhon et al., 2021; Bhandari et al., 2021; Islam et al., 2021a; Islam et al., 2021b), and the use of recycled asphalt pavement and recycled concrete as pavement base and subbase

(Bhandari et al., 2019; Imtiaz et al., 2020), among others have demonstrated their promising sustainable innovations. Controlling rainwater intrusion in pavement subgrade can lead to less repair and maintenance on the long run and thus, lower the overall life cycle cost of the selected approach.

The main sources of moisture variation in the subgrade soil are rainfall and evapotranspiration. The presence of excess moisture content reduces the bearing capacity of the subbase and the subgrade causing failure of the pavement system. Constant moisture content of expansive soil reduces soil movement that might cause damage to the pavement. Equilibrium moisture content can be maintained in the subgrade soil with the proper mechanism to prevent the infiltration of moisture and drain the water away from the system. Collecting the water at the edge of pavement can be one of the simplest methods to do so.

M-E Design Guide recommends subsurface drainage to lower the ground water level, intercept the lateral flow of subsurface water beneath the pavement structure, and remove the water that infiltrates the pavement's surface (Manosuthikij, 2008). Rollins and Christie (2002) states improper or lack of drainage causes problems in collapsible and expansive subgrade soils with the development of ponding and soft spots. The authors suggest cross drain through the median for lateral drainage and lining in the drainage ditches using asphalt and gravel to prevent leakage.

2.8 Moisture Control Using Barriers

Moisture barriers can isolate the subgrade soil from the seasonal change in climatic conditions. There are different types of moisture barrier such as horizontal moisture barrier, vertical moisture barrier, modified moisture barrier etc. The geomembrane as a moisture barrier was first used in Victoria in 1985 when a section of Sunraysia Highway at Morton

Plains was reconstructed due to pavement damage caused by expansive soils. This trial (described in detail by Holden, 1992; Evans and Holden, 1997) showed that the vertical moisture barrier significantly increased the life of the pavement.

Liu et al (2018) studied the effectiveness of geosynthetics clay liners as a barrier to minimize the fluctuation of moisture and temperature in highway subgrades through numerical analysis. The barrier was found to effectively prevent the rainfall infiltration and maintain equilibrium moisture in the subgrade. The author concluded that the presence of GCL resulted in the unchanged porewater pressure in the underlying soil and hence the strength of the subgrade soil was not compromised.

2.8.1 Vertical Moisture Barrier

In the past few decades, Vertical Moisture Barrier (VMB) has been used to control the problems associated to expansive subgrade soil across United States. Jayatilaka et al. (1992) states vertical moisture barrier to be more suitable for wet and semi-arid climates with cracked soils and shallow root zones.

Vertical moisture barriers were used by the Texas Department of Transportation from mid-1990s when expansive clays required frequent maintenance work (Jayatilaka and Lytton, 1997). The barriers are installed at the edge of the pavement to isolate the subgrade soil beneath the pavement from changing climatic conditions. The vertical moisture barrier extended to a depth of 6 ft -8 ft is designed to prevent the possible moisture intrusion from the edge. The barriers were successful in reducing the pavement roughness and the performance was observed to be improving with increased depth of VMB. However, the construction of vertical moisture barrier involves great difficulty as well as increased cost.

2.8.2 Horizontal Moisture Barrier

Geosynthetics are primarily used in pavements for separation, reinforcement, and drainage (Barksdale et al., 1989). Horizontal moisture barrier is placed at the base-subgrade interface to isolate the subgrade soil from the environmental conditions. The research on horizontal moisture barrier is limited as compared to vertical moisture barrier.

Geocomposite Capillary Barrier Drain (GCBD) developed by Henry and Stormont (2000) removes the water from the soil at negative pore water pressure. The system with the fine soil underlain by a coarse soil forms a capillary barrier due to the difference in their hydraulic characteristics. The infiltrating water accumulates at the interface in such system until the air entry value of the underlying soil is attained after which the water breaks into lower layers (Henry et al., 2002) as shown in (Figure 2–30). Placing a fine sand at the interface (which acts as a transport layer) accelerates the drainage of water significantly (Figure 2–30). According to Stormont and Morris (1998), sand and gravel as a transport layer and capillary barrier respectively can make the system effective. Same action is performed by Geocomposite capillary barrier which consists of geonet sandwiched in between geotextiles. The top geotextile, geonet and bottom geotextile acts as a transport layer, capillary barrier and separator layer respectively. One of the major limitations of this system is that it allows breakthrough of rainwater during extended rainfall period.

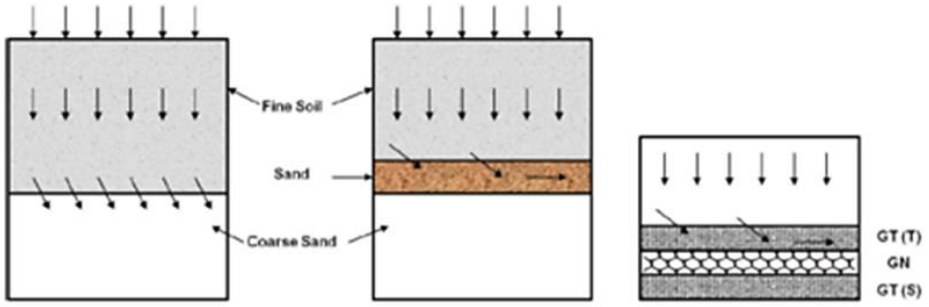

Figure 2–30 Lateral Drainage in Unsaturated Soil with the incorporation of GCBD (Redrawn from Henry et al., 2002)

Chen and Bulut (2016) studied the effect of outside crack on the performance of horizontal moisture barrier using numerical modeling. The outside crack resulted in the increased suction value to deeper depth as seen in Figure 2–32. The author also incorporated the effects of unsaturated soil moisture diffusion coefficient, drying time on the suction distribution and vertical displacement in ABAQUS.

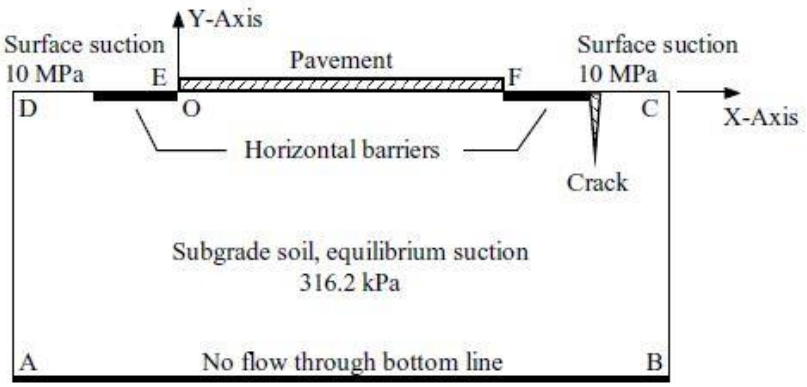

Figure 2–31 Geometrical Model for Finite Element Analysis (Chen and Bulut, 2016)

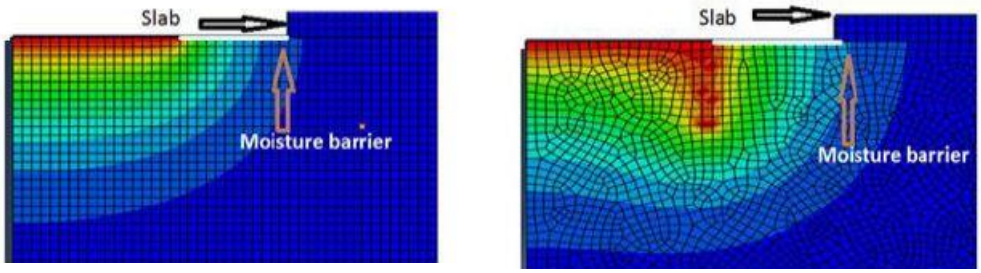

(a) (b)

Figure 2–32 Suction Profile (a) Without and (a) With Outside Cracks (Chen and Bulut, 2016)

2.8.3 Modified Moisture Barrier

Modified moisture barrier is the modification of a geo-composite capillary barrier drain (GCBD). It overcomes the limitation of GCBD by incorporating an additional component of geomembrane which is an impermeable geosynthetics material and is capable of preventing moisture infiltrating through geocomposite layer after a breakthrough point (Ahmed, 2017; Sapkota et al.,2019). With GCBD, some part of infiltrated moisture might reach the subgrade soil, but the impermeable layer of geomembrane can inhibit the moisture to reach the subgrade soil. The mechanism of modified moisture barrier is illustrated in the figure below.

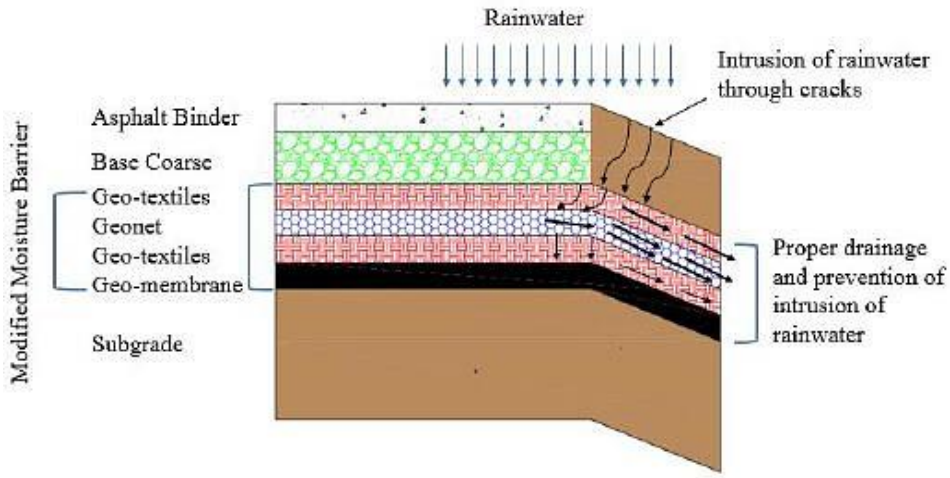

Figure 2–33 Mechanism of Modified Moisture Barrier (Sapkota et al., 2019)

2.9 Previous Studies on Moisture Barriers

The Texas State Department of Highways and Public Transportation conducted a study by implementing horizontal and vertical geomembrane in several sites to stabilize the deteriorated pavement section (Steinberg, 1989). The horizontal barrier was installed in one site while the vertical barrier was utilized in eleven pavement sites. Based on the continuous monitoring of these sites, it was observed that the fabric protected sections generally showed higher serviceability index than the control section.

The geomembrane was first utilized in Texas on General McMullen Drive as a horizontal moisture barrier (Steinberg, 1989). The pavement was stabilized after witnessing severe distortions due to swelling clays. The monitoring results showed the higher serviceability in the section installed with geomembrane. However, the decreasing trend of serviceability index (SI) was observed for all the sections with time.

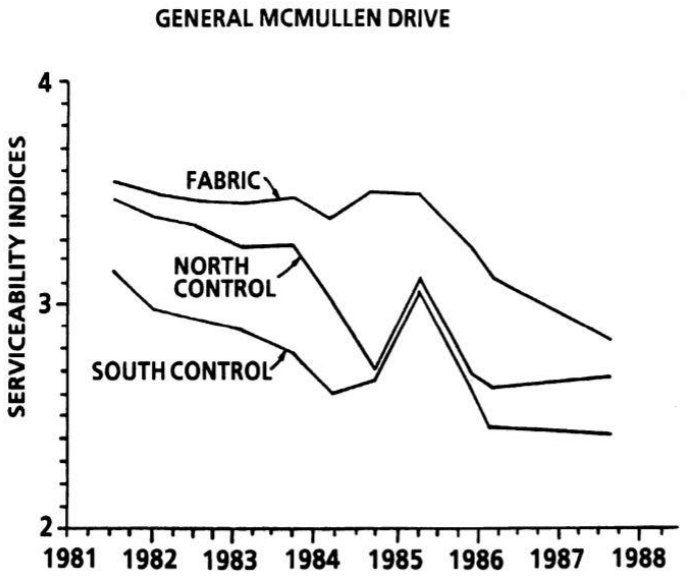

Figure 2–34 Serviceability Index of the Stabilized and Control sections of McMullen Drive (Steinberg, 1989)

The first implementation of vertical moisture barrier was done on Highway Loop 410 in 1979 followed by its implementation in Highway 37 in the year 1980 (Steinberg, 1989). The performance of the barrier was evaluated through sensor testing, photo logging and profilometer testing. The photo logging indicated improved performance of the protected lanes with relatively very few pavement cracking. The relatively lower roughness with the implementation of vertical moisture barrier led to more utilization of the system in other sites Steinberg (1980;1985;1989;1992). The studies concluded deep vertical moisture barrier as being effective in controlling expansive soil movement on pavement. Figure 2–35 shows a typical cross section of a pavement using vertical moisture barrier.

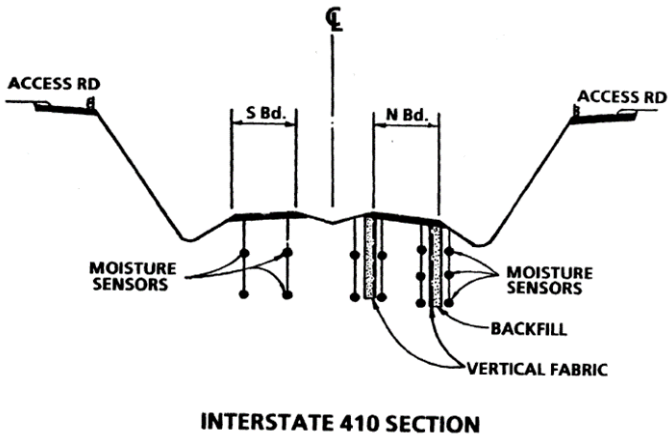

Figure 2–35 Schematic of Vertical Moisture Barrier in Interstate 410 Section (Steinberg, 1989)

Figure 2–36 shows the serviceability index of interstate 410 which was plotted after the long-term monitoring data. The success of the application of vertical moisture barrier in this section established a base for using this stabilization technique in the other pavement sections as well which had serious maintenance problem.

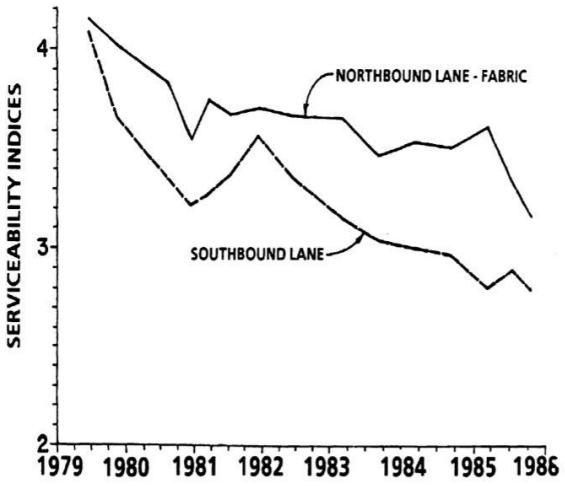

Figure 2–36 Comparison of Serviceability Index in the Fabric Protected and Control Sections of Interstate 410 (Steinberg, 1989)

The second application of vertical moisture barrier was done on Interstate 37 which also experienced heavy distresses. The monitoring of the stabilized section showed reduced pavement cracking than the control section where no barrier was provided. However, significant change in moisture was recorded in the sensors outside the vertical moisture barrier as compared to the sensors installed inside (Picornell et al., 1984). The stabilized sections with the reduced pavement cracking did not require maintenance until 1988. Similar observations were made on other sites due to the enhanced serviceability of pavement with the use of vertical moisture barrier.

Even though the initial results indicated the reduced moisture change with the deep vertical moisture barrier, the serviceability indices were observed to decrease over time. Pavements are not completely impermeable as revealed by several tests (Dempsey and Robnett, 1979) and water may penetrate from them. This water reaches the swelling soil subgrade resulting in its excessive movement. Moreover, great difficulties in construction were encountered during the implementation of vertical moisture barrier. The backfilling of the trench is also a crucial criterion with the higher installation depth (at least 2.4 m in most of the cases). An improper backfilling can act as a passage for moisture intrusion and formation of cracks as can be seen in Figure 2–37.

Figure 2–37 Crack at Pavement Edge after Installing Vertical Barrier (Steinberg, 1989)

The roughness development on pavements was also studied by Gay (1994) and found the moisture barriers to be effective in reducing roughness of the pavement. Three types of barrier were used: Ethylene vinyl acetate (EVA)-coated fabric, injected lime slurry, and injected lime-fly ash slurry and two depths were considered. Periodic measurements of the stabilized section were carried out with the matric suction measurements taken more frequently using sensors embedded both inside and outside the moisture barriers at different depths.

The behavior of a paved road reinforced with geosynthetics at the bottom of the road section was studied by Dondi (1994) using ABAQUS. The non-linear constitutive laws of the multilayer materials were simulated by the appropriate models, taking in to account the frictional behavior on the geotextile soil interfaces surfaces. Cam clay model was used as for cohesive subsoil layer and geosynthetic was modelled using membrane elements. The study showed that the friction developed between the geosynthetic and the granular soil in the foundation layer considerably reduced the shear stress between the geosynthetics and the subsoil. This increased life of the pavement. Moreover, the geosynthetic acts as the

base of the foundation layer, absorbing part of shear stresses, and strains that would otherwise affect the subsoil.

Picornell et al. (1984) also concluded moisture barriers to be effective in controlling the roughness of the pavement. The author evaluated the performance of barrier by measuring pavement roughness and matric suction potential at both sides of barrier. The performance evaluation included roughness spectra analysis, percentage of distressed area from photo logging and determination of present serviceability index for stabilized and control section. For the matric suction determination, the laboratory-calibrated sensors were installed at three different depths. The study showed constant matric suction value on the inner side of barrier with drastic changes on the outer side. In addition, the barrier was able to maintain lower loss in serviceability and lower distresses as compared to control section.

Jayatilaka and Lytton (1997) developed the vertical movement model and roughness model in terms of Serviceability Index and International Roughness Index using computer program. The field-based study of the effectiveness of vertical moisture barrier was carried out at ten different sites in terms of Present Serviceability Index (PSI) and International Roughness Index (IRI). All PSI and IRI data collected were analysed and mathematical models were developed to predict the roughness with time. At first the model for vertical movement was developed using two computer programs MOPREC (climate-based model from moisture balance procedure) and FLODEF (FEM program for calculating vertical movement profile across a pavement section with and without vertical moisture barrier). Then roughness model was developed in terms of PSI and IRI. Both the models were incorporated in a computer program PRES, written in FORTRAN language to predict the roughness over time. The roughness prediction model can be used in determining the

effectiveness of vertical moisture barrier. The author identified vertical moisture barrier to be effective in reducing the development of roughness.

Many moisture barriers in Texas extend to a depth 2.4 meters. Picornell et al., (1987) proposed a method to find the depth of vertical moisture barrier as a function of climate and soil characteristics. The author suggested maximum volume changes as being governed by the wettest and driest moisture profiles that can occur in an exposed soil. Therefore, the effect of vegetation in the moisture removal from the soil mass was evaluated to obtain the driest profile that can possibly cause the shrinkage cracks. The extraction of water was simulated in the numerical environment by knowing the root density distribution and rooting depth of the vegetative cover. The finite element method was used to model the moisture flow and in the analysis of nonlinear elastic deformation of the soil. The author used edge distortion and maximum crack depth for the determination moisture barrier's depth. Picornell and Lytton (1987) suggest the barrier to be extended to a depth of root to prevent cracking and 25 percent deeper to prevent roughness in pavement.

Furthermore, Rahim and Picornell (1989) developed a computer program to evaluate different types of barrier. The soil was considered to be divided into several blocks and the moisture movement was allowed only along the cracks between two soil blocks. The program showed that the barrier accelerated swelling of subgrade soil in the presence of surface cracks that allow the moisture to infiltrate into lower layers of pavement. The information on size of soil blocks is needed to be provided in the program to form shrinkage crack fabric and evaluate the behavior of barrier. However, the data is not readily available in Texas.

Chen and Bulut (2015) studied the performance of vertical moisture barrier in the presence of cracks outside the protected area. The study was done in numerical environment using

Abaqus software. The author compared the suction distribution with outside cracks to the suction distribution in the case without outside cracks and the case without vertical moisture barrier. The author concluded that the outside cracks greatly affect the performance of vertical moisture barriers. Moreover, the increasing depth of cracks was found to have negative impact on the performance of vertical moisture barrier, hence suggest using horizontal moisture barriers.

Al-Qadi et al. (2004) studied the effect of a horizontal geocomposite membrane as a moisture barrier underneath the Virginia Smart Road. The barrier was placed during the construction of Virginia Smart Road. The membrane was installed over half the length of a pavement test section while the other half was left without geocomposite membrane. To evaluate the effectiveness of barrier, ground penetrating radar (GPR) and time-domain reflectometry were utilized. The study showed the horizontal geocomposite membrane to be effective in maintaining constant moisture profile and less pavement deflection.

GPR result analysis showed that the membrane was able to reduce the moisture infiltration by as much as 40% after rainfall event in the stabilized section. The moisture content was found to be constant beneath the pavement and independent of rainfall which is the primary source of transient moisture variation in pavement. Figure 2–38 shows the moisture content variation plotted against the rainfall event. From the results, it is clearly observed that the despite the rainfall events, the moisture content is observed to be constant. The authors concluded that the barrier was effectively reducing the amount of water that could have reached the subgrade soil.

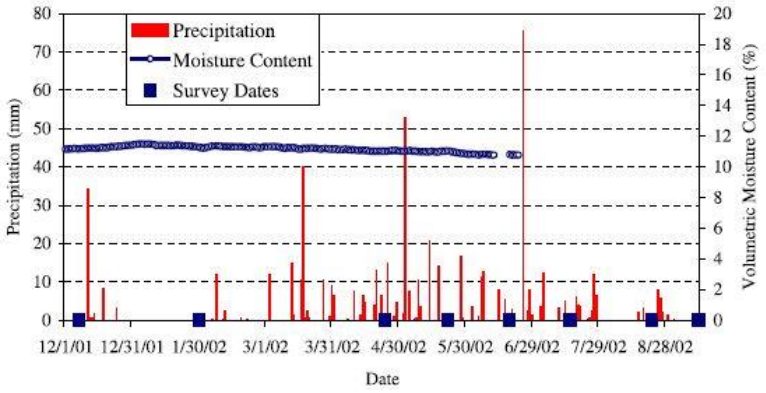

Figure 2–38 Moisture Content Measured by TDR under Moisture Barrier (Al- Qadi et al., 2004)

The average moisture content for the sections with and without Geo-composite membrane from the test site is shown in Figure 2–39. It is clearly evident from the figure that average moisture content in the section with geo-composite membrane is less than the section without geo-composite membrane. This indicates that the geo-composite membrane is draining the water away from the pavement structure and hence less moisture is recorded in that section at any time of monitoring. Despite the seasonal change in climatic condition, i.e., the wet or dry period the value of moisture content in the section without barrier is always higher.

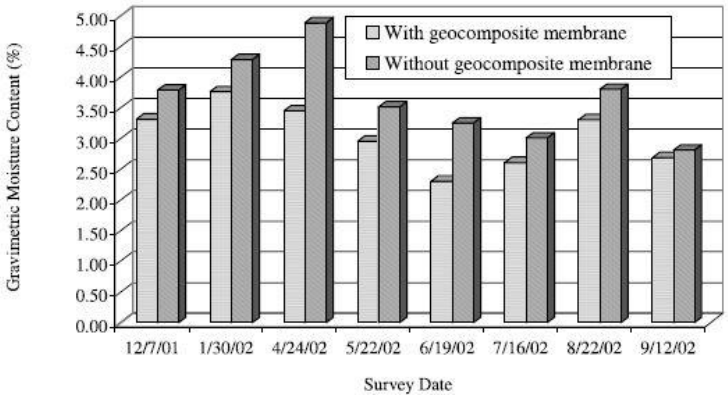

Figure 2–39 Average Moisture Content at the Sections with and without Geo-composite

Falling weight deflectometer (FWD) was also done at the test section to evaluate the impact of moisture on pavement deflection. Figure 2–40 illustrates the deflections measured at two sections- with and without barrier from March 2000 to December 2001. The section with geo-composite membrane exhibited less deflection than the section without membrane. The study concluded that moisture accumulation in the section without geocomposite compromised the bearing capacity of the subbase and subgrade material and eventually led to more deflection.

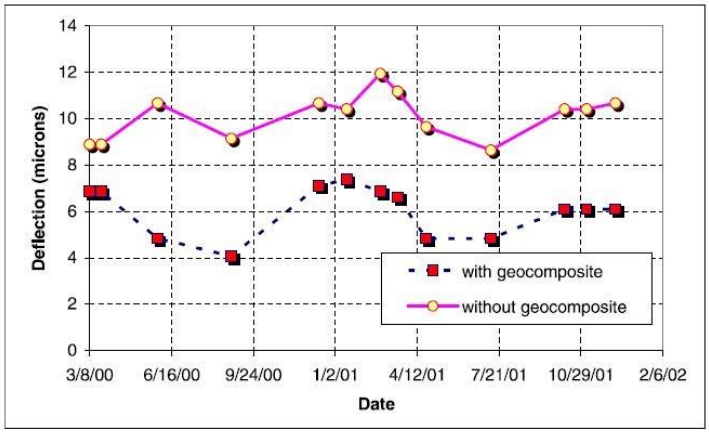

Figure 2–40 Measured Deflection with and without Geo-composite Membrane (Al- Qadi et al., 2004)

Christopher et al. (2000) evaluated horizontal moisture barrier to control the drainage in different types of pavements in Maine (Figure 2–41). The study utilized special geocomposite consisting of geotextile and geonet. The system was found to be effective in preventing water from entering subgrade. However, system required the need of constructing separate drainage collection system with perforated pipe increasing construction complexities.

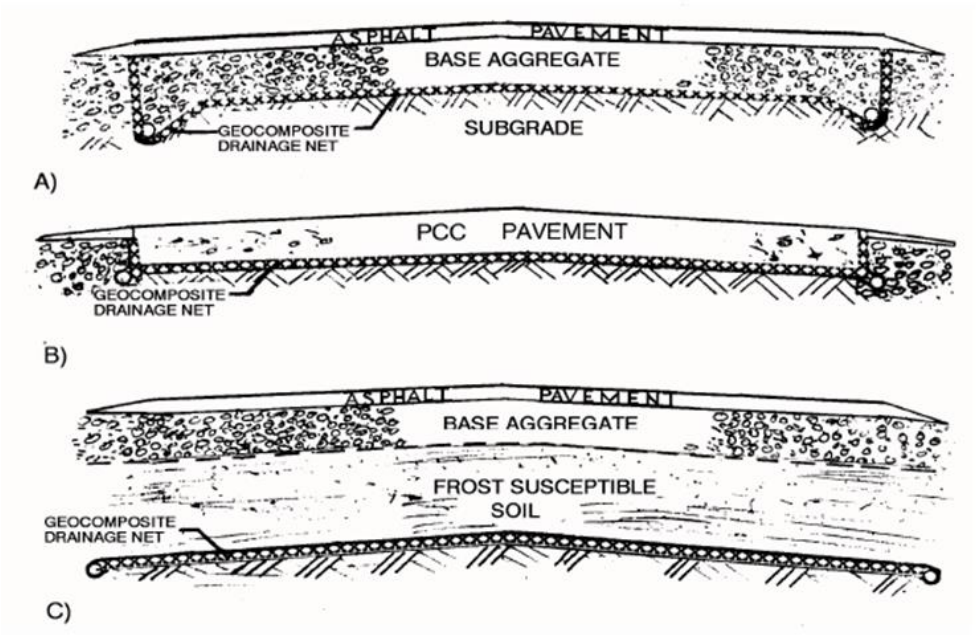

Figure 2–41 Horizontal Geo-composite Drainage Layers (Christopher et al. 2000)

A research conducted by Ahmed et al. (2018) utilized the modified moisture barrier in stabilizing the pavement section at FM 987 after witnessing a longitudinal crack at the edge of the pavement. A 50 ft section was considered to be stabilized with the modified moisture barrier and an adjacent 50 section was considered a control section. Similar instrumentation was installed in both the section to compare and evaluate the effectiveness of moisture barrier in reducing the moisture intrusion and controlling the subsequent deformation. Figure 2–42 illustrates the moisture variation at 3 ft depth in both the test sections. As can be seen, the barrier section was able to maintain constant moisture value while significant moisture fluctuation due to climatic loading was observed in the control section. The results indicated the effectiveness of modified moisture barrier in avoiding the rainwater from reaching the subgrade soil, thus avoiding its detrimental effect on the pavement structure.

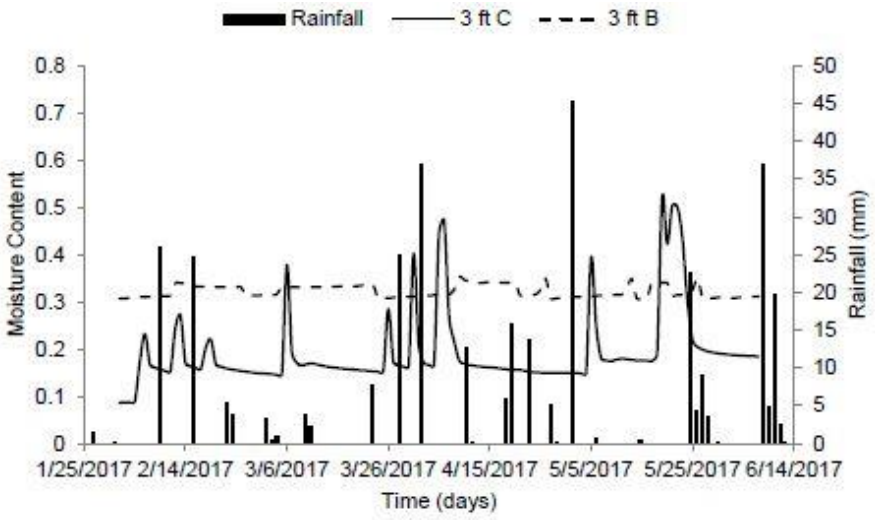

Figure 2–42 Moisture Content Comparison in Control and Barrier section at 3 ft depth of FM 987 roadway (Ahmed et al., 2018)

The deformation monitoring of the same site revealed that the section without the barrier exhibited the most movement. A considerable swelling of 25 mm was recorded in the control section as a result of increased rainfall in May 2017. Also, the area experienced shrinkage with the onset of summer when the temperature is usually at its peak and rainfall is minimal. In contrast, almost insignificant movement was observed in the barrier. Figure 2–43 illustrates the measured deformation in the control and barrier section at the edge.

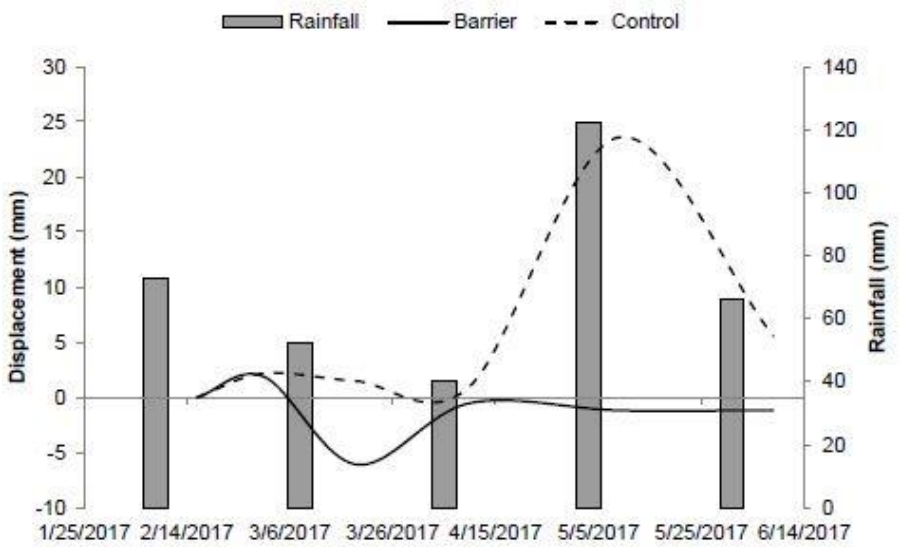

Figure 2–43 Measured deformation at Edge of Pavement with and without Barrier (Ahmed et al., 2018)

After the successful use of modified moisture barrier in FM 987, it was utilized again in stabilizing a highway slope at US 287 by Sapkota et al. (2019). It has been reported by previous studies that the cracks at the crest of the highway slope provide the pathway for the moisture intrusion into the subgrade soil causing softening of the expansive subgrade soil. This results in the instability of the highway slope causing failure. Therefore, the modified moisture barrier was used along with recycled plastic pins in a highway slope of US 287 to maintain equilibrium moisture content and avoid the potential slope failure. In this study, three sections were considered for comparison and evaluation of the adopted approach- control section, pin only section and pin plus barrier section. Figure 2–44 shows observed moisture profile in different test sections during the monitoring period. As can be seen, insignificant moisture variation was observed in the barrier section while the other two section showed peaks and drops in moisture corresponding to the observed rainfall events.

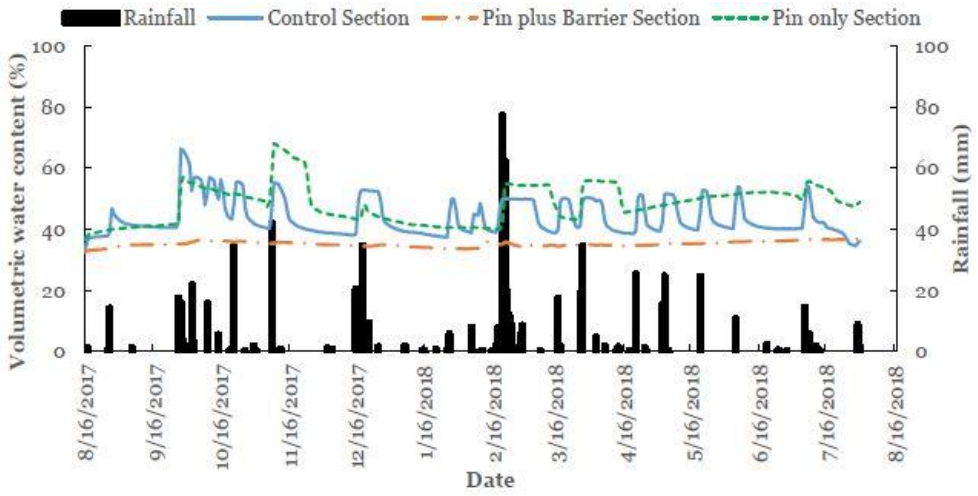

Figure 2–44 Moisture Variation Observed at the Sections with and without Modified Moisture Barrier at 2 ft. Depth (Sapkota et al., 2019)

2.10 Limitation of Previous Studies

Previous studies have shown the importance of maintaining the constant moisture content in the subgrade soil to control the probable moisture variation due to rainfall events and reduce the subsequent deformation. Different kinds of moisture barriers have been introduced and its effectiveness in controlling moisture variation was evaluated. Among them, modified moisture barrier has been found to be effective in maintaining equilibrium moisture content within subgrade soil, however no studies have been conducted with its implementation throughout the width of actual pavement section. Previous studies on modified moisture barrier were performed in a small test section along the pavement shoulder. The moisture barrier placed throughout the width can prevent moisture intrusion that may take place form pavement surface and fine cracks. Therefore, it is very important to analyze the performance of modified moisture barrier when placed throughout the pavement width for a better design and rehabilitation process.

Chapter 3

SITE SELECTION AND INVESTIGATION

3.1 Introduction

This chapter presents the adopted methodology to fulfil the current research objectives. The objective of this study is to evaluate the performance of modified moisture barrier as a potential solution to the observed expansive soil associated pavement distresses around North Texas through actual field implementation and monitoring. Field studies constitute a major part of this dissertation research as it can reflect the actual performance of structures in presence of all the uncertainties existing in the field. Therefore, an actual compromised pavement section with underlying expansive clay was selected and instrumented with the proposed moisture barrier to evaluate its performance. The details on the site selection and investigation, subgrade soil assessment, and assessment of site investigation results are discussed in this chapter.

3.2 Project Background and Visual Inspection

Several criteria such as presence of expansive subgrade soil, surficial pavement distresses with a need of repair services were primarily considered for the site selection. The project site for the current study is located in a farm to market road (FM 639) in Frost, Navarro County, Texas. The location of pavement is presented in Figure 3–1.

It is a two-lane pavement serving two-way traffic. Each lane measure 3.35 m (11 ft.) with 15.24 cm (6 in.) wide shoulders on both sides. The pavement was found to be heavily distressed along the centerline as per the visual examination performed in October 2018. The crack measured about 91 m (300 ft.) long, 5 cm (2 in.) wide and 46 cm (18 in.) deep and largely affected the traffic flow. The geological records of the area showed the presence of high plastic clayey soil in the vicinity which is susceptible to seasonal swelling

and shrinkage. The observed cracks during initial reconnaissance are shown in Figure 3–2.

Figure 3–1 Location of Project Site

Figure 3–2 Observed Pavement Distresses During Initial Field Inspection

3.3 Preliminary Site Investigation

A detailed investigation of the selected project site was conducted in December 2018 using ground penetrating radar and pavement coring. The main purpose of these investigations was to evaluate pavement layers and the severity and extent of observed surface distresses in the deeper layers of pavement and subgrade soil. GPR scanning was able to identify the existing asphalt and base layer thickness which was further verified by coring. The test procedure and the results are explained in the following sections.

3.3.1 Pavement Coring

Pavement coring was performed at four locations on the distressed portion of the FM 639 roadway to evaluate the existing pavement thicknesses and the integrity of underlying pavement layers. The coring layout is shown in Figure 3–3. All the coring were performed near the cracked region using core barrel 10 cm (4 in.) in diameter and 46 cm (18 in.) in height. The sampling process is presented in Figure 3–4 and the extracted samples are shown in Figure 3–5.

Of all the cored samples, two samples were extracted intact while other two were distorted. Table 3–1 summarizes the estimated layer thicknesses. The extracted samples revealed the pavement thickness to be in the range of 30-38 cm (12-15 in.).

Table 3–1 Pavement layers

Pavement layers	Thickness (cm)
Asphalt wearing course	5 to 8
Cement treated base layer	25 to 30

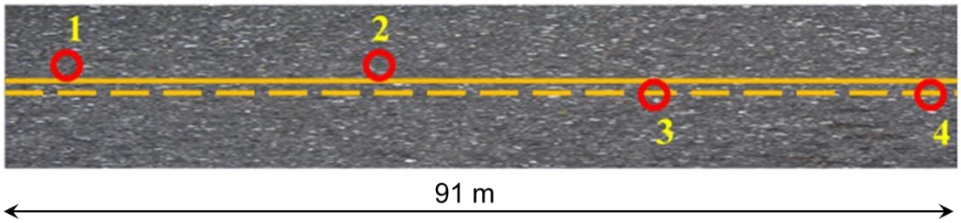

Figure 3–3 Coring Location.

(a) (b) (c) (d) (e)

Figure 3–4 Sample Coring Process: (a) Marking Coring Location, (b) Coring with Coring Rig, (c) Core Hole, (d) Sample Extraction, and (e) Final Cored Sample.

(a) (b)

(c) (d)

Figure 3–5 Core Sample From: (a) Location 1, (b) Location 2, (c) Location 3, and (d) Location 4.

3.3.2 GPR Scanning

In addition to pavement coring, GPR scanning was performed along fives lines in the distressed section of selected farm to market road. GPR is an extensively used non-destructive testing method with a wide range of applications in pavement assessments. This method emits electromagnetic waves in the subsoil which reflects back with varying amplitude. The arrival time of reflected waves depends on dielectric properties of the materials or mediums being scanned (Chen & Wimsatt, 2010), thereby capturing a continuous image of the subsurface condition. It has been successfully used in pavements for measuring layer thickness, estimating asphalt densities, determining the moisture content of base materials, identifying stripping zones in asphalt layers, detecting voids, locating subsurface cracks, locating anomalies, and analyzing rutting mechanism (Loken, 2007).

In the current study, GPR system consisting of three components: the SIR-30 main frame, 400 MHz and 2.6 GHz frequency antenna, and a hand cart with wheels comprising Distance Measuring Instrument (DMI) was used (Figure 3–6 a, b). The penetration depth of the 2.6 GHz antenna was 0.3 m (1 ft.) while the penetration depth of 400 MHz antenna was 3 m (10 ft.) which were adequate to distinguish different pavement layers at various depths. The methodology for GPR scanning included site preparation, traffic control, layout of survey lines (Figure 3–6 c), and GPR scanning along the marked lines. The estimated pavement layer thicknesses from the GPR output were consistent with the thicknesses of cored pavement retrieved from the site.

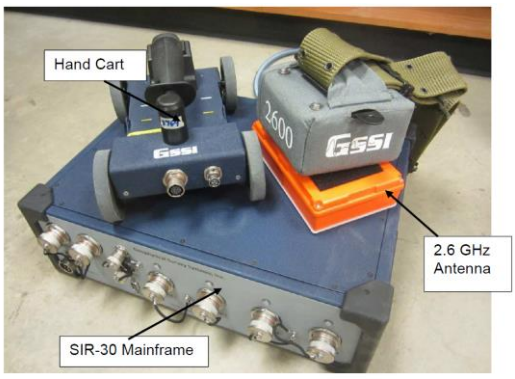

(a)

(b)

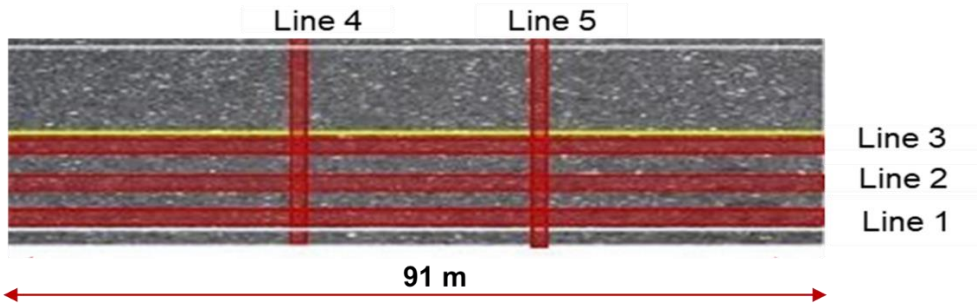

(c)

Figure 3–6 (a) GPR System (b) Typical Cart Mounted GPR Scanning System and (c) Survey Lines for GPR Scanning

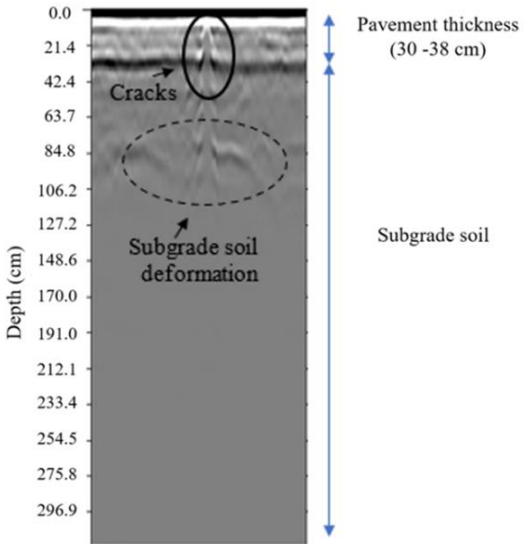

Figure 3–7 GPR Image across the Pavement Capturing Subgrade Soil Deformation

Figure 3–7 show the scanned image obtained using the 400 MHz frequency antenna in transverse direction. As expected, the scanned result showed crack along the centerline of the pavement which was consistent with the visual survey. In addition, an irregular profile was captured right below the cracks to a depth of 114.3 cm (45 in.) in the subgrade soil. As suggested by Dessouky et al. (2015), this evidence points towards soil movement taking place in that region. Such soil movement may be due to swelling of underlying soil, which is highly expansive in nature in response to excessive moisture infiltration. Therefore, a remedial measure that would prevent the potential moisture seepage into the subgrade soil and mitigate the volumetric deformation of highly expansive subgrade soil was needed to enhance serviceability of the pavement.

3.3.3 Soil Sampling and Laboratory Testing

The subgrade soil assessment was conducted through soil borings which extended to a depth of 3 m (10 ft). In total, six boreholes were drilled at two sections of pavement using hollow stem auger. The borings were done under the centerline and edges of the roadway

and disturbed and undisturbed samples were collected. For the collection of undisturbed samples, thin-walled Shelby tube sampler with exterior diameter of 7.62 cm (3 inches) was utilized. Standard penetration testing was performed in one of the boreholes at 1.52 m (5 feet) depth interval to assess in-situ soil strength. Based on in-situ observations, the predominant soil strata were dark brown high plasticity clay. The bore logs are presented in the Appendix section.

a) In-situ Gravimetric Moisture Content Tests

The moisture content profile of the subgrade soil was determined through moisture content test procedures described in ASTM D2216 “Standard Test Methods for Laboratory Determination of moisture content of soil and Rock by Mass”. Figure 3–8 show the measured soil moisture profile along depth for all boreholes. As can be seen in the figure, gravimetric moisture content of the collected soil samples was found to vary in between 21% to 35%.

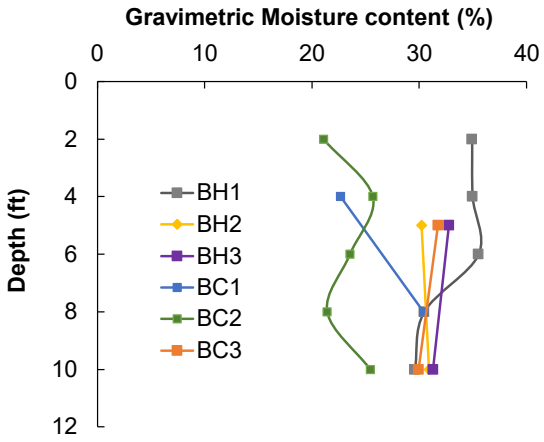

Figure 3–8 Moisture Profile of Collected Soil Samples

b) Grain Size Distribution Tests

The particle size distribution in the collected samples was determined as per ASTM D 422-63 Standard Test Method for Particle-Size Analysis of Soils. For the full range of particle

size distribution, results from sieve analysis and hydrometer soil tests were combined. The soil samples were first oven dried and washed through sieve #200. The retained soil from the wash sieve was oven dried and sieved using different sieve sizes. Again 50 gm of sample passing sieve #10 from the same soil sample was used for hydrometer tests. Sodium hexametaphosphate was used as dispersing agent during the process. A control solution was made for the combined correction in the hydrometer readings. The hydrometer readings were taken at an elapsed time of 2, 4, 8, 15, 30, 60, 120, 240, 480 minutes and 24 hours. The grain size distribution is generally presented by semi-logarithmic plots in which the particle diameters are plotted in log scale and the corresponding percent finer in arithmetic scale. Figure 3–9 (a) and (b) show the hydrometer test and depth-wise particle size distribution curves for borehole 1 respectively. The results showed that soil samples consisted of 89% to 94% fines in all layers.

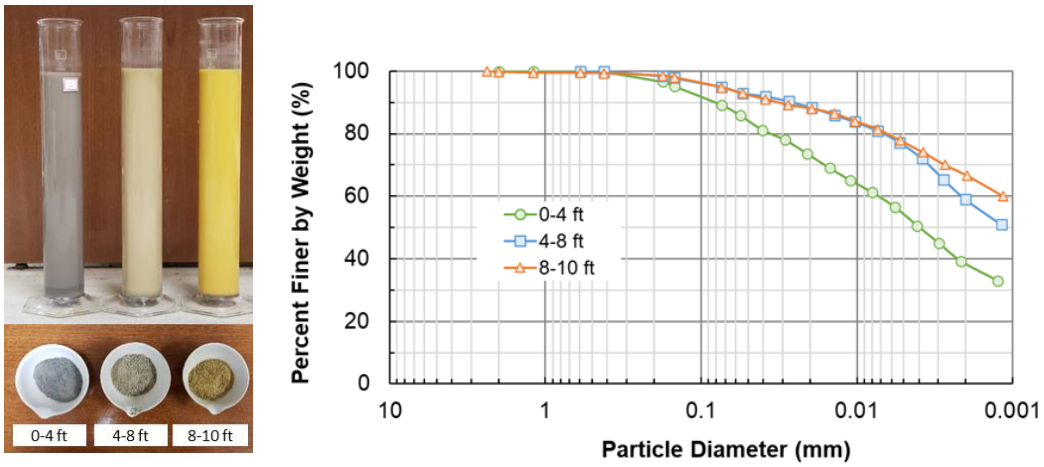

(a) (b)

Figure 3–9 (a) Hydrometer tests (b) Grain Size Distribution Curve from combined results of sieve analysis and hydrometer

c) Atterberg Limit

The Atterberg limits of soil samples were measured according to ASTM 4318 Standard Test Methods for Liquid limit, Plastic Limit, and Plasticity Index of soils. The tests revealed a very high liquid limit and plastic limit values. The liquid limit and plasticity index of the soil varied between 70% to 85% and 39% to 53% respectively. The plasticity chart of the soil samples is presented in Figure 3–10. The soil was classified as high plastic fat clay at all depths according to Unified Soil Classification System (USCS).

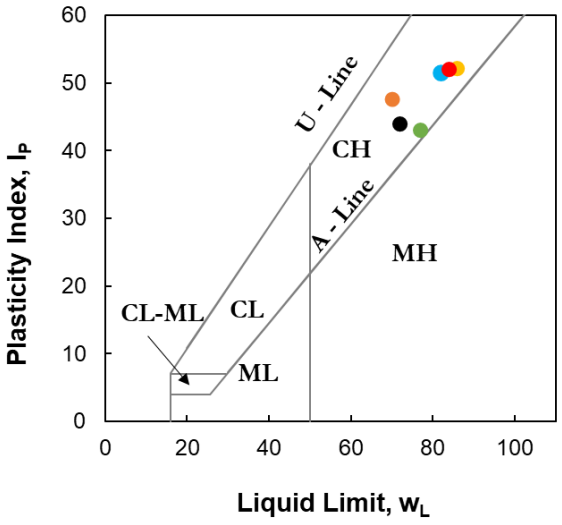

Figure 3–10 Plasticity Chart

d) Specific Gravity Test

The specific gravity of the collected soil samples was determined based on ASTM 854 Standard Test Methods for Specific Gravity of Soil Solids by water pycnometer. The test showed the specific gravity of the samples to be in the range of 2.7 to 2.75.

e) Swell Test

Swell potential of expansive soil was determined using one-dimensional swell test. This test can be used to quickly identify the expansive nature of soil and is relatively easier than

three- dimensional volume change study. Swell test was performed on the soil based on ASTM D-4546 “Standard Test Methods for One-Dimensional Swell or Collapse of Soils”. Test Method B was followed as the samples were collected from the field in intact condition.

For the test, an intact sample extruded from the Shelby tube from 0.6 m (2 ft.) and 1.52 m (5 ft.) depth was placed in the consolidometer with filter paper and porous stone on both sides of the sample and overburden pressure was applied to the sample. The height of the sample was 2.54 cm (1 in.).

After allowing the sample to consolidate for about 30 minutes under the overburden pressure, water was added to the sample and the dial gauge deformation was recorded immediately at 15 s, 30 s, 1 min, 2 min, 4 mins, 8 mins, 15 mins, 1 hr., 2 hrs., 4 hrs., 8 hrs., 24 hrs. and so on. The dial gauge deformation is recorded usually up to 72 hours.

The free swell potential for the soil sample at 2 ft under existing overburden pressure was observed to be 6.5%. The observation was made for 72 hours after which the swelling was complete. The free swell potential for the soil sample at 5 ft under existing overburden pressure was observed to be 0.55%. The observation was made for 72 hours after which the swelling was complete.

Unlike very high swell potential observed at 2 ft, the swell potential observed at 5 ft was low. Swell potential is dependent upon number of factors, including initial moisture condition and swell pressure. As the overburden depth for the soil at 5 ft is higher as compared to the overburden depth for the soil at 2 ft, reduced swell potential was observed for the soil at 5 ft which also concludes that overburden pressure is greater than the swell pressure at this depth.

3.4 Assessment of Site Investigation Results

Site investigation results revealed that the failed pavement was constructed over high plastic clayey soil with liquid limit and plasticity index varying in between 70% to 85% and 39% to 53%, respectively. These types of soils are highly problematic due to its intrinsic property to undergo swelling and shrinkage with moisture variation. The soil undergoes significant deformation in response to seasonal climatic variations which gradually reflects over the pavement's surface.

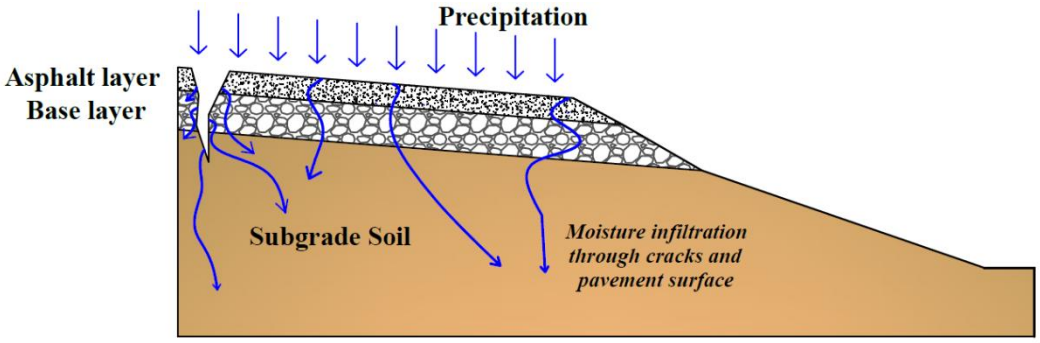

Figure 3–11 Moisture Infiltration into Subgrade Soil

Moisture intrusion may take place from cracks in pavement surface, through shoulder and side ditches, free water from pavement base, capillary rise from ground water table etc. (Ridgeway, 1982). In the current study, the rainwater infiltration can be considered the major source of moisture variation in the subgrade soil as no ground water table was detected during the time of investigation. The fine cracks formed on the pavement surface by the wearing and ageing of asphalt layers over the years can also greatly alter the moisture distribution in pavement. Pavement surface itself can allow 33 to 50% of moisture infiltration in pavement as per the research conducted by FHWA (Cedergren, 1974). Figure 3–11 illustrates the moisture infiltration that can take place from pavement surface and cracks. Excess moisture in the pavement layers can reduce the strength and bearing

capacity of pavement system as a whole. Lack of adequate drainage is another factor that is very crucial to the stability of pavement.

3.5 Controlling Rainwater Intrusion in Pavement System

The moisture intrusion into the pavement system can be controlled with the use of moisture barrier system (Ahmed et al., 2018; Elseifi et al., 2001). In recent years, geosynthetic products have gained popularity in pavement application to control moisture intrusion into the underlying pavement layers and drain the excess moisture away from the pavement structure. These products act as barrier against moisture infiltration and exfiltration and as a result are found to be efficient in reducing the shrink swell potential of highly expansive soil (Steinberg, 1985; Stalin et al., 2010).

Vertical moisture barriers, horizontal moisture barriers, geo composite capillary barrier, modified moisture barriers are some of the barriers that are used for controlling moisture infiltration (Ahmed et al., 2018). Among several types of moisture barrier, Modified Moisture Barrier (MMB) offers a great potential in the overall stability of pavement structure by preventing rainwater to intrude into the subgrade soil and draining the infiltrated rainwater (Ahmed et al., 2018; Sapkota et al., 2019).

3.6 Moisture Control Mechanism of Modified Moisture Barrier

MMB is a newly developed technology for pavement application and is a modification of Geo composite Capillary Barrier Drain, GCBD (Ahmed et al., 2018). GCBD was originally proposed by Henry and Stormont (2000) and consists of a geonet sandwiched in between geotextiles. The system limits the percolation of rainwater into the subsoil with the combined effect of top geotextile as a transport layer, geonet as a capillary barrier and bottom geotextile as a separator layer (Stormont et al., 2009). The capillary barrier effect developed in the geo composite inhibits rainwater permeating through pavement layers

and laterally draining the water. However, the system allows percolation after it reaches a breakthrough point (Rahardjo et al., 2012).

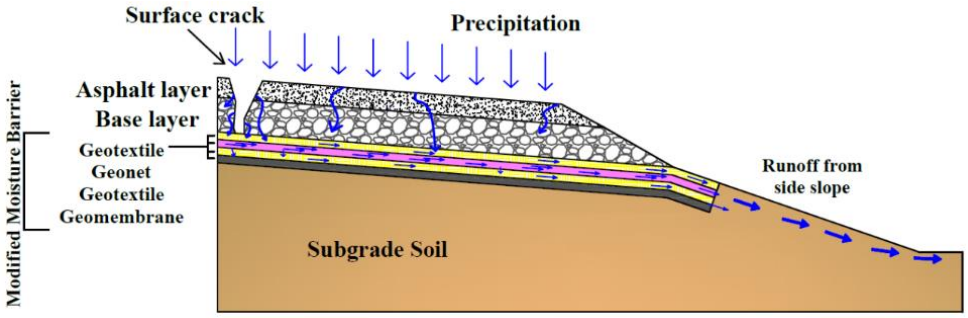

Figure 3–12 Modified moisture barrier isolating subgrade soil from infiltrating rainwater.

The additional component of geomembrane underneath the geo composite system overcomes the limitation of GCBD by sealing the subgrade soil and preventing the breakthrough to penetrate into deeper soil layers (Ahmed et al., 2018). This combination of geosynthetics materials i.e., geo composite and geomembrane are referred as Modified Moisture Barrier. The underlying geomembrane prevents downward movement of moisture when the capillary barrier effect attains a breakthrough point in the upper geo composite system increasing the efficiency of the system. In addition, the geomembrane can prevent fine particles' movement across the base-subgrade interface. In contrast to the conventional drainage system, this method can provide drainage while the soil is unsaturated which prevails most of the time in real field (Stormont et al., 2009). The increased drainage of rainwater in its unsaturated state from the base layer can also prevent the detrimental effect of moisture in base materials. Figure 3–12 illustrates the mechanism by which modified moisture barrier isolates the subgrade soil from infiltrating rainwater.

Chapter 4

MOISTURE BARRIER APPLICATION AND INSTRUMENTATIONS

4.1 Introduction

This chapter presents the detail regarding the modified moisture barrier application and instrumentations involved. The modified moisture barrier was installed in the distressed pavement section for controlling the potential moisture intrusion into highly expansive clayey subgrade and reducing subsequent swelling and shrinkage. Several instrumentations including integrated temperature and moisture sensors, suction sensors and inclinometers were installed in the project site for performance monitoring.

4.2 Pavement Stabilization Plan

Modified moisture barrier was used in the selected pavement section to control the seasonal moisture variation that can potentially take place through rainwater seepage from pavement surface and cracks. Two sections were designed - one with the barrier and the other without barrier to evaluate the effectiveness of modified moisture barrier. A 91 m (300 ft) long roadway section which experienced significant damages was stabilized with the modified moisture barrier while adjacent 30.48 m (100 ft) section was considered as a control section. A 91 m (300 ft.) long and 7.31 m (24 ft.) wide modified moisture barrier was placed in the interface between the base course and expansive subgrade soil. The combination of 8 oz. HDPE geo composite (geotextile + geonet + geotextile) and 1 mm (40 mil) smooth, black LLDPE geomembrane material was selected for the installation. The layout of the section with the modified moisture barrier and appropriate instrumentations are shown in Figure 4–1.

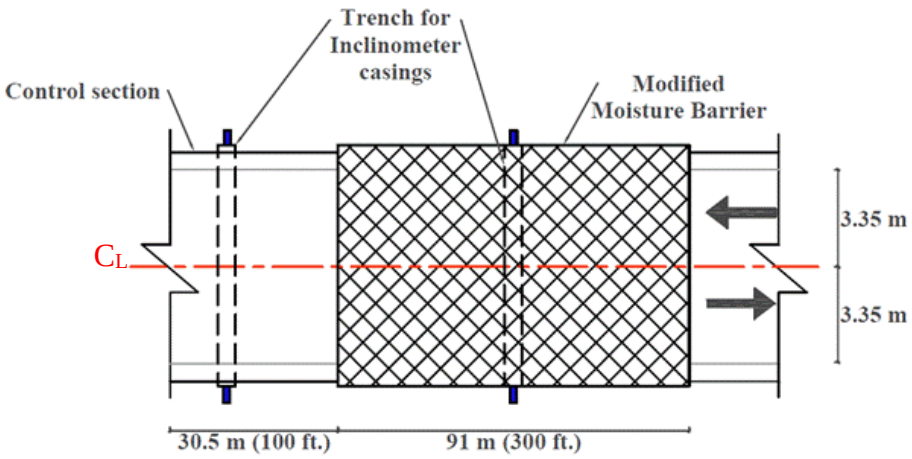

(a)

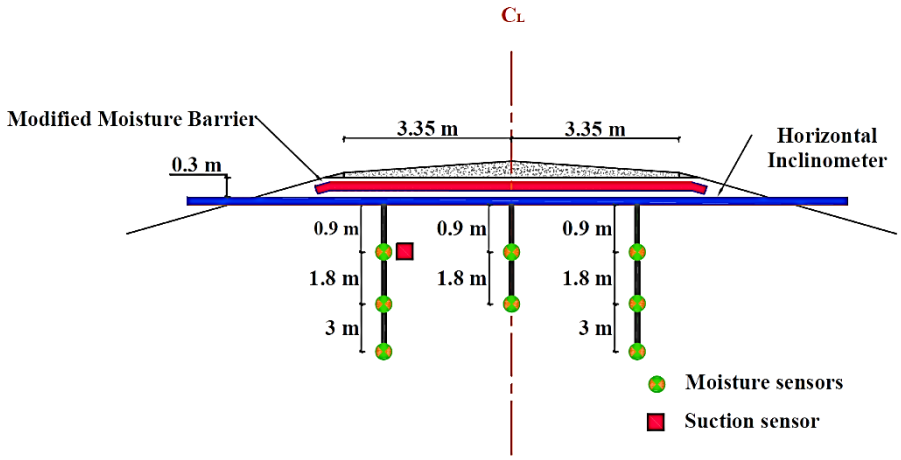

(b)

Figure 4–1 (a) Layout of Modified Moisture Barrier (b) Field Instrumentation Layout of Barrier Section.

4.3 Material Selection

Commercially available geosynthetic materials were selected for the current study. The selection criteria and properties of geo composite and geomembrane are discussed in the section below.

4.3.1 Selection of Geo composite

The main purpose of using 8 oz. HDPE geo composite consisting of a layer of geonet sandwiched between layers of geotextile in this study, is to provide adequate drainage in the pavement system. It is suggested that the materials should have enough stiffness to sustain traffic loading without significant deformation along with adequate flow capacity to drain water (Christopher et al., 2000). The material selection was carried out following the specification based on AASTHO standard (M288) for both flow and strength properties. The material was selected such that the geotextile layer has AOS less than 0.22 mm, permittivity value greater than 0.1 sec $^{-1}$ and grab tensile strength greater than 700N. The transmissivity of geocomposite in between 0.00035 and 0.001 m^2/s were considered which is capable of providing similar drainage capacity as 4-inch OGBL. Considering these criteria commercially available SKAPS TRANSNET geocomposite consisting of SKAPS Geonet made from HDPE resin with non-woven polypropylene geotextile fabric heat bonded on both sides of geonet was used, the properties of which is shown in Table 4–1.

4.3.2 Selection of Geomembrane

In this study, 1 mm (40 mil) smooth, black LLDPE geomembrane material was used. The impermeable property of this material helps in preventing the moisture flow across it. The specified geomembrane material manufactured by SOLMAX was used for the study. The properties of the Geomembrane used in the study are summarized in Table 4–1.

Table 4–1 Properties of Geosynthetic Materials

Components of MMB	Material Property	Value
Geonet	Thickness (mm)	6.98
	Tensile Strength (N/mm)	11.35
	Transmissivity (m^2/sec)	6 X 10^{-3}
Geocomposite	Ply Adhesion (g/cm)	178
	Transmissivity (m^2/sec)	7 X 10^{-4}
Geotextile	AOS (mm)	0.18
	Permittivity (s^{-1})	1.26
	Permeability (cm/s)	0.3
	Grab Tensile Strength (N)	1001
Geomembrane	Thickness (mm)	1
	Tensile Strength (KN/m)	29
	Puncture Resistance (N)	275

4.4 Instrumentation Details

The study area was instrumented with moisture sensors and inclinometer casings to monitor soil moisture and vertical movement of the subgrade soil, respectively. Eight moisture sensors were installed in the barrier section, three at the edges and two at the center of pavement. To compare and evaluate the effectiveness of modified moisture barrier, sensors were installed in the control section as well. Integrated moisture and temperature sensor - Teros 12 was used in the current study for volumetric moisture content measurement and temperature from the dielectric constant of surrounding media. In addition, Teros 21 suction sensors were installed to monitor the suction variation in subgrade soil with time. The cables from the sensors were connected to the data logger

for easy data acquisition. The utilized sensors and data loggers are shown in Figure 4–2. Table 4–2 show the instrumentation details.

(a) (b) (c)

Figure 4–2 (a) Moisture/Temperature Sensors (b) Suction Sensors (c) Data Logger

15 m long inclinometer casings were installed across the pavement in both the barrier and control sections to measure the deformation in subgrade soil Figure 4–3. The casings were extended beyond the pavement to facilitate the monitoring and were fixed at one end using concrete grout. The site was monitored thoroughly using the field instrumentations to assess the effectiveness of the proposed method.

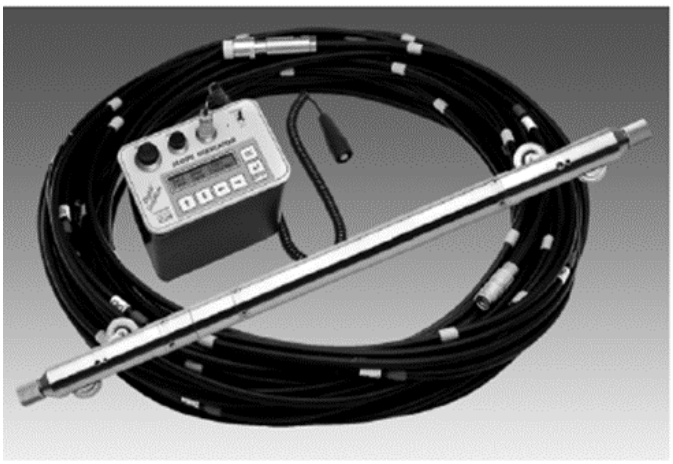

Figure 4–3 Horizontal Inclinometer

Table 4–2 Instrumentation Details

Sections	Location	Depth (m)	Sensor	Number of Sensors
Barrier	Right Edge	0.9	Moisture Sensor	3
		1.8	Moisture Sensor	
		3	Moisture Sensor	
	Center	0.9	Moisture Sensor	2
		1.8	Moisture Sensor	
	Left Edge	0.9	Moisture Sensor	4
		1.8	Moisture Sensor	
		3	Moisture Sensor	
		0.9	Suction Sensor	
Control	Right Edge	0.9	Moisture Sensor	4
		1.8	Moisture Sensor	
		0.9	Suction Sensor	
		1.8	Suction Sensor	

4.5 Field Installation

4.5.1 Phase-I

The barrier was installed in the failed pavement section in February 2019. The road was closed for the traffic and the asphalt layer and base materials of distressed section were pulverized using Reclaimer/ Stabilizer TEREX RS446 (Figure 4–4). Once the materials were completely pulverized and blended till the subgrade layer, they were piled on two sides of the pavement to make space for the installation of modified moisture barrier over the subgrade soil. The subgrade soil was then graded using pavement grader GALION 830 for making the surface smooth.

Figure 4–4 Removal of Top layer and Base Layer of pavement

4.5.2 Phase-II

Two trenches (45cm W x 30cm D) were excavated across the pavement to install inclinometer casings beneath the pavement - one in the barrier section and the other in the control section (Figure 4–5). Soil borings were drilled, and moisture sensors were installed at varying depths as per the instrumentation plan. The borehole was backfilled using in-situ materials after each sensor instrumentation and compacted to field density. Wires from the sensors were covered using protective foam and taken outside the pavement to connect them to a data logger. The inclinometer casings were connected to each other and then placed in the trench over a sand bed of about 15 cm thick and aligned carefully. Finally, the trench was backfilled and compacted.

(a)

(b)

(c)

(d)

(e)

(f)

Figure 4–5 (a) Layout of Trench Across the Pavement (b) Excavation of Trench (c) Levelling of Trench (d) Installing Sensors in the Boreholes (e) Checking sensors with Data Loggers (f) Placing Inclinometer and Backfilling the Soil

4.5.3 Phase-III

During this phase, modified moisture barrier was placed over the subgrade (Figure 4–6). At first, the exposed surface was cleaned properly to remove any bulky aggregate that could puncture the geosynthetic material and then a thin layer of sand was placed in some

locations to level the base. A 91 m (300 ft.) long 7.31 m (24 ft.) wide geomembrane was then placed over the soil and cleaned again to remove remaining debris. Once the geomembrane was laid and leveled, the geo composite material was placed on the top. The pavement was then backfilled using the recycled base materials and compacted using pneumatic roller. Pavement surfacing in the form of chip seal surface was then provided after few days of installation and the road was opened to traffic.

(a)

(b)

(c)

(d)

(e)

Figure 4–6 (a) Preparing Subgrade Soil for MMB Installation (b) Laying Geomembrane Material (c) Road Section with Geomembrane (d) Laying Geocomposite layer (e) Final View of Pavement after Backfilling and Repaving.

4.6 Performance Monitoring Plan

The section stabilized with modified moisture barrier and adjacent control section was monitored regularly to evaluate the effectiveness of the proposed barrier system. The monitoring schedule of the project site is shown in Table 4–3. The data collection was initially conducted in a biweekly basis for first few months which was done in a monthly basis after six months.

Table 4–3 Monitoring Frequency

Instrumentation	Monitoring Frequency
Moisture Sensors	Continuous
Suction Sensors	Continuous
Inclinometer	Monthly

Figure 4–7 Data Collection and Field Monitoring

Chapter 5

FIELD RESULTS AND DISCUSSION

5.1 Introduction

This chapter presents the monitoring results from field instrumentations and evaluates the effect of modified moisture barrier on pavement's performance. The seasonal change in moisture and suction along with the deformation of the subgrade soil in the barrier and control sections were monitored which are discussed in this chapter. The effectiveness of the proposed approach has been thoroughly discussed by comparing the performance of barrier and control sections. The results are further compared with the findings from previous studies.

5.2 Performance Monitoring of Control Section

The performance of the control section was monitored by measuring hourly soil moisture content and vertical movement using sensors and horizontal inclinometer, respectively. The control section is 30.48 m (100ft.) in length and was primarily considered to compare and evaluate the performance of modified moisture barrier installed at the adjacent section. It should be noted that the sensors initially installed at the control section were non-functional after few months. Hedayati (2014) reports the survivable rate of these types of sensors to be 70%. New sets of moisture/ temperature and suction sensors were installed at the edge of control section on 346th day after first installation i.e., in February 2020. The sensors and inclinometers in the subgrade soil were able to capture the effect of seasonal climatic loading which is discussed in the following section.

5.2.1 Moisture and Suction Variation in Control Section

Figure 5–1 shows the daily average soil moisture content observed in the control section plotted against real time rainfall events. Day 1, in the figure represents February 9, 2020.

The sensors, installed at 0.9 m (3 ft.) and 1.8 m (6 ft.) depth at the edge of the pavement section captured the seasonal change as well as temporary saturation due to climatic loading. The average soil moisture content was found to be higher in wet period than in dry period. An equilibrium moisture content of 50% was recorded initially since the sensors were embedded into the soil during the wet period when the ambient temperature is usually low, and the soil is near to its full saturation due to frequent rainfall events. After 70th day, the decreasing trend in moisture was observed as a result of increased temperature and less rainfall causing the soil to lose excess moisture. At 0.9 m depth, the recorded moisture content ranged from minimum value of 33% in dry period to maximum value of 50% during the period of rainfall. On the other hand, range of 40% to 50% was observed at 1.8 m depth, indicating significant effect of climatic loading in shallow sensors than in deeper sensors. The observed seasonal and temporal moisture variation at different time of year in expansive subgrade soil has been reported to be the main cause of pavement failure by previous studies (Hedayati, 2014; Ahmed, 2017; Sapkota, 2019).

Figure 5–2 shows matric suction of subgrade soil at 0.9 m depth from February 2020 to January 2021. The plot compares the field suction with observed rainfall at different time of year. As the figure suggests, the subgrade soil was found to maintain minimum suction value of -10 kPa at the time of rainfall when the rainwater caused the soil moisture content to increase significantly. On the other hand, suction increased as high as -733. 73 KPa during summer when the temperature was at its peak. The minimum suction corresponded to 50% volumetric water content while the maximum recorded suction corresponded to 33% volumetric water content in the field. The subsequent rainfall events in summer resulted in the drop of matric suction value to -10 kPa, thus indicating the section being highly affected by the climatic conditions.

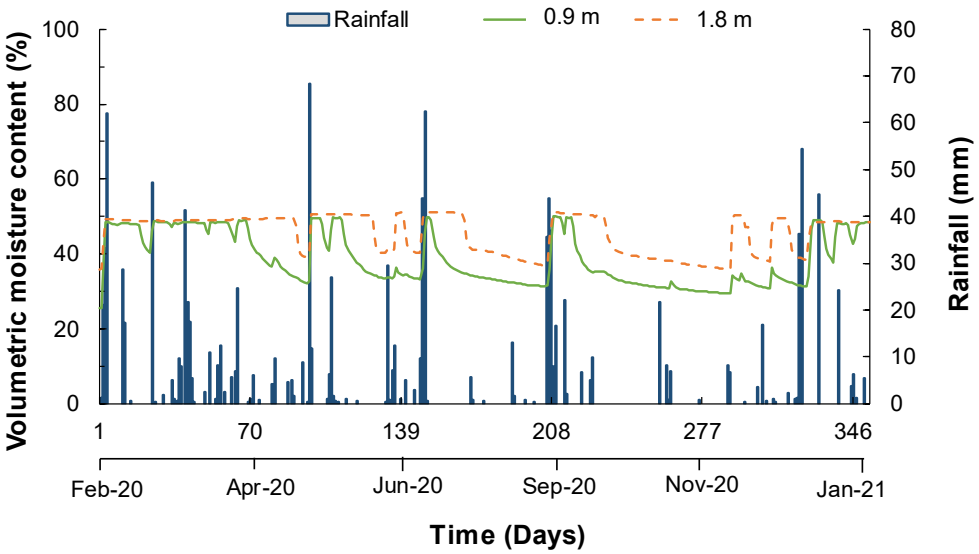

Figure 5–1 Volumetric Moisture Content Variation at the Edge of Control Section

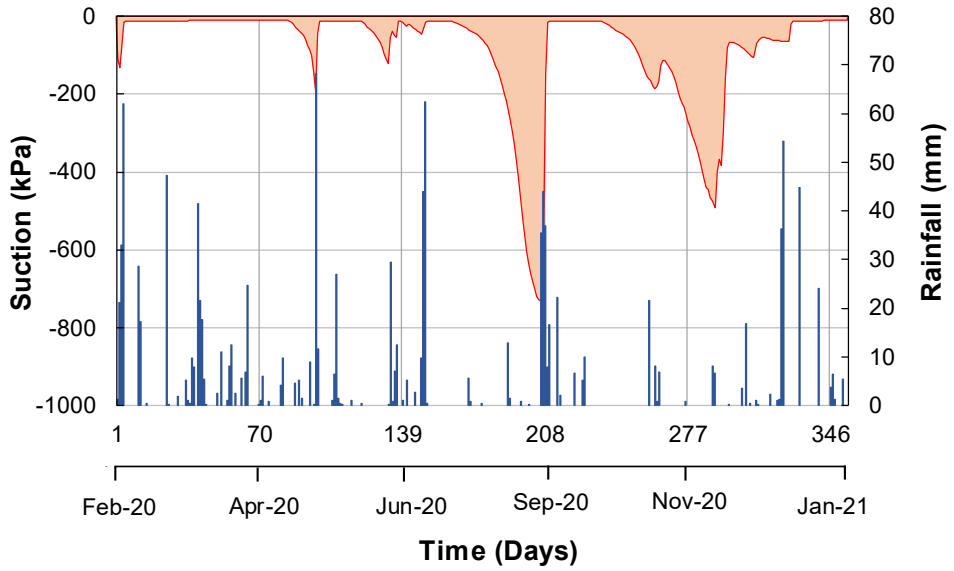

Figure 5–2 Suction Variation at 0.9 m Depth in Control Section

Several studies in the past have reported significant moisture and suction variation in the active zone of the soil mass due to seasonal drying and wetting (Bayomy and Salem, 2004; Nguyen et al., 2010; Hossain, 2013; Sapkota et al., 2019; Pandey et al., 2019). This was reported as the main cause of pavement distresses. The continuous moisture and suction variation cause swelling and shrinkage of subgrade. This ultimately leads to development of pavement cracks.

5.2.2 Deformation in Control Section

Figure 5–3 shows the movement of subgrade soil in the control section. The initial reading taken on March 21, 2019 was considered as a base reading represented by Day 1 in the figure. Significant upward and downward movement was observed in the control during the monitoring period. The section experienced maximum movement in the form of shrinkage in late September 2019 (represented by Day 192) owing to increased temperature and less rainfall. The soil moved to -61.7 mm from the base reading at a distance of 1.83 m (6 ft.) from the edge during that time. At the right edge, maximum drop to -54.83 mm from the base reading was observed. In contrast, no such significant movement was observed in the barrier section. An increase in rainfall and decrease in temperature in the following months caused the soil to again move upwards from its maximum shrinkage value. However, the same amount of shrinkage was not observed in the second cycle (Summer 2020) probably because the site experienced more rainfall during summer 2020 compared to summer 2019. The overall pattern of deformation captured the cyclic upward and downward movements corresponding to the climatic conditions.

The subgrade soil movement at the edge of control section was compared with the moisture variations at 0.9 m depth from February 2020 to January 2021, as shown in Figure 5–4. The results showed increased movement of subgrade soil in the form of swelling with

an increase in moisture content and vice versa with some lag period. For instance, the volumetric moisture content maintained a maximum value of 50% until mid-April 2020 in response to frequent rainfall events and low ambient temperature after which peaks, and drops were observed. However, the maximum swelling was observed after almost a month in May 2020.

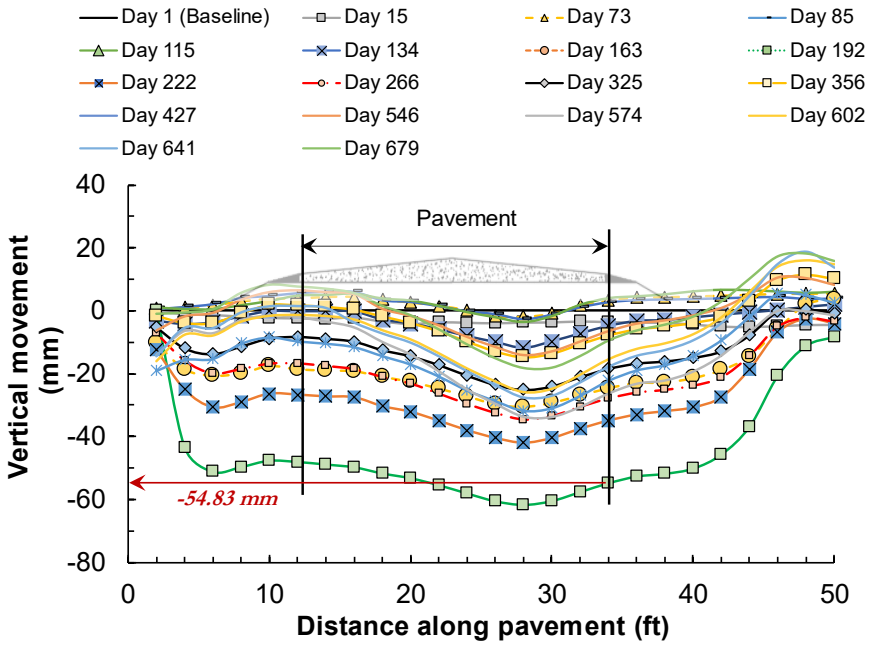

Figure 5–3 Vertical Movement in Subgrade Soil of Control Section

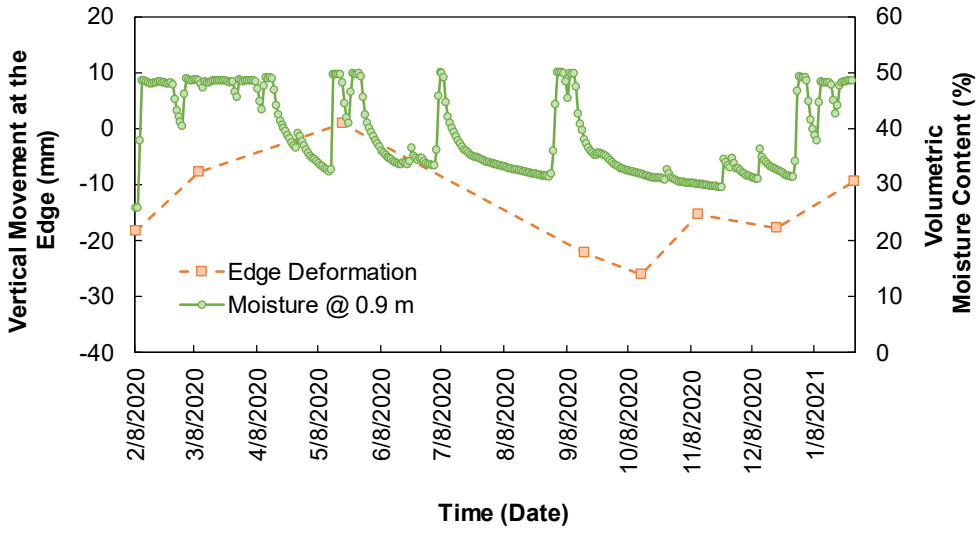

Figure 5–4 Comparison of Subgrade Deformation with Moisture Variation in Control Section

5.3 Performance Monitoring of Barrier Section

In total, 8 integrated moisture and temperature sensors were installed at different depths of subgrade soil with the moisture barrier system to capture temporal and spatial moisture variation. The inclinometer casing was 15.24 m (50 ft) long and installed across the pavement. It is to be noted that the casing installed in the barrier section was damaged and repaired during the installation due to which the readings were limited to 10.4 m (34 ft) only. The inclinometer readings were taken biweekly for first six months after which monthly readings were taken.

5.3.1 Moisture and Suction Variation in Barrier Section

The performance of pavement section stabilized with modified moisture barrier is continuously monitored since March 2019. Figure 5–5 and Figure 5–6 present moisture variation observed at the edge and center of the stabilized pavement section against the real time rainfall events from March 2019 through January 2021, respectively. A cumulative

rainfall of 2080 mm was observed during the monitoring period. The frequency of rainfall was observed to be more during the wet period and less during summer. However, insignificant change in the moisture content was observed in the barrier section despite the rainfall events. The values showed non-dependency with precipitation events at all depths and locations. The volumetric moisture values at the right edge of pavement were maintained at 38%, 47% and 55% at 0.9 m, 1.8 m, and 3 m depth respectively throughout the monitoring period. The insignificant change in moisture values can be associated to the effectiveness of modified moisture barrier placed at the base-subgrade interface. Some increase in moisture was recorded during first few months after the installation which is considered as adjustment period when the disturbed soil tries to attain the same state as surrounding soil. Once the moisture content reached to a value that of the surrounding soil, equilibrium moisture content was observed throughout the monitoring period.

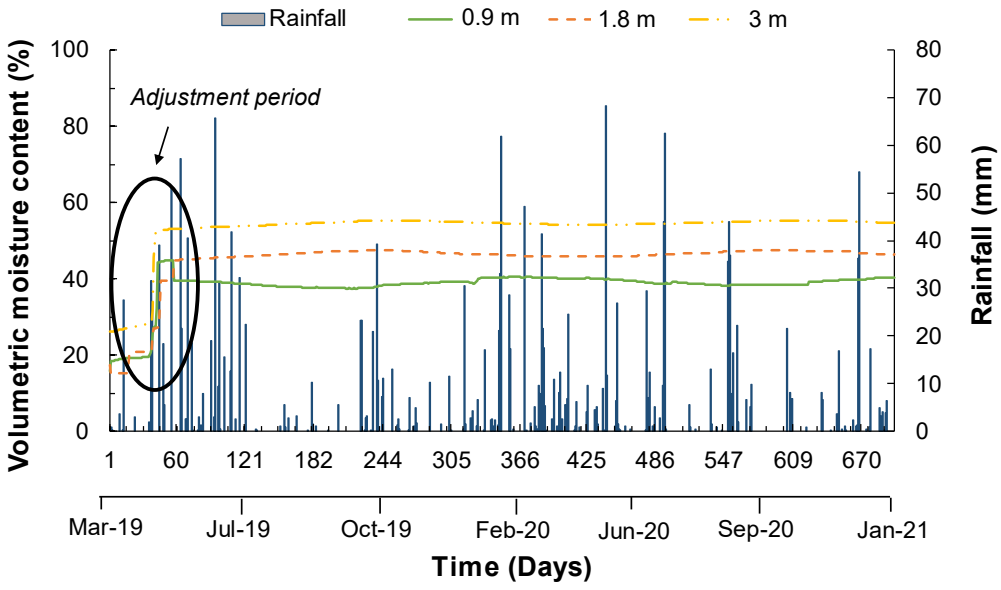

Figure 5–5 Volumetric Moisture Content Variation at the Edge of Barrier Section

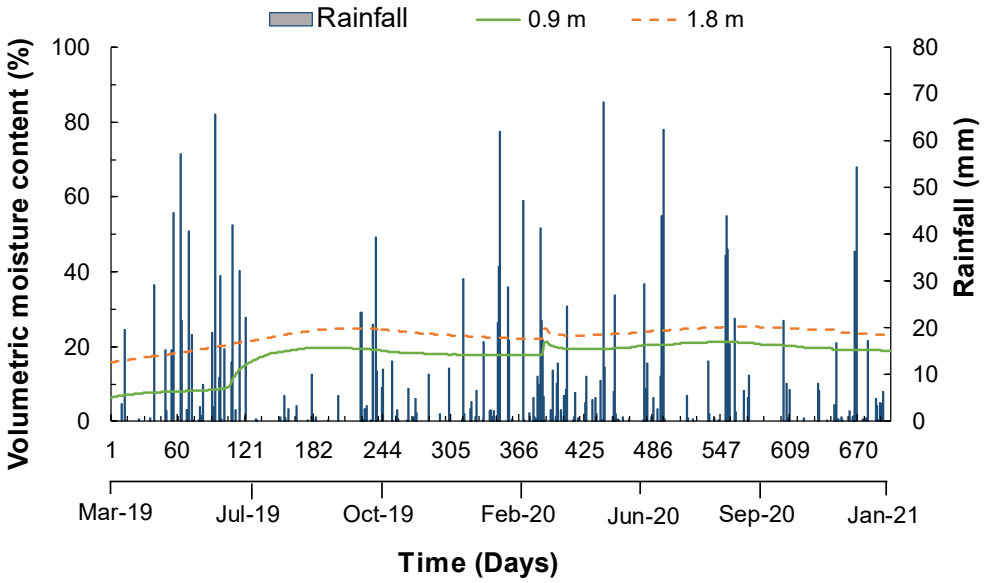

Figure 5–6 Volumetric Moisture Content Variation at the Center of Barrier Section

Similar to the edge sensors, the sensors at the center maintained almost the same saturation level with the average moisture values maintained at 18% and 23.3% at 0.9 m and 1.8 m depth, respectively (Figure 5–6). No rainfall dependent behavior was observed in the moisture values, indicating no moisture intrusion into the subgrade soil from pavement's surface. All these results show the potential of moisture barrier in preventing the moisture to reach the subgrade and mitigate the probability of pavement failure.

Figure 5–7 shows suction variation at 0.9 m depth in barrier section during the monitoring period. As can be seen in the figure, minimum suction value of -10 kPa was maintained throughout the monitoring period. This indicates neither rainwater infiltration nor exfiltration is occurring beneath the stabilized section after the barrier was laid in the wet period. The higher suction values recorded immediately after the installation can be associated to the adjustment period when the soil around the sensor was in a relatively disturbed condition.

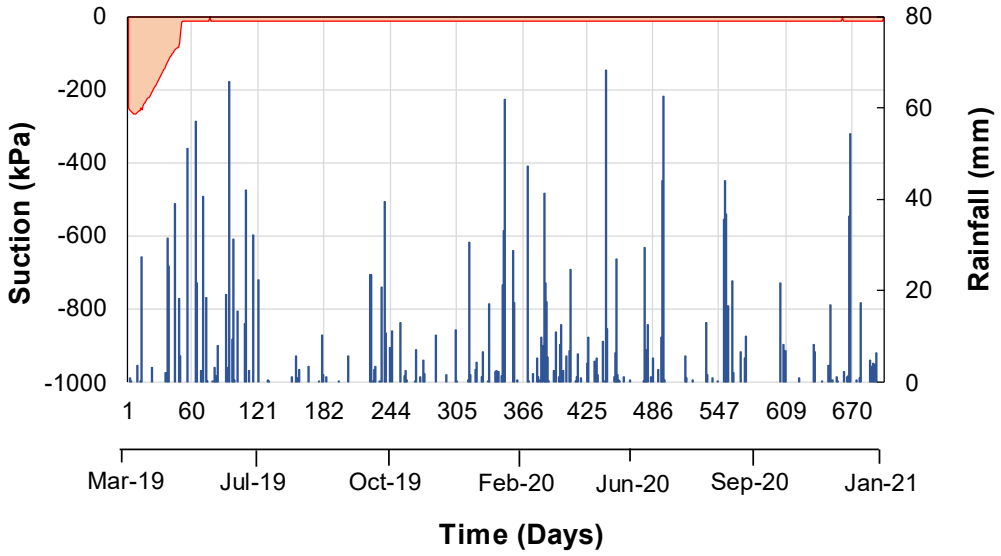

Figure 5–7 Suction Variation at 0.9 m Depth in Barrier Section

5.3.2 Deformation in Barrier Section

Figure 5–8 shows the movement of subgrade soil at a cross-section of 91 m long pavement section which is stabilized with modified moisture barrier. The initial reading from the inclinometer is considered as a base reading based on which the vertical deformation of the pavement was analyzed. The base reading was taken after the roadway section was repaved using chip seal to avoid any probable disturbance. Day 1 in the figure represents the first reading of inclinometer measured on March 21, 2019. Based on two years of monitoring results, the subgrade soil underneath modified moisture barrier experienced a maximum movement of 7.36 mm from the base reading at a distance of 1.83 m (6 ft) from the edge. At the edge, total movement of 6.6 mm was recorded. The subgrade soil movement at the edge of barrier section was also compared with the moisture variations over a period of time for 0.9 m depth, as shown in Figure 5-9.

The results showed insignificant variation of soil moisture content and subgrade soil movement at all times despite the pavement surface being subjected to seasonal climatic

loading. This less movement can be attributed to the adequate drainage and prevention of moisture infiltration in the underlying soil layers by the modified moisture barrier placed at the base-subgrade interface.

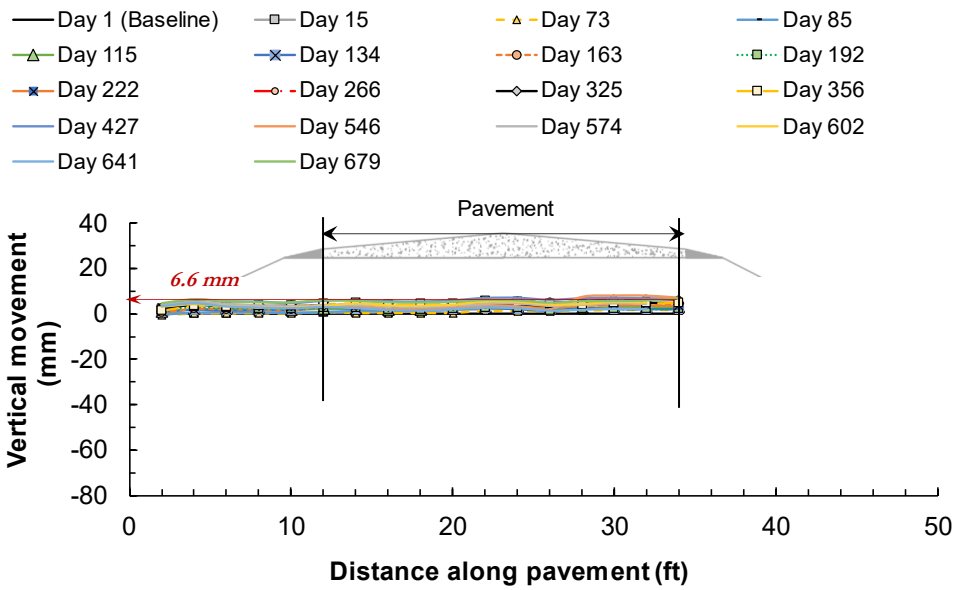

Figure 5–8 Vertical Movement in Subgrade Soil of Barrier Section

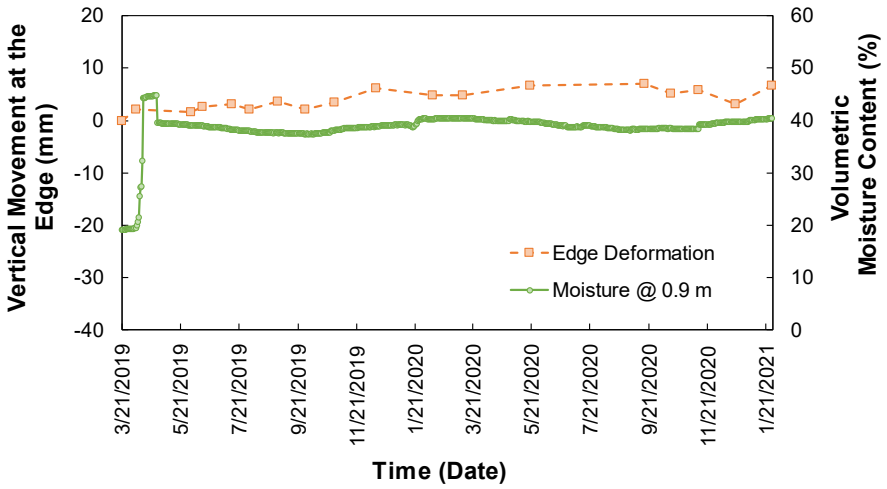

Figure 5–9 Comparison of Subgrade Deformation with Moisture Variation in Barrier Section

5.4 Comparison Between Barrier and Control Sections

5.4.1 Moisture Variation- Barrier Vs Control Section

The moisture variation in the subgrade of stabilized pavement section and adjacent control section was evaluated using the hourly moisture content data recorded by the sensors. The 24- hours moisture data were converted to daily average and evaluated against the cumulative daily rainfall. Figure 5–10 shows the comparison between observed moisture profile at 0.9 m depth from both the sections from February 2020 to January 2021. Sensors in the barrier section showed near-constant moisture profile while a maximum of about 17% change in volumetric moisture content occurred in the control section at a depth of 0.9 m. The cyclic fluctuation in moisture may significantly alter the mechanical property of subgrade soil, thereby causing different types of distresses in pavement (Wanyan et al., 2010). Although AASHTO suggests considering equilibrium moisture content under the covered areas for the determination of soil parameters for the design of pavement, several studies have reported the seasonal and temporal moisture variation underneath the pavement (Ngyuen et al., 2010; Hedayati, 2014), implying pavement surface is not completely impermeable and may allow some moisture intrusion which needs to be considered for the pavement design procedure. Hedayati (2014) investigated the real time moisture variation in expansive subgrade soil by installing moisture sensors underneath distressed low volume pavement of North Texas. The author reported sensitivity of all sensors towards the climatic loading and concluded that moisture content may vary significantly under the pavement's surface mainly in narrow two-lanes roadway in the form of seasonal and transient variation. A research conducted by FHWA also reports moisture intrusion as much as 33 to 50 % occurring from the surface of pavement (Cedergren, 1974). In the current study, constant moisture profile at the edge and center of barrier section

indicates that modified moisture barrier was able to reduce potential moisture fluctuation as a result of environmental loading.

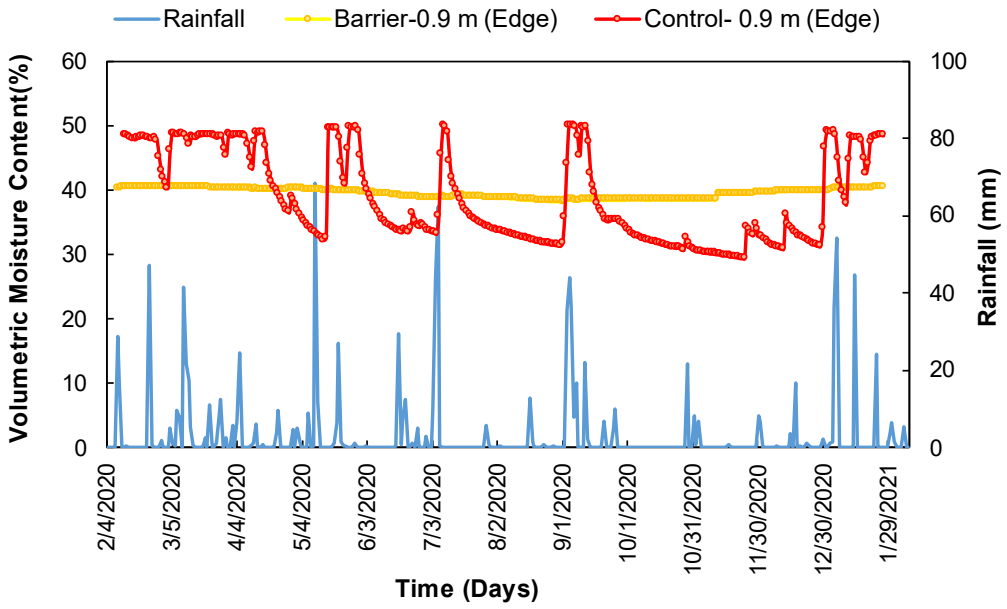

Figure 5–10 Comparison Between Volumetric Moisture Variation in Barrier and Control Sections

5.4.2 Deformation- Barrier Vs Control Section

Horizontal inclinometer captured the seasonal movement of highly expansive subgrade soil. Figure 5–11and Figure 5–12 illustrate the movement of the pavement edges with and without moisture barrier throughout the monitoring period. As discussed earlier, the section without any modified moisture barrier exhibited the most movement while there is almost insignificant movement in the barrier section despite being subjected to same climatic conditions. The moisture barrier was able to control the swelling and shrinkage potential of highly expansive subgrade soil. As a result, almost constant soil profile was observed in the barrier while maximum movement of -48 mm and -54.83 mm were observed at the left and right edge of the control section, respectively. The barrier was able to reduce the

movement of subgrade soil approximately by 89% based on the performance monitoring results.

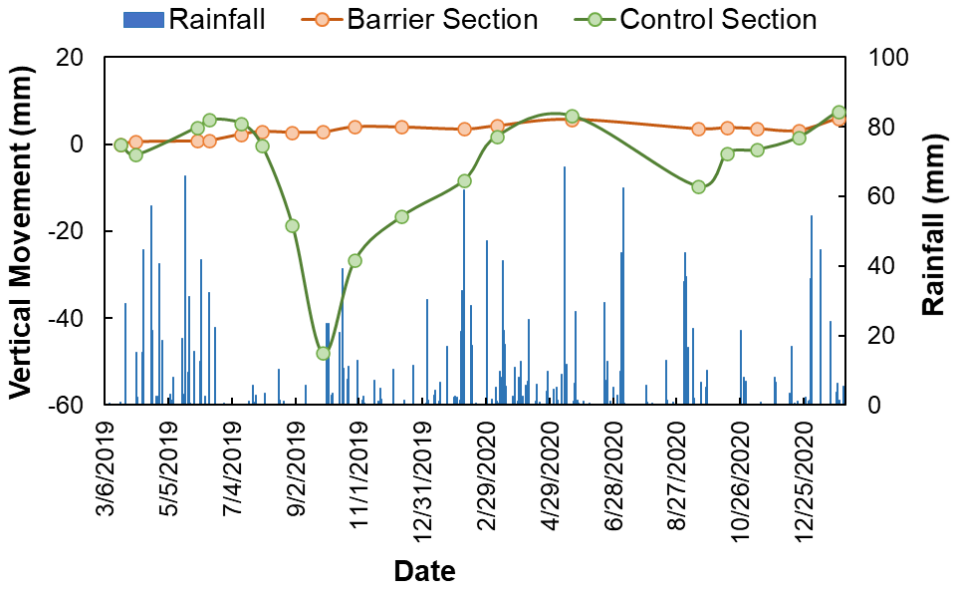

Figure 5–11 Subgrade Soil Movement at the Left Edge of Pavement

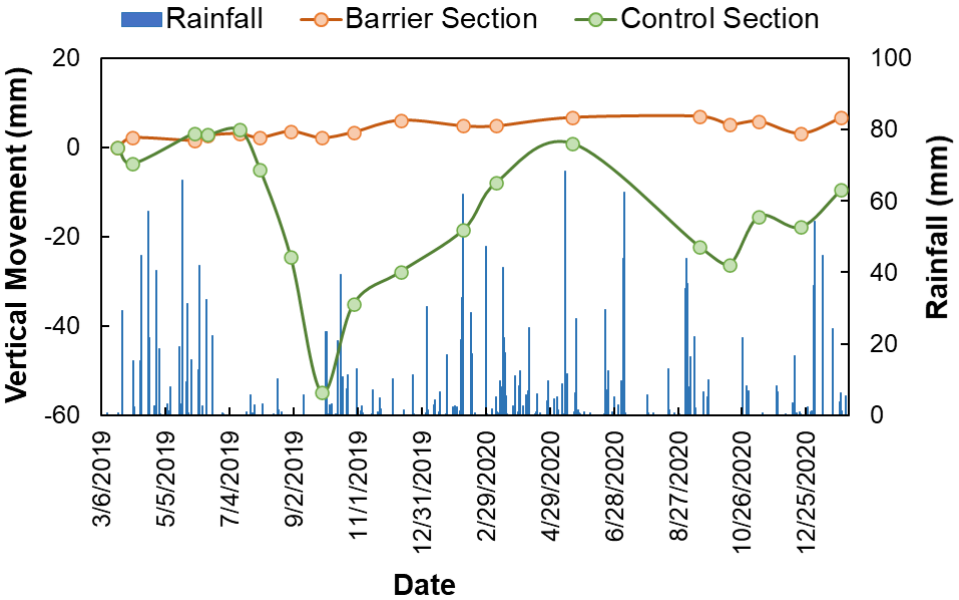

Figure 5–12 Subgrade Soil Movement at the Right Edge of Pavement

5.4.3 Incremental Movement- Barrier Vs Control Section

Figure 5–13 compares the maximum incremental movement of the subgrade soil observed at the right edge of barrier and control sections. The swelling of the subgrade soil can be represented by positive incremental movement while the shrinkage of the soil can be represented by negative incremental movement. The figure represents the extent of swelling and shrinkage in the subgrade soil at different time of year.

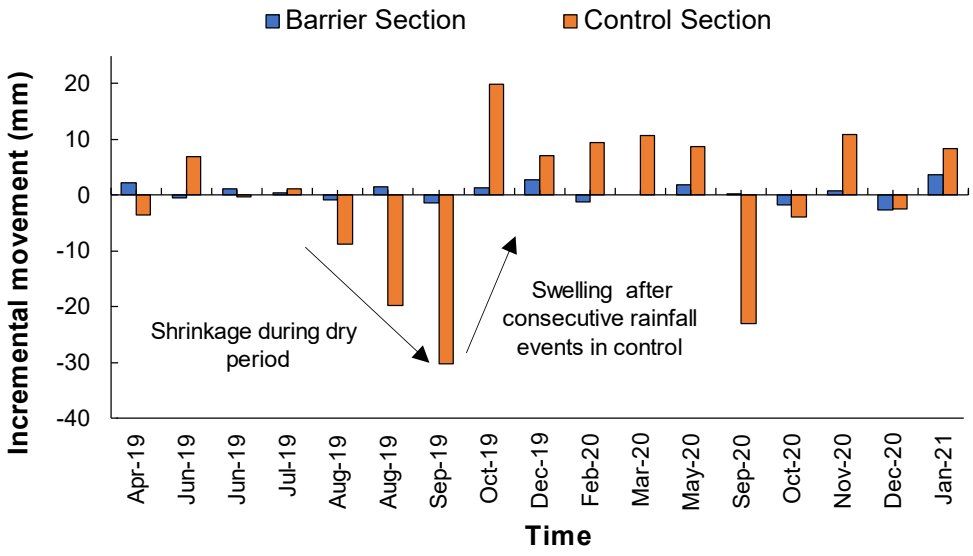

Figure 5–13 Incremental Movement of Subgrade Soil at the Right Edge of Pavement Section

As the figure suggests, modified moisture barrier was able to significantly reduce excessive seasonal movement throughout the monitoring period. The maximum incremental movement observed in the barrier section was only 3.55 mm. Furthermore, the movement was not found to follow any particular pattern. On the contrary, considerably higher movement was observed in the section with no moisture control system, especially at the end of summer. The control section exhibited incremental movement in the form of swelling

during wet period and shrinkage during dry period. The effect of long dry summer 2019 was well reflected in the control with the incremental movement of -30.23 mm which was the highest movement during the monitoring period. Comparing the incremental movement of the expansive subgrade soil at the two sections, it is clearly evident that the movement is more prominent in the control section with higher values than in the barrier section.

5.5 Comparison with Previous Studies

A study by Elseifi et al. (2001) used geo composite membrane in a test section of Virginia Smart Road and reported constant moisture values in the barrier section while a maximum of 5% moisture change was reported in control section due to rainfall of 47 mm. The authors concluded high dependence of soil moisture on rainfall events in pavement sections with no moisture barrier as observed in the current study. Likewise, the study conducted by Ahmed et al. (2018) in a Farm to Market road of North Texas demonstrated moisture fluctuation independent of precipitation with slight variations beneath the shoulder of pavement where the modified moisture barrier was laid. On the other hand, volumetric moisture content ranged in between 20% to 60% at 0.9 m depth in control section. (Figure 5–14). Another study by Sapkota et al. (2019) reported a maximum moisture variation of 31.17% and 32.81% in sections without modified moisture barrier while the section with barrier showed maximum variation up to 3.89% (Figure 5–15).

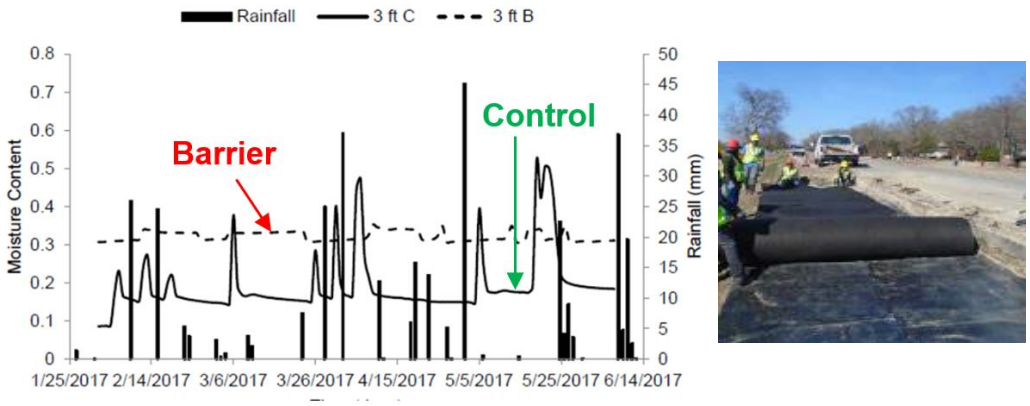

Figure 5–14 Moisture Variation in a MMB Stabilized Pavement Shoulder at FM 987 (Ahmed et al., 2018)

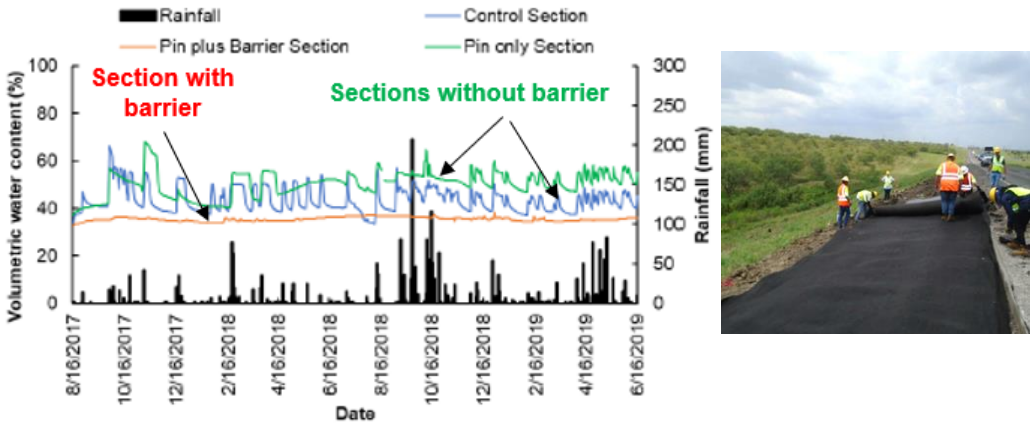

Figure 5–15 Moisture Variation in a MMB Stabilized Highway Slope at US 287 (Sapkota, 2019)

The effectiveness of the proposed stabilization method was compared with previous literatures in terms of percentage reduction in deformation. Figure 5–16 illustrates the comparison of percentage reduction in deformation of expansive subgrade soil from different field-based studies conducted in the past. Ahmed et al. (2018) studied the behavior of expansive subgrade soil after stabilizing 15.24 m (50 ft.) of pavement with modified moisture barrier in which barrier section exhibited deformation reduction by 80%

as compared to adjacent control section. Unlike the current study, the author placed the moisture barrier only at one edge of the pavement. Likewise, Tailor and Shah (2014) conducted a study to improve the performance of flexible pavement constructed on expansive soil with the help of geotextile. The authors reported reduction in shrinkage by 50% in an average when geotextile was used beneath the pavement. In another study conducted by Pardo et al. (1998), vertical moisture barrier consisting of geomembrane was used over highly expansive alluvial subgrade soil. While a relative settlement of 85 mm was witnessed at unsealed shoulder, the edge-line settlement of the stabilized pavement was only 5 mm. The vertical moisture barrier was effective in reducing the differential subgrade movement by 95% following a record dry summer temperature. When compared to the results obtained by Pardo et al. (1998), the present study differs by only 6% in reducing the deformation at edge of the pavement. By placing modified moisture barrier all over the pavement, the proposed method of stabilization resulted relatively uniform profile and reduction in swelling and shrinkage of highly expansive subgrade soil by about 89%.

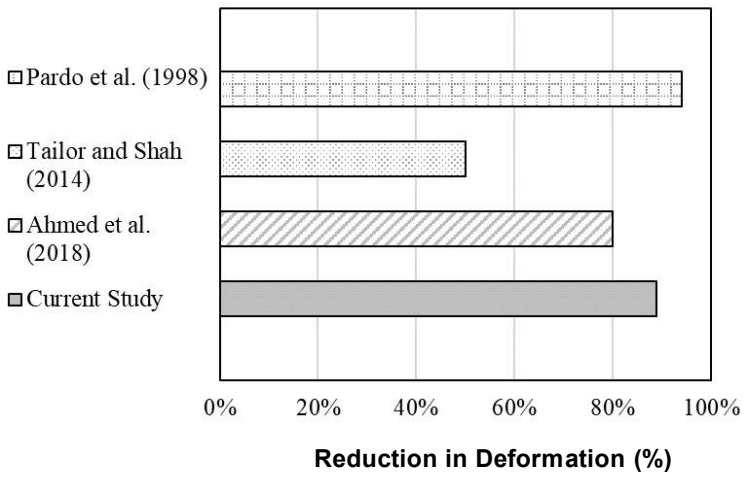

Figure 5–16 Comparison of Percentage Reduction of Subgrade Soil Deformation with Previous Studies

5.6 Visual Survey

Figure 5–17 shows the pictures of the test sections taken during the field visit of June 2020. No cracks were observed in the pavement section stabilized with modified moisture barrier while surficial distresses were observed in other parts of pavement. This was because the modified moisture barrier installed at the base-subgrade interface was able to prevent the cyclic moisture variation in the highly expansive subgrade soil and control the excessive swelling and shrinkage of soil while the control experienced significant swelling and shrinkage with no measures to control the moisture infiltration. The new cracks formed in the control section along with old cracks in the vicinity were sealed using sealing product.

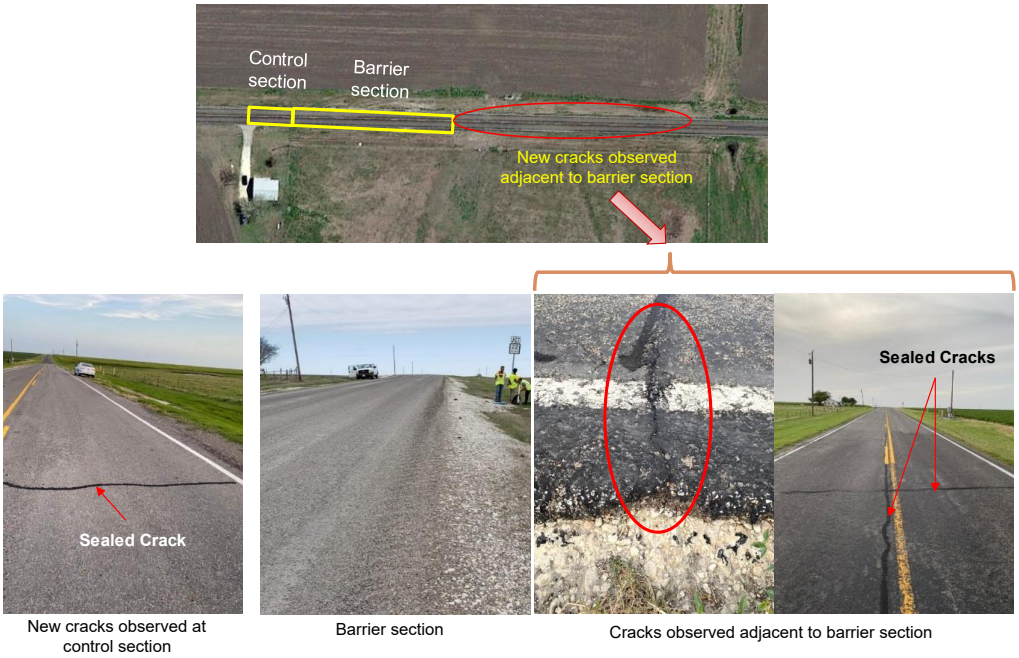

Figure 5–17 Visual Inspection During Field Monitoring

5.7 Effectiveness of Proposed Remedial Method

The main purpose of using modified moisture barrier in the current study was to isolate the subgrade soil from variable environmental conditions throughout the year. This would

ensure no fluctuation of subgrade moisture which would eventually control the recurrence of pavement cracks due to highly expansive nature of subgrade soil.

The overall observation of moisture variation in the current study indicated the effectiveness of modified moisture barrier in maintaining equilibrium moisture content under the pavement surface. This may have otherwise altered through moisture infiltration from pavement surface or lateral movement of water from pavement edge. The present study shows very promising results in effectively controlling the deformation in expansive subgrade soil with high value of percentage reduction in seasonal movement. Moreover, the installation of modified moisture barrier is comparatively more convenient than other conventional methods. The installation method does not alter or hamper the pavement system in any way. The various steps involved in construction of a pavement, such as compaction, placement of base, application of asphalt, among others are not affected due to the barrier system. Considering all the above-mentioned points, horizontally placed modified moisture barriers can be deemed very effective and efficient for controlling environmentally induced pavement distresses.

Chapter 6

MOISTURE AND DEFORMATION MODELING

6.1 Background

The field monitoring results showed that both the moisture and deformation in the control section varied throughout the year. A seasonal fluctuation was seen for both the results. The seasonal variation can be attributed to the change in climatic conditions at different time of the year. In general, the wet period, which is characterized by more rainfall and less temperature, showed higher subgrade moisture contents, and swelling of the subgrade. On the other hand, the dry period, which is characterized by less rainfall and higher temperature, showed lower subgrade moisture content and shrinkage of the subgrade. Apart from the seasonal trend, there were incidents with sudden peaks and drops due to temporary changes in rainfall and ambient temperature. It would be beneficial to develop prediction models based on the field results which can predict moisture content and deformation of subgrade soil. These models can be used for similar types of soil in the North Texas region. The prediction of moisture changes and deformation of subgrade based on anticipated climatic conditions can immensely help transportation authorities, researchers, or any other interested parties in evaluating the performance of pavements constructed over expansive subgrade. This chapter demonstrates the steps involved in developing such prediction models. The developed models are also validated with field results to assess the predictability of the models.

6.2 Data Analysis

Non-parametric analysis was performed on the moisture and deformation variation of the control section. Non-parametric methods are best suited for data which do not follow any specific order with time. Previous studies have shown the applicability of non-parametric

analysis on data varying over time (Hedayati, 2014; Ahmed, 2017). The following points can be summarized for such data sets:

- The data does not follow any specific distribution trend, so there is no direct numerical interpretation.
- The data does not fall into any specific statistical distribution.
- The only information present about the data is its variation with time.

The non-parametric method does not follow the normal statistical methods. It does not rely on typically used statistical identifiers, such as mean, standard deviation, and variance, to explain the variation observed in the data points. An accepted technique of carrying out these analyses is dividing the date into sub-categories. Generally, they are categorized into two sets: main signal and noise. The main signal characterizes a trend seen over a time period of interest. Smoothing techniques are applied to make the prediction trend interpretable. Care must be taken while selecting a smoothing parameter, so as not to underfit or overfit the data. The noise, or the peaks and drops, can be characterized by sudden changes in independent (predictor) variables. The main signal and noise can be combined to get the final model. The final model should be able to fairly predict both the seasonal trend over time along with the occasional changes. MATLAB R2020b was used for fitting the seasonal trend (main signal) of the moisture and deformation variation.

6.3 Moisture Modeling

The subgrade moisture content of the control section showed variations in response to different time of year and rainfall. The average moisture was relatively higher during the wet period, while there was a decrease in the overall trend during the dry period. This showed a high dependency of moisture on climatic loading. At the same time, there were occasional peaks and drops of moisture content in response to excessive temporary

changes in rainfall and temperature. The trend was thus differentiated into two categories: an annual seasonal trend, and occasional peaks and drops (noises). Similar trends have been observed by previous field studies as well (Nguyen et al., 2010; Hossain, 2013; Manosuthikij, 2008; Hedayati, 2014; Ahmed, 2017). As mentioned in the literature review section, a first-degree Fourier series (Sastry, 2012) can be used to explain the annual seasonal variation of subgrade moisture such as:

$$f\ (t) = \ a_o + \sum_{n=1}^{\infty}\left(a_n cos\frac{2n\pi x}{T} + \ b_n sin\frac{2n\pi x}{T}\right)$$

The series follows the form:

$$f\ (x) = \ a_o + \ a_1 * \cos(x * w) + b_1 * \sin(x * w)$$

where, a_o represents the average value of the dataset or the annual average moisture content of the field, a_1 and b_1 represent the amplitude of the dataset, and w is the frequency (day^{-1}). The variable x is the day of the year.

The moisture sensor installed at the edge of the control section at 0.9 m depth was used for the model development. The data used for the model starts from February 9, 2020 (Day 1) and ends on January 27, 2021 (Day 354). The data was plotted against the Day in MATLAB. It is to be noted that the beginning of the dataset was during wet period with heavy rainfall accumulations. Thus, it was decided to omit the peak moisture contents for the first 70 days (based on the extent of heavy rainfall events). Furthermore, the moisture content during this time attained almost the saturated moisture content range of the soil. Thus, including this data for the seasonal trend would be misleading. After removing the outliers and numerous trial and error, a model was selected to fit the annual seasonal trend.

The model parameters are as shown below. The adjusted R^2 was estimated to be 95.61%. The dataset plot is shown in Figure 6–1.

$$\textit{Seasonal M.C.} = 35.29 + 1.974 * \cos(x * 0.01717) + 3.41 * \sin(x * 0.01717)$$

Where, *Seasonal M.C.* = Volumetric moisture content at day *x* (%)

a_o = Annual average volumetric moisture content (%) = 35.29 %

Day 1 = February 09, 2020

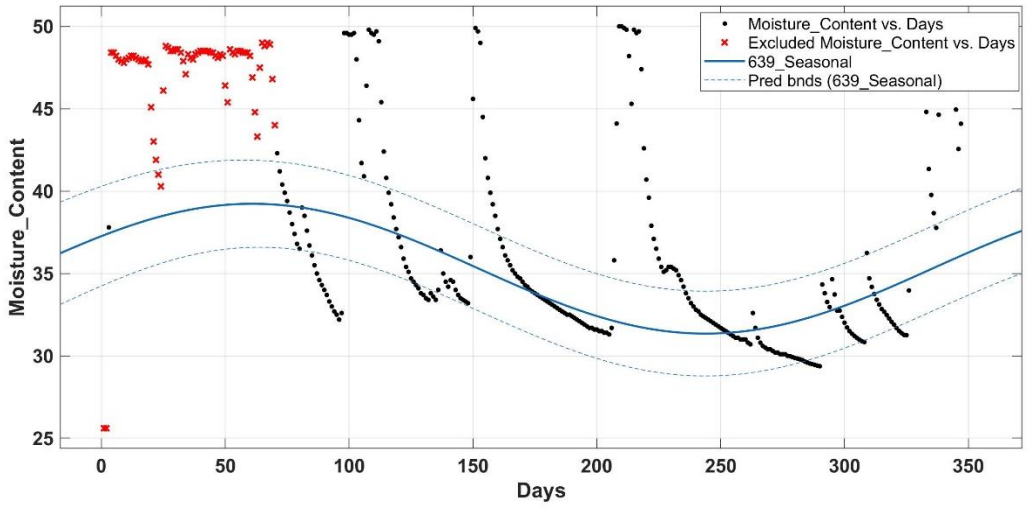

Figure 6–1 Seasonal Trend of Moisture Content

The seasonal fit showed the average variation seen with time. The wet period showed higher moisture contents, while the dry period exhibited relatively less moisture contents. However, only this trend could not capture the instantaneous changes in moisture due to the temporary change in rainfall and temperature. Thus, separate studies were conducted to evaluate the individual effects of rainfall and temperature on the subgrade moisture.

6.3.1 Effect of Rainfall on Subgrade Moisture

The next step was to capture the temporary peaks and drops in the subgrade moisture content. Two key assumptions were followed for this which are explained below:

1. The peaks in moisture content were separated such that there was at least 1% change from the previous rainfall event. Ahmed (2017) followed a similar approach as well. This was done because in some instances when the rainfall was very high, the moisture content increased by less than 1%. This was seen mostly when the subgrade moisture was at its peak value (saturation point). Any amount of rainfall would not increase the subgrade moisture beyond its peak capacity. Inclusion of such points would disarray the prediction model.
2. Focus was given to moisture changes from the equilibrium position. These moisture changes truly reflect the effect of temporary increase of rainfall events.

The peak moisture content changes were tabulated along with the corresponding rainfall values. Several regression methods were tried (linear, logarithmic, polynomial), however, keeping in mind the ease of use, a linear regression was selected to best explain the model variability. The regression coefficient (R^2) was found to be 67.49% (Figure 6–2). Similar R^2 values were reported by Ahmed (2017) which were between 57-74%. Comparable trends were shown by other studies as well where temporary increase in rainfall events caused an instantaneous increase in the subgrade moisture (Xu et al., 2012; Hedayati, 2014). The effect of rainfall can be formulated as follows:

$$\textit{Increase in M.C. (Due to Rainfall)} = 0.2407 * x_R + 0.9639$$

where, x_R denotes rainfall in mm.

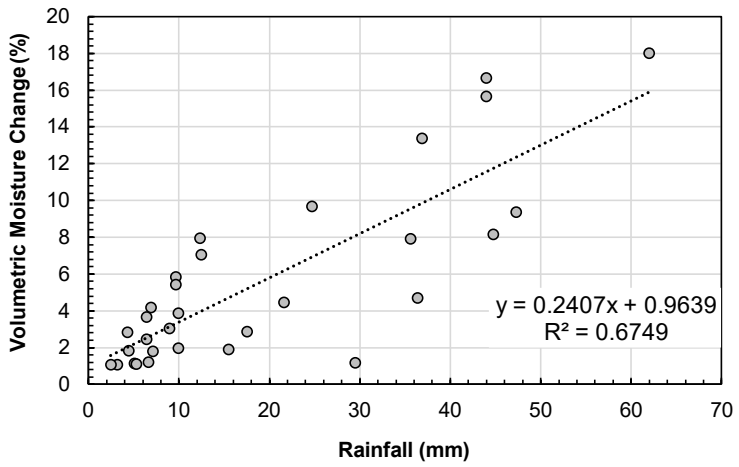

Figure 6–2 Linear Relationship Between Change in Moisture Content and Rainfall

6.3.2 Effect of Temperature on Subgrade Moisture

As high rainfall events brought a spike in the subgrade moisture, an increase in soil temperature above the average can cause the subgrade moisture to decrease. An important point to be stated here is that the effect of the average temperature throughout the year is already reflected by the seasonal fit as shown earlier. It is the change from the average temperature that is of interest. The seasonal trend already predicted the variation in subgrade moisture in response to the average soil temperatures throughout the year. However, some instantaneous events when the temperature rises suddenly from the expected temperature of that time, can dry out some moisture from the soil. Thus, the objective of this section is to quantify that decrease in moisture content due to the temporary increase in soil temperature. This was done in two steps as explained below:

1. First, the average soil temperature throughout the year was modeled using non-parametric analysis. A similar approach as was done earlier for the seasonal variation of moisture was followed.

2. Then, the difference in actual soil temperature and average seasonal soil temperature was calculated. This difference was plotted against the change or decrease in subgrade moisture to quantify a relationship.

Soil temperature is dependent on many factors such as time of the day, season, weather patterns, rainfall, drought, and depth of soil among others. It can be accurately measured using temperature sensors installed in the soil at required depth. Hillel (1982) stated that the temperature variation of soil can be modeled in such a way that it oscillates in a sinusoidal pattern around an average value. Previous studies have demonstrated the successful development of sinusoidal temperature variation models (Lei et al., 2011; Hedayati, 2014; Ahmed, 2017).

The soil temperature from the same sensor (0.9 m depth) that was used before was used to develop a seasonal soil temperature model. MATLAB R2020b was used to fit a first-degree Fourier series to the soil temperature data. The model fitting is shown in Figure 6–3. The adjusted R^2 was estimated to be 97.86%. The seasonal soil temperature can be predicted using the following equation:

$$Seasonal\ S.T. = 21.32 - 8.266 * \cos(x * 0.01624) + 1.611 * \sin(x * 0.01624)$$

Where, *Seasonal S.T.* = Soil temperature at day x (^oC)

a_o = Annual average soil temperature (^oC) = 21.32 ^oC

Day 1 = February 09, 2020

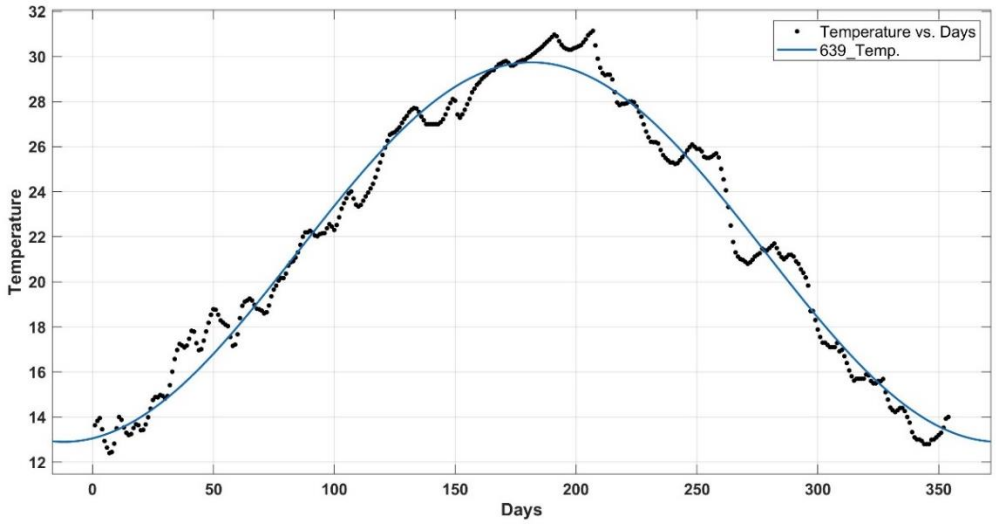

Figure 6–3 Seasonal Trend of Soil Temperature

As expected, the soil temperature model predicts higher temperatures during the summer days and vice versa during winter. Now, the difference between the actual soil temperature and model predicted soil temperature was calculated. This difference was then tabulated and compared with the change in subgrade moisture from the average seasonal trend. For the purpose of catching the effect of high temperatures, and thereby subsequent decrease in moisture contents, only those subgrade moistures were chosen which were less than the seasonal expected values. Decrease in moisture contents were chosen where there was at least 2% change. This was done to model only the extreme events and reduce scatter in data. Figure 6–4 shows the linear regression fit on the data. The temperature changes could explain 61.2% of the variability in the moisture. The effect of soil temperature change can be formulated as follows:

$$\textit{Decrease in M.C. (Due to Soil Temperature)} = -0.3912 * x_t - 1.9757$$

where, x_t denotes increase in soil temperature from the seasonal value in ^{o}C.

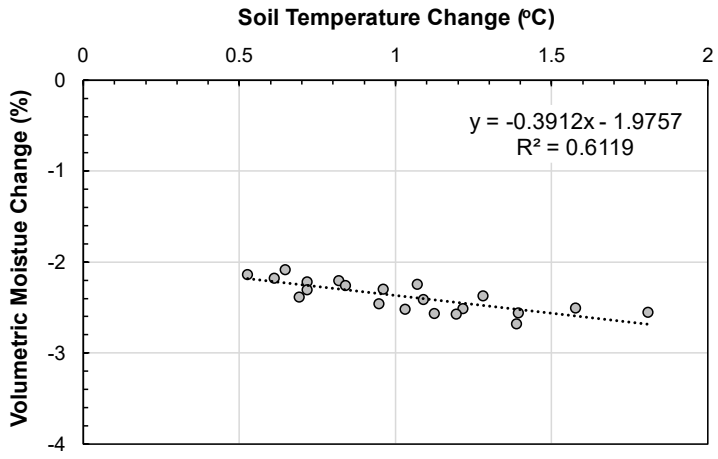

Figure 6–4 Linear Relationship Between Change in Moisture Content and Soil Temperature

6.3.3 Final Moisture Model

Following the quantification of rainfall and soil temperature effect on subgrade moisture, the final model was formulated as follows:

M.C. = Seasonal M.C. + Increase in M.C. (Due to Rainfall) - Decrease in M.C. (Due to Soil Temperature)

$M.C. = [35.29 + 1.974 * \cos(x * 0.01717) + 3.41 * \sin(x * 0.01717)] + [0.2407 * x_R + 0.9639] - [0.3912 * x_t + 1.9757]$

where,

x = Day number (February 09, 2020 regarded as Day 1)

x_R = Rainfall in mm

x_t = Increase in soil temperature from the seasonal value in ^oC.

The model generated moisture contents were plotted against the sensor/field data to evaluate the predictability of the model, which is shown in Figure 6–5. The model shows

satisfactory fit with the field values. It was successful in capturing the seasonal trend as well as the temporary rise due to rainfall events. The field results indicated that the moisture stayed at the peak value for few days before dropping after every rise. This is due to the permeability of the soil. It takes certain time for any moisture increase to dissipate or exfiltrate which is called desaturation time. However, the predicted moisture did not stay at the maximum level for few days but rather dropped instantaneously. This was expected since the mathematical model does not consider the soil permeability or other factors affecting the lag period for moisture to drop. The rate of desaturation of the soil was not considered during the model development. It is to be noted that the predicted peak values of subgrade moisture were almost the same as seen in the field. Thus, this model can be used to predict subgrade moisture content for similar type of subgrade soil conditions and at similar depths. The first term of the model, which represents the average moisture content for that location, needs to be entered accordingly.

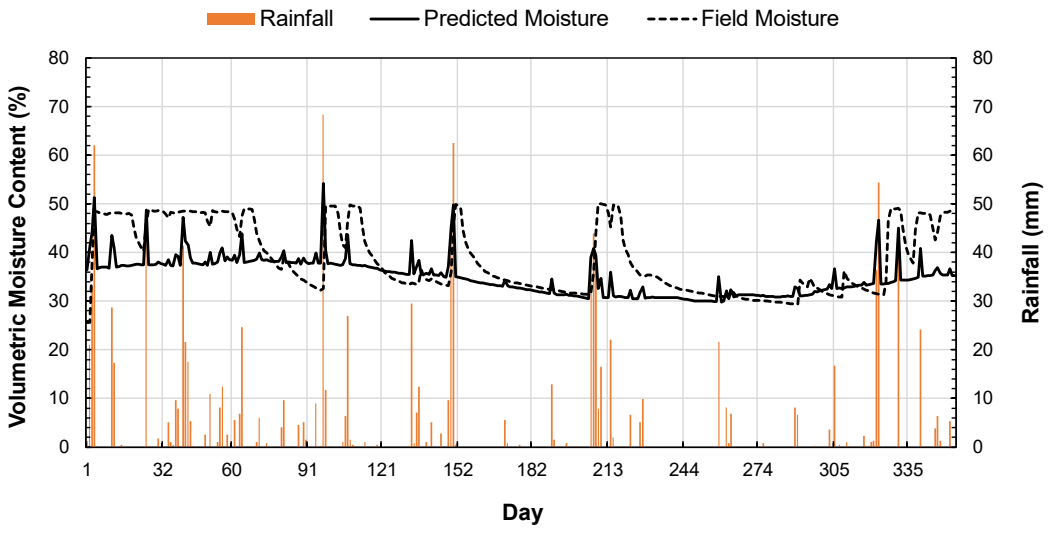

Figure 6–5 Comparison of Model Predicted and Field Subgrade Moisture in FM 639

The input parameters for the model are day number, rainfall, and soil temperature change. However, the soil temperature is not readily available unless a sensor is installed. This will create a hindrance for the user to apply the model. Therefore, it was decided to create a general model which could predict changes in soil temperature readily.

6.3.4 Change in Soil Temperature Model

A prediction model should be such that the user can predict the output using readily available input parameters. This makes the prediction model user-friendly and applicable. The soil temperature change which is required in the developed model is not easily available to the user. An equation relating the soil temperature to any easily available parameter can be beneficial. Soil temperature is mainly dependent on the air/ambient temperature. Regardless of time of the day, season, or any other factors, air temperature dictates the major variation in soil temperature. To demonstrate the relationship between air temperature change and soil temperature change, it was first needed to develop an air temperature model. A similar approach that was followed to develop the soil temperature model can be used here as well. Since the air temperature model can be a generic one for North Texas, available data from various locations in North Texas was chosen. One year of air temperature data for different years at different locations were fitted using first degree Fourier series. The coefficient values of each model were then averaged to get a final generic model which can be used in any part of North Texas. The year and location of air temperature data used in the model development are tabulated in Table 6–1. The coefficients obtained from each model are presented in Table 6–2. The fitted models for each year and location are presented in Figure 6–6.

Table 6–1 Year and Location of Air Temperature Data for Model Development

Year	Location
2013	FM 2757, Kauffman County
2014	FM 2757, Kauffman County
2017	SH 342, Ellis County
2018	FM 987, Kauffman County
2020	FM 639, Navarro County

Table 6–2 Air Temperature Model Coefficients

Location	Model Coefficients				Adjusted R^2 (%)
	a_0	a_1	b_1	w	
FM 2757, Kauffman County	19.68	-11.88	-1.443	0.01865	79.12
FM 2757, Kauffman County	16.2	-10.97	8.366	0.01431	80.29
SH 342, Ellis County	17.56	-7.995	7.098	0.0146	75.32
FM 987, Kauffman County	19.39	-11.36	3.056	0.01727	83.46
FM 639, Navarro County	18.55	-9.254	5.09	0.01564	99.15
Average	**18.276**	**-10.292**	**4.433**	**0.01609**	-

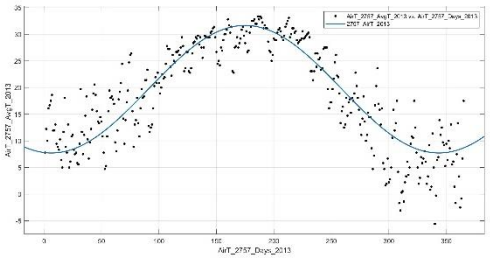

FM 2757, Kauffman County (2013)

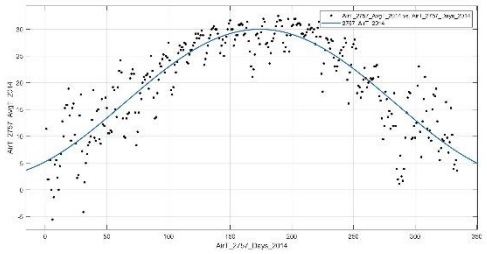

FM 2757, Kauffman County (2014)

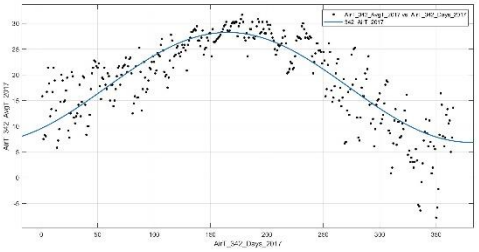

SH 342, Ellis County (2017)

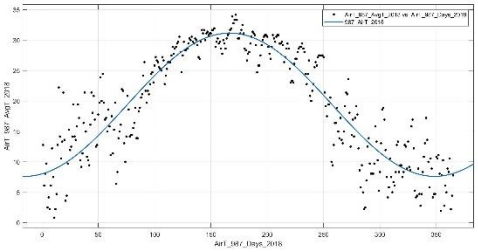

FM 987, Kauffman County (2018)

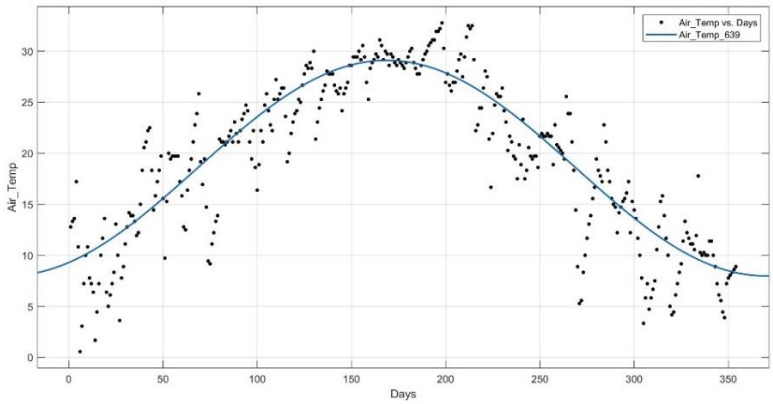

FM 639, Navarro County (2020)

Figure 6–6 Seasonal Trend of Air Temperature in North Texas

The final seasonal air temperature model can be represented as follows:

$$Seasonal\ A.T. = 18.276 - 10.292 * \cos(x * 0.01609) + 4.433 * \sin(x * 0.01609)$$

Where, *Seasonal A.T.* = Seasonal air temperature at day x (^{o}C)

Day 1 = February 09

The final air temperature model can be illustrated as Figure 6–7. The chart can be directly used without using the equation to estimate the average air temperature for a certain day.

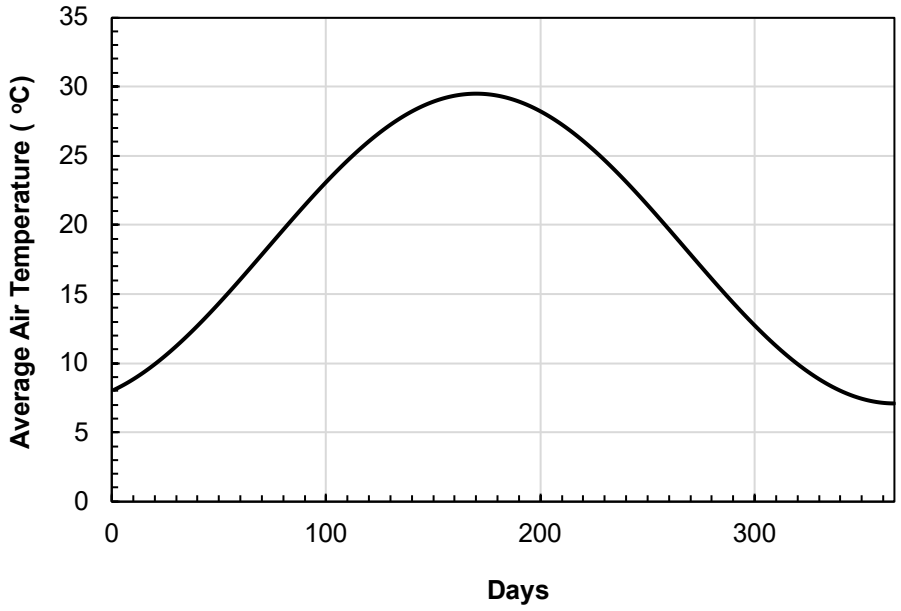

Figure 6–7 Final Generic Air Temperature Model for North Texas

After the formulation of the final air temperature model, the data of the current study was used to develop the soil temperature change relation with air temperature change. So, first the difference of actual air temperature and the predicted seasonal air temperature was calculated. Then, the difference between actual soil temperature and predicted seasonal soil temperature was estimated. The two sets of differences were plotted against each other so as to establish a relationship between them. For the purpose of simplicity, only two categories were used for developing the relation, which are:

1. When the air temperature rises above the average expected temperature, the soil temperature rises as well.
2. When the air temperature drops below the average expected temperature, the soil temperature drops as well.

Any other relation will have effect from different sources. For instance, if the air temperature rises above the expected temperature and the soil temperature decreases below the average seasonal temperature at the same time, it could be due to effect of rainfall events. Various relationship between the data was tried (linear, exponential, polynomial), after which a polynomial relation showed the best fit. The R^2 value of the fit was 61.14%. The plotted data and fitted trend are shown in Figure 6–8.

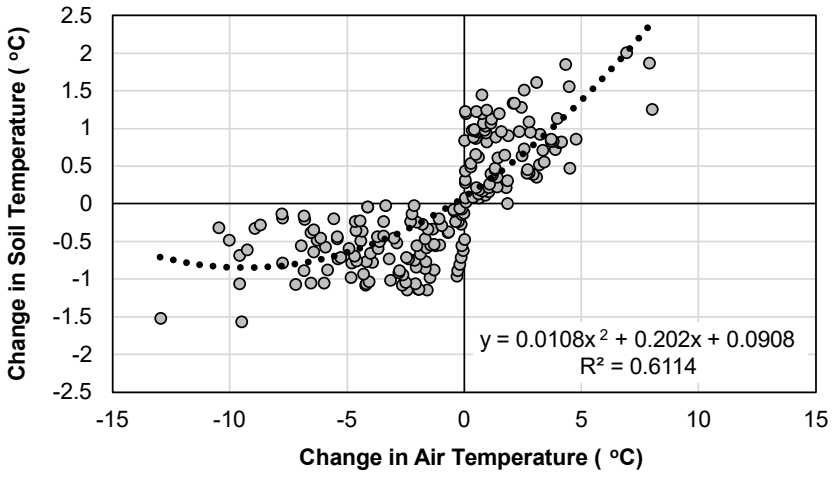

Figure 6–8 Relationship Between Changes in Air and Soil Temperature

Thus, the change in soil temperature as per the change in air temperature can be calculated as follows:

$$\textit{Change in S.T.} = 0.0108 * x_{AT}^2 + 0.202* x_{AT} + 0.0908$$

where, x_{AT} = Change in air temperature (°C)

This change in soil temperature can now be directly used in the subgrade moisture prediction model. The steps involved in using the model to predict subgrade moisture are outlined in Figure 6–9.

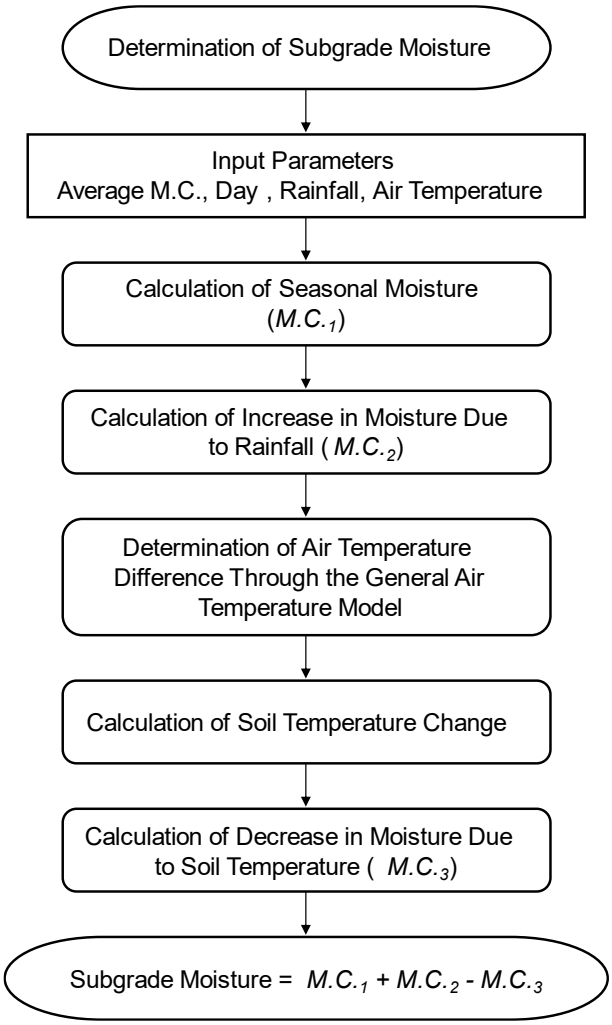

Figure 6–9 Flowchart for Calculation of Subgrade Moisture

6.3.5 Validation of the Moisture Model

The model was developed for the current study located in Navarro County, Texas using the data of 2020. To check the accuracy of the model and its applicability in North Texas, it was cross validated using data from other locations. Furthermore, the validation included data from different years. Table 6–3 shows the location, road name, and year of the data used for the validation of the developed moisture model.

Table 6–3 Location and Year of Moisture Model Validation Data

Location	**Roadways**	**Year**
Kauffman County	FM 2757	2013
Ellis County	SH 342	2017
Kauffman County	FM 987	2020

Hypothesis testing was conducted for each validation to justify the predictability of the model. Ahmed (2017) demonstrated the use of two-sample t-test assuming unequal variances to determine if there were significant differences between the field and model predicted subgrade moisture. The mean of the field and model predicted moisture values were compared against each other. The test was conducted at 95% confidence interval. Thus, the significance level (α) was 0.05. The hypothesis of the two-sample t-test can be depicted as follows:

H_o: $m_1 - m_2 = 0$

H_a: $m_1 - m_2 \neq 0$

where,

m_1 = mean of the field subgrade moisture

m_2 = mean of the model predicted subgrade moisture

The criteria which had to be satisfied so that the null hypothesis could not be rejected are:

- The t-value from the analysis should be lower than the positive critical value, or greater than the negative critical value of the two-tailed t-test.
- The p-value of the analysis should be higher than the significance level.

FM 2757

FM 2757 is a farm to market road located in Kauffman, Texas which exhibited expansive soil associated pavement cracks in 2012. Hedayati (2014) conducted a detailed study on the expansive subgrade soil of FM 2757 through extensive field instrumentations and evaluated the real time effect of environmental loading on pavement performance. The instrumentations captured subgrade moisture content as well as the vertical movement from 2012 to 2014 which indicated seasonal variation as well as temporary change due to rainfall events.

The subgrade soil moisture contents starting from Feb 9, 2013 were taken for the validation purpose. The rainfall and average air temperature for each day of the year were tabulated as well. The average moisture content of the location was calculated. The generic air temperature model in Figure 6–7 was used to calculate the daily air temperature differences. Then, the soil temperature change for each day was calculated using the air temperature change. Finally, the moisture model was used to calculate the daily subgrade moisture variation. Figure 6–10 shows the comparison plot between field and model predicted moisture contents. The model could capture the rainfall effect and the temporary

rise in moisture content. The field moisture did not follow a clear seasonal pattern, which explains some of the anomaly with the validation. Nevertheless, the model was successful in capturing the overall trend of moisture variation. This can also be verified from the plot between field and predicted moisture against a 1:1 45^{o} line (Figure 6–11). Since a majority of the points are clustered around the line, it can be stated that the moisture model provided satisfactory predictions. A two-tailed t-test was also conducted to justify the model, the summary of which is presented in Table 6–4. The t-value is greater than the negative critical value. The p-value of the analysis was higher than the significance level. Based on the analysis, it can be concluded that the null hypothesis could not be rejected, indicating that there is no significant difference between the field and model predicted means of the subgrade moisture. This justifies the moisture prediction model.

Table 6–4 Summary of Hypothesis Testing on FM 2757

	Mean	**St. Dev.**	**t-value**	**p-value**	**Critical t-value**
Field	41.514	1.798	-0.49	0.624	± 1.96
Predicted	41.609	3.123			

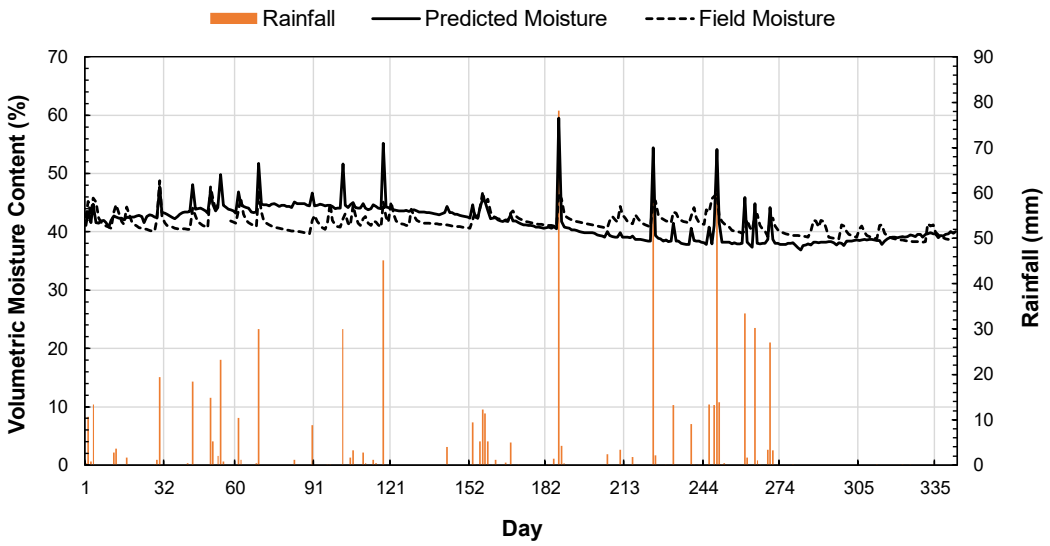

Figure 6–10 Comparison of Model Predicted and Field Subgrade Moisture in FM 2757

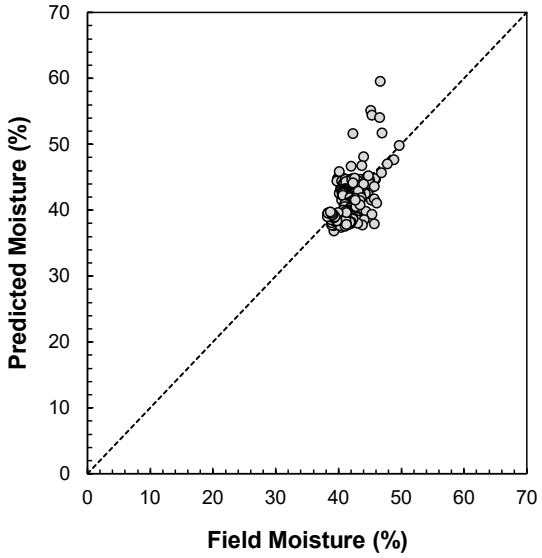

Figure 6–11 Accuracy of the Prediction Model in FM 2757

SH 342

SH 342 is a State Highway in Ellis County, Texas which is constructed over high-plasticity clayey soil (CH) with plasticity index in between 28 to 42%. Ahmed (2017) instrumented the pavement section with moisture sensors to observe the effect of real time rainfall events on subgrade soil moisture condition. In 2016, series of sensors were installed at the side slope of the pavement which exhibited seasonal moisture fluctuation over time and has been utilized in the current study for model validation.

The subgrade soil moisture contents starting from Feb 9, 2017 were taken for the validation purpose. The rainfall and average air temperature for each day of the year were tabulated as well. The average moisture content of the location was calculated. The generic air temperature model in Figure 6–7 was used to calculate the daily air temperature differences. Then, the soil temperature change for each day was calculated using the air temperature change. Finally, the moisture model was used to calculate the daily subgrade moisture variation. Figure 6–12 shows the comparison plot between field and model predicted moisture contents. The model could capture the rainfall effect and the temporary rise in moisture content. The model was also successful in capturing the overall trend of moisture variation. This can also be verified from the plot between field and predicted moisture against a 1:1 45^{o} line (Figure 6–13). Since a majority of the points are clustered around the line, it can be stated that the moisture model provided satisfactory predictions. A two-tailed t-test was also conducted to justify the model, the summary of which is presented in Table 6–5. The t-value is greater than the negative critical value. The p-value of the analysis was higher than the significance level. Based on the analysis, it can be concluded that the null hypothesis could not be rejected, indicating that there is no

significant difference between the field and model predicted means of the subgrade moisture. This justifies the moisture prediction model.

Table 6–5 Summary of Hypothesis Testing on FM 342

	Mean	St. Dev.	t-value	p-value	Critical t-value
Field	16.595	2.670	-0.84	0.401	± 1.96
Predicted	16.771	2.794			

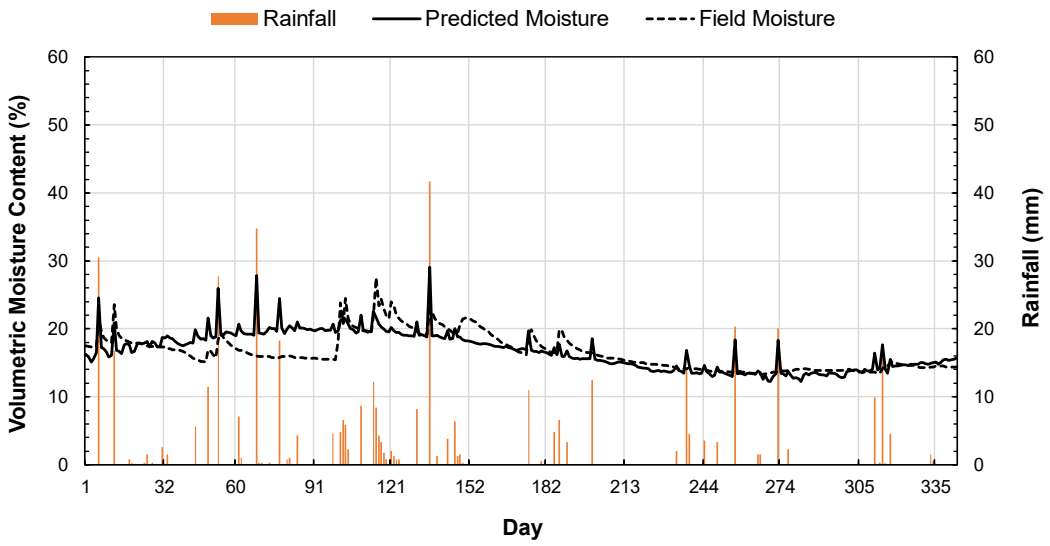

Figure 6–12 Comparison of Model Predicted and Field Subgrade Moisture in FM 342

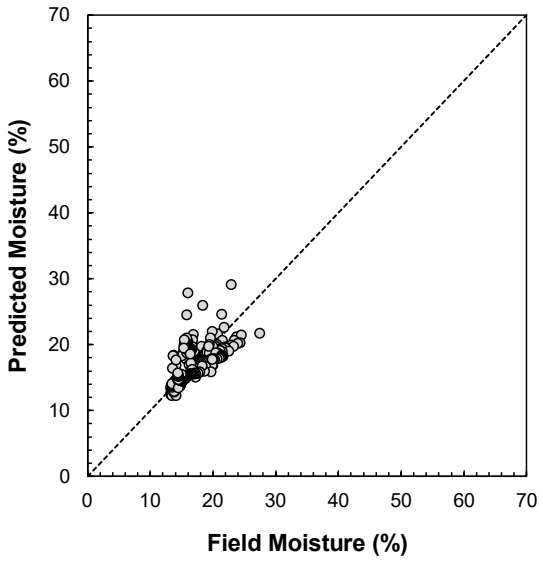

Figure 6–13 Accuracy of the Prediction Model in FM 342

FM 987

FM 987 is located in Post Pak Bend at Kauffman County, Texas. The site consists of high plastic clayey soil as other sites and was reported to exhibit longitudinal cracking along the shoulder of pavement (Ahmed, 2017). The site was instrumented with moisture sensors to evaluate the performance of pavement with and without moisture control mechanism. To facilitate the long-term monitoring of site, an array of sensors was installed at the side slope of control section which captured both the seasonal and temporary moisture variation due to climatic loading. The monitoring results from the one of the sensor at the side slope has been utilized here for model validation.

The subgrade soil moisture contents starting from Feb 9, 2020 were taken for the validation purpose. The rainfall and average air temperature for each day of the year were tabulated as well. The average moisture content of the location was calculated. The generic air

temperature model in Figure 6–7 was used to calculate the daily air temperature differences. Then, the soil temperature change for each day was calculated using the air temperature change. Finally, the moisture model was used to calculate the daily subgrade moisture variation. Figure 6–14 shows the comparison plot between field and model predicted moisture contents. The model could capture the rainfall effect and the temporary rise in moisture content. The model was also successful in capturing the overall trend of moisture variation. This can also be verified from the plot between field and predicted moisture against a 1:1 45^{o} line (Figure 6–15). Since a majority of the points are clustered around the line, it can be stated that the moisture model provided satisfactory predictions. A two-tailed t-test was also conducted to justify the model, the summary of which is presented in Table 6–6. The t-value is lower than the positive critical value. The p-value of the analysis was higher than the significance level. Based on the analysis, it can be concluded that the null hypothesis could not be rejected, indicating that there is no significant difference between the field and model predicted means of the subgrade moisture. This justifies the moisture prediction model.

Table 6–6 Summary of Hypothesis Testing on FM 987

	Mean	**St. Dev.**	**t-value**	**p-value**	**Critical t-value**
Field	24.295	5.417	1.42	0.157	± 1.96
Predicted	23.797	3.629			

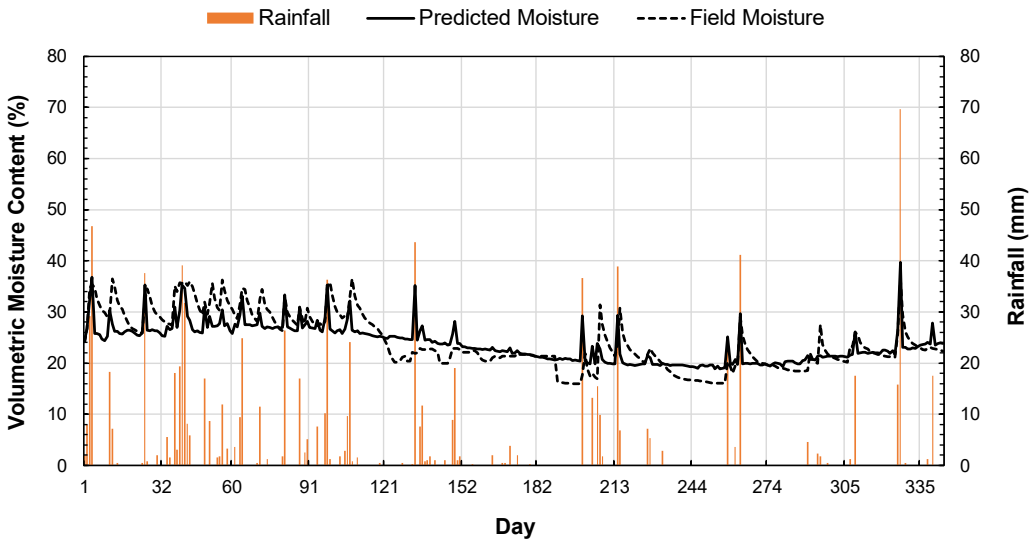

Figure 6–14 Comparison of Model Predicted and Field Subgrade Moisture in FM 987

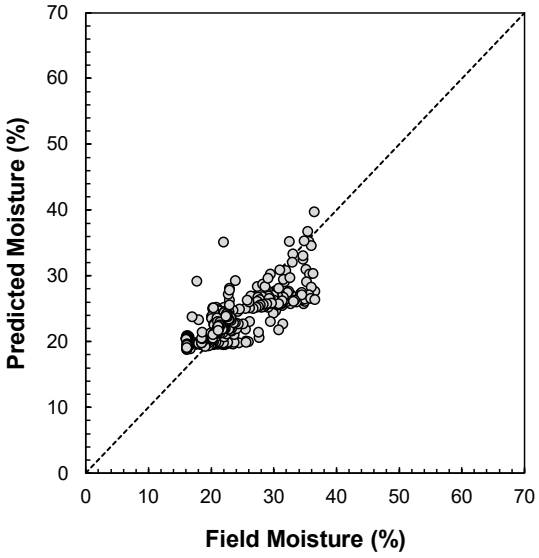

Figure 6–15 Accuracy of the Prediction Model in FM 987

Previous studies (Hedayati, 2014; Kodikara et al., 2014; Ahmed, 2017) have shown the accuracy of their model by plotting similar comparisons as in the current study. Figure 6–

16 shows some of the comparison plots. The similarity or improvement of predictability with those from the literature also justifies the applicability of the current moisture model.

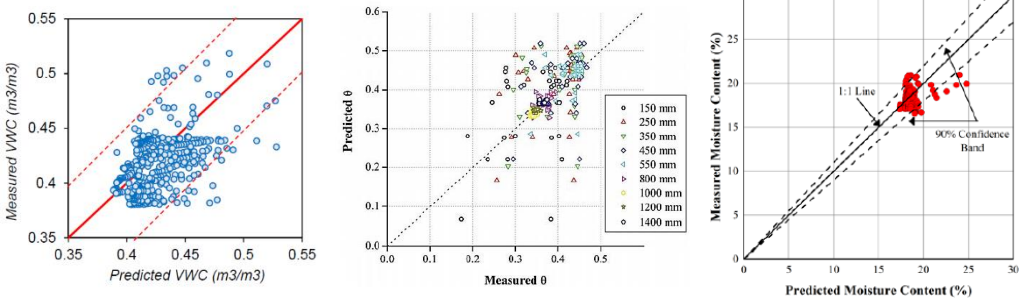

Hedayati (2014) Kodikara et al. (2014) Ahmed (2017)

Figure 6–16 Accuracy Plots of Prediction Models from the Literature

6.4 Deformation Model

The subgrade vertical deformation of the control section showed variations in response to different time of year and rainfall. The subgrade soil exhibited swelling during the wet period and shrinkage during the dry months. This was due to the amount of water intrusion into the soil. More amount of water intrusion during rainfall events brought about swelling of the high plasticity subgrade soil. Similarly, high temperatures and less rainfall made way for more evaporation of soil moisture. Eventually, when the loss of moisture was more than the influx, the subgrade soil shrank. This showed a high dependency of deformation on climatic loading as was seen for the moisture.

Various predictors can be used to develop a deformation model since the subgrade deformation is affected by rainfall, temperature, time of the year, and suction, among others. Moisture content of the soil is another important predicting factor; however, it is dependent on the amount of precipitation. Thus, including both precipitation and moisture

content in the model will create multicollinearity among the predictors which is regarded to degrade the predictability of a model (Kutner et al., 2005). Ahmed (2017) reported about the inefficiency of using suction for development of a model. Due to the low life and less reliability of suction sensors, it was decided not to include them in the model development. The expected trend was thus differentiated into three categories: an annual seasonal trend, effect of rainfall, and effect of temperature. Seasonal variations have been reported to be the primary cause of subgrade deformation (Hossain et al., 2016; Ahmed et al., 2017).

As mentioned in the literature review section and the demonstration in the moisture model development, a first-degree Fourier series (Sastry, 2012) can be used to explain the annual seasonal variation of subgrade deformation such as:

$$f\ (t) = \ a_o + \ \sum_{n=1}^{\infty} \left(a_n cos \frac{2n\pi x}{T} + \ b_n sin \frac{2n\pi x}{T} \right)$$

The series follows the form:

$$f\ (x) = \ a_o + \ a_1 * \cos(x * w) + b_1 * \sin(x * w)$$

where, a_o represents the average value of the dataset or the annual average deformation, a_1 and b_1 represent the amplitude of the dataset, and w is the frequency (day^{-1}). The variable x is the day of the year.

The vertical deformation of the subgrade soil was recorded on a monthly basis using a horizontal inclinometer. The deformation values at the right edge of the pavement were utilized for developing the model. One year of data starting from March 21, 2019 (Day 1) was used to capture the seasonal variation. The data was plotted against the Day in MATLAB. After numerous trial and error, a model was selected to fit the annual seasonal

trend. The model parameters are as shown below. The adjusted R^2 was estimated to be 77.41%. The dataset plot is shown in Figure 6–17.

$$\textit{Seasonal Deformation} = -17.6 + 12.55 * \cos(x * 0.01751) + 22.04 * \sin(x * 0.01751)$$

Where, *Seasonal Deformation is in mm*

a_o = Annual average deformation (mm) = -17.6 mm

Day 1 = March 21, 2019

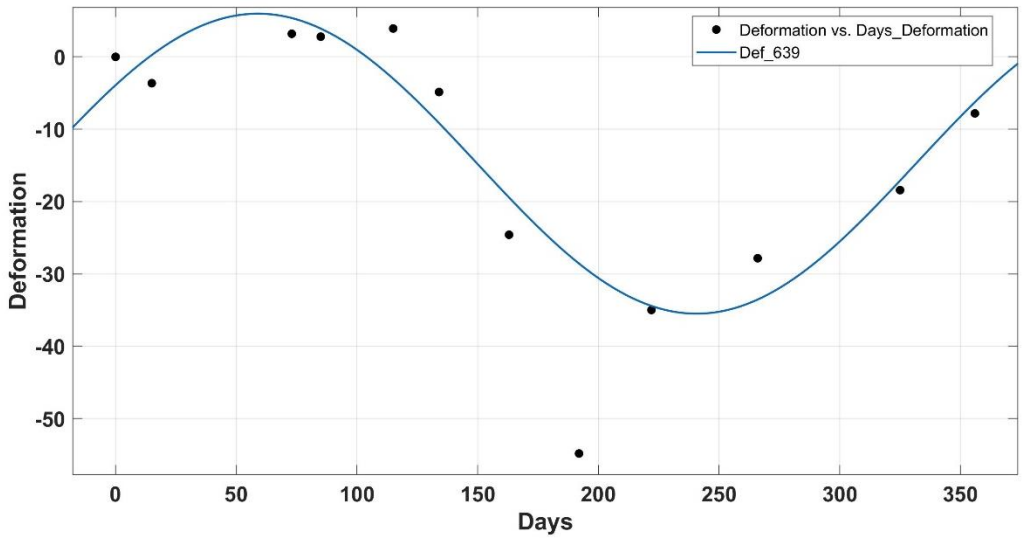

Figure 6–17 Seasonal Trend of Subgrade Deformation

The seasonal fit showed the average variation seen with time. The wet period showed swelling, while the dry period exhibited shrinkage. Figure 6–18 shows the comparison of field measure and model predicted deformation. It can be seen that the model could capture the seasonal variation of deformation fairly well. However, the peak values of swelling and shrinkage were not forecasted accurately. The model underpredicted the peak

shrinkage during the dry period of 2019. Similarly, it overpredicted the shrinkage during the dry period of 2020. It is to be noted that the rainfall was comparatively higher during 2020 compared to 2019. Due to this the subgrade did not shrink as much in 2020. Conversely, the model predicted similar shrinkage for both the years. This indicates that it is very important to add the effect of rainfall and temperature. Only a seasonal variation cannot explain all the variations seen at the field. Thus, separate studies were conducted to evaluate the individual effects of rainfall and temperature on the subgrade deformation.

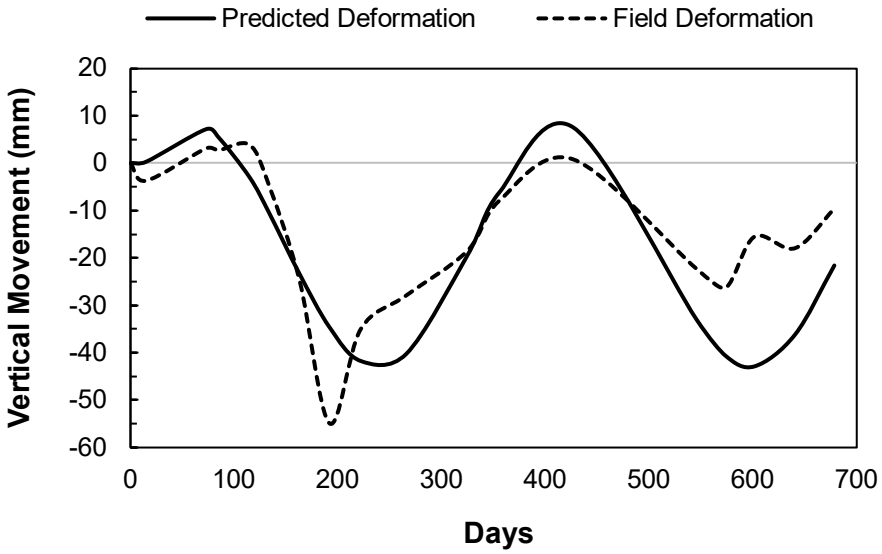

Figure 6–18 Comparison of Field Deformation and Predicted (Seasonal) Deformation

6.4.1 Effect of Rainfall on Subgrade Deformation

The next step was to capture the influence of rainfall in the subgrade deformation. Cumulative rainfall between each deformation readings were calculated. An interesting response was observed in the swelling of the subgrade. Swelling is a direct effect of moisture increase which is due to rainfall. However, due to the low permeability of pavement asphalt, base, and subgrade itself, it takes some time for the water to reach the

subgrade. Furthermore, the subgrade does not instantaneously swell after the moisture increases. There is a certain time period between the onset of rainfall and swelling of subgrade. This time can be regarded as the lag period as shown in Figure 6–19. So, based on the field behavior, it was decided that the effect of a rainfall will be reflected on the swelling after about 45 days. The point of interest here was the change in subgrade deformation due to the rainfall. So, at first, the difference between the field and model predicted deformation was calculated for each reading. Then, this difference was plotted against the cumulative rainfall between consecutive readings. However, the cumulative rainfall which accumulated 45 days before the day of interest was taken.

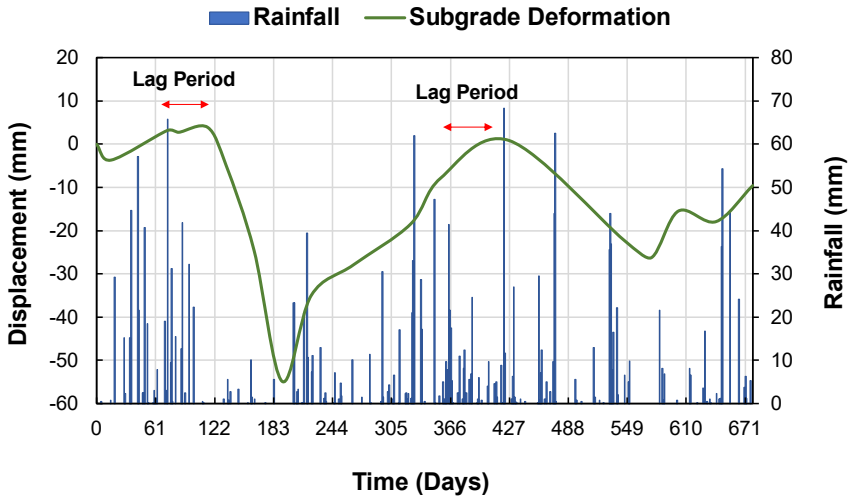

Figure 6–19 Lag Period Between Rainfall and Swelling

Several regression methods were tried (linear, logarithmic, polynomial), however, keeping in mind the ease of use, a linear regression was selected to best explain the model variability. The regression coefficient (R^2) was found to be 65.83% (Figure 6–20). The effect of rainfall can be formulated as follows:

$$\textit{Swelling (Due to Rainfall)} = 0.0537 * x_R + 1.6262$$

where, x_R denotes cumulative rainfall in mm.

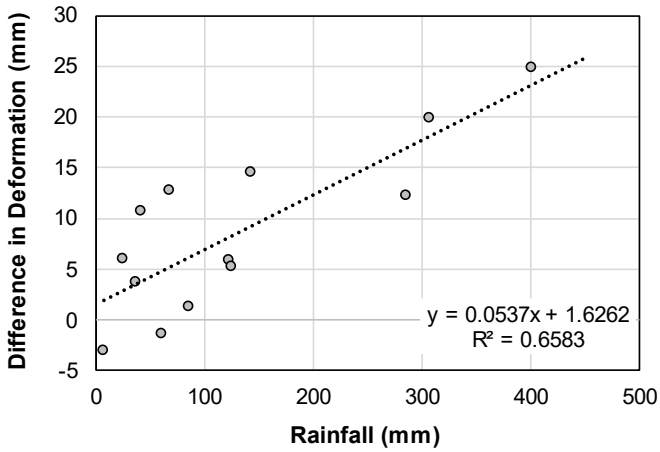

Figure 6–20 Linear Relationship Between Change in Deformation and Rainfall

6.4.2 Effect of Temperature on Subgrade Deformation

As high rainfall events resulting in swelling of the subgrade soil, an increase in soil temperature above the average can cause the subgrade to shrink. The average daily temperatures between two consecutive readings were again averaged to simulate the temperature effect. This average temperature was then plotted against the difference between field and model predicted deformation values. This was a similar approach as that was taken for the rainfall effect; however, no lag period was assumed here. Since the effect of air temperature does not take as much time as the rainfall effect, the lag period was not considered. After several iterations with different regression methods, the linear fit was chosen for its simplicity. Figure 6–21 shows the linear regression fit on the data. The air temperature changes could explain 76.81% of the variability in the vertical movement. The effect of air temperature can be formulated as follows:

$$\textit{Shrinkage (Due to Temperature)} = 1.6192 * x_t - 30.935$$

where, x_t denotes air temperature in ^oC.

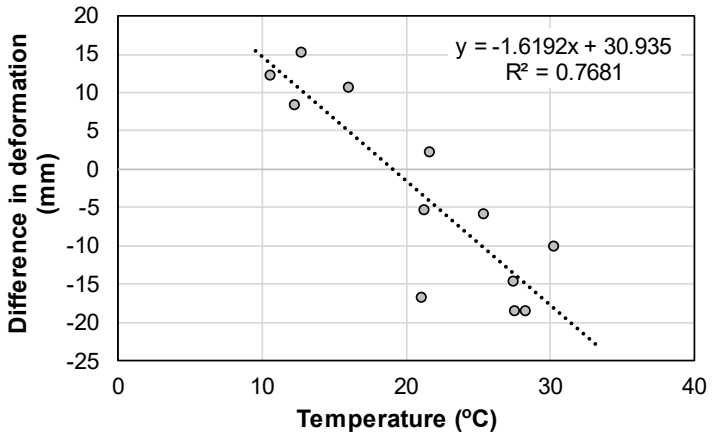

Figure 6–21 Linear Relationship Between Change in Deformation and Temperature

6.4.3 Final Deformation Model

Following the quantification of rainfall and temperature effect on subgrade deformation, the final model was formulated as follows:

Subgrade Deformation = Seasonal Deformation + Swelling (Due to Rainfall) - Shrinkage (Due to Temperature)

Subgrade Deformation = [-17.6 + 12.55 * cos (x * 0.01751) + 22.04 * sin (x * 0.01751)] + [0.0537 * x_R + 1.6262] – [1.6192 * x_t – 30.935]

where,

x = Day number (March 21, 2019 regarded as Day 1)

x_R = Rainfall in mm

x_t = Air Temperature in ^oC.

The model generated subgrade deformations were plotted against the field measured data to evaluate the predictability of the model, which is shown in Figure 6–22. The model shows satisfactory fit with the field values. It was successful in capturing the seasonal trend as well as matching the peak values. The peak values of shrinkage and swelling matched comparatively better than the model with just the seasonal deformation factor. There was some variation during March to June 2020 (Day 350-450) where the prediction model exhibited higher swelling than the actual value. In actual field condition, the overburden pressure from the pavement layers and traffic surcharge may tend to restrict some amount of swelling. The prediction model did not incorporate this factor, which might be a probable reason for the higher swelling shown during Day 350-450. Apart from that, all other variations seemed to be reflected well by the prediction model. An interesting point to state here is that the model was effective in replicating the lag period seen at field.

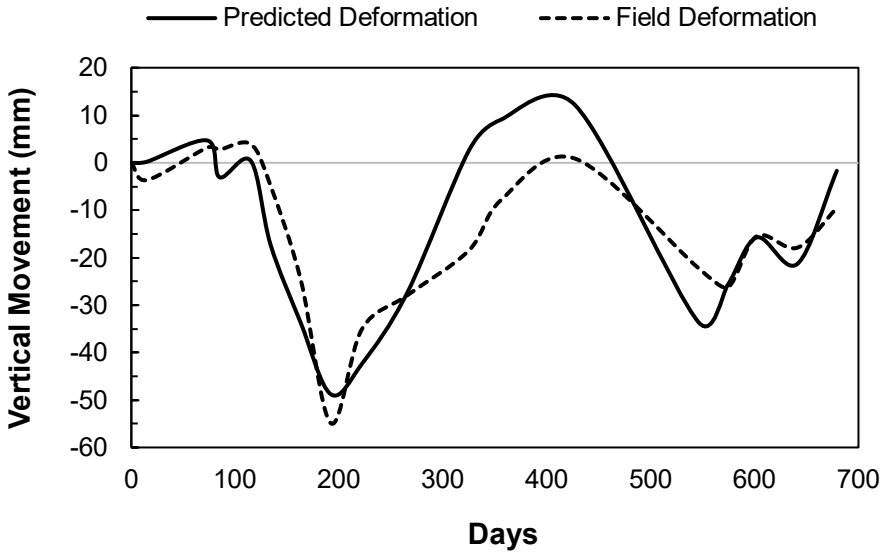

Figure 6–22 Comparison of Field Deformation and Final Predicted Deformation

The input parameters for the model are day number, rainfall, and air temperature. All these parameters are easily available which makes the model readily applicable.

6.4.4 Validation of the Deformation Model

The final deformation model was validated using the deformation values of the same pavement at the left edge and the center. Figure 6–23 and Figure 6–24 show the comparisons at the left edge and center of pavement, respectively.

It can be stated that the model could fairly predict the deformation values throughout the pavement. Hypothesis testing was conducted for each validation to justify the predictability of the model. Two-sample t-test assuming unequal variances was conducted to determine if there were significant differences between the field and model predicted subgrade deformations. The mean of the field and model predicted deformation values were compared against each other. The test was conducted at 95% confidence interval. Thus, the significance level (α) was 0.05. Table 6–7 summarizes the results of the hypothesis testing. The t-value satisfies the critical value criteria for all the cases. The p-value of the analysis was higher than the significance level. Based on the analysis, it can be concluded that the null hypothesis could not be rejected, indicating that there is no significant difference between the field and model predicted means of the subgrade deformation. This justifies the deformation prediction model.

Table 6–7 Summary of Hypothesis Testing of Deformation Model

Location		Mean	St. Dev.	t-value	p-value	Critical t-value
Left Edge	Field	-5.699	14.179	1.39	0.172	± 2.04
	Predicted	-13.395	18.610			
Center	Field	-16.424	15.790	-0.53	0.602	± 2.03
	Predicted	-13.395	18.610			
Right Edge	Field	-14.309	15.771	-0.16	0.874	± 2.03
	Predicted	-13.395	18.610			

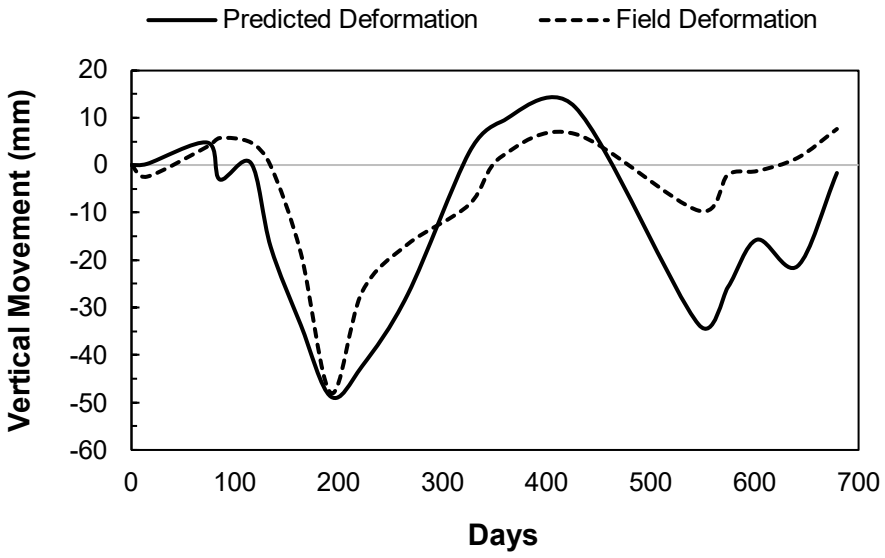

Figure 6–23 Comparison of Field Deformation and Predicted Deformation (Left Edge)

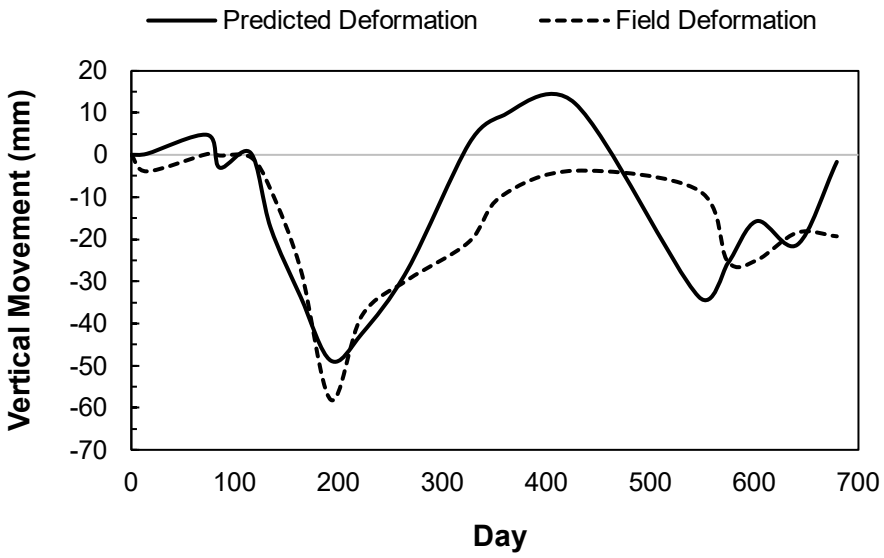

Figure 6–24 Comparison of Field Deformation and Predicted Deformation (Center)

6.5 Limitations of the Prediction Model

Both the subgrade moisture and deformation prediction models provided very satisfactory fit with the field data. The validations also satisfied the statistical assumptions. Moreover, the moisture model was validated with field results from different locations and year. However, there are certain limitations on the use of the model which are outlined below:

- The first term in the seasonal part of both the models requires the input of average values. For instance, the user needs to manually input the average subgrade moisture content observed throughout the year at a particular location.
- The soil was assumed to be homogeneous; however, this is not the actual case in field.

- The deformation model predicted the same deformation throughout the width of the pavement. In reality, and as seen from the field data, there are slight variations in deformation throughout the width of the pavement.

- The prediction models did not consider the depth effect. Both the moisture and deformation can differ with depth which could not be explained through the developed models. However, the models were developed for the depth with the maximum variations. Thus, they can be effectively used to evaluate the moisture and deformation variation in pavement subgrade.

Chapter 7

NUMERICAL MODELING

7.1 Introduction

The objective of the current study is to evaluate the effectiveness of modified moisture barrier (MMB) in controlling the potential rainwater seepage into expansive subgrade soil and laterally drain the infiltrated water away from the pavement system for its overall stability. As a part of the study, a distressed pavement section in Frost, Navarro County was stabilized by incorporating MMB at the interface of base and subgrade soil. The barrier system served several functions such as separation, prevention of rainwater seepage, and drainage of infiltrated water. Based on the performance monitoring of the barrier and control sections, it was evident that MMB prevented the excessive movement of highly expansive subgrade soil underneath the barrier by isolating the subgrade soil from the impact of seasonal climatic variation. The impact of climatic loading in the hydro-mechanical behavior of expansive subgrade soil with and without moisture barrier was further studied numerically and is presented in this chapter.

In recent years, computer models have been extensively used in engineering practice due to their ability to simulate the real field conditions and solve complex soil -structure interaction through rigorous calculation. The current study utilizes GeoStudio software to numerically study the unsaturated moisture flow due to climatic loading and the subsequent volume change in expansive subgrade soil with and without moisture barrier. In addition, flow through geo composite was evaluated for different transmissivities and rainfall intensities. Figure 7–1 shows the analysis performed and discussed in this chapter.

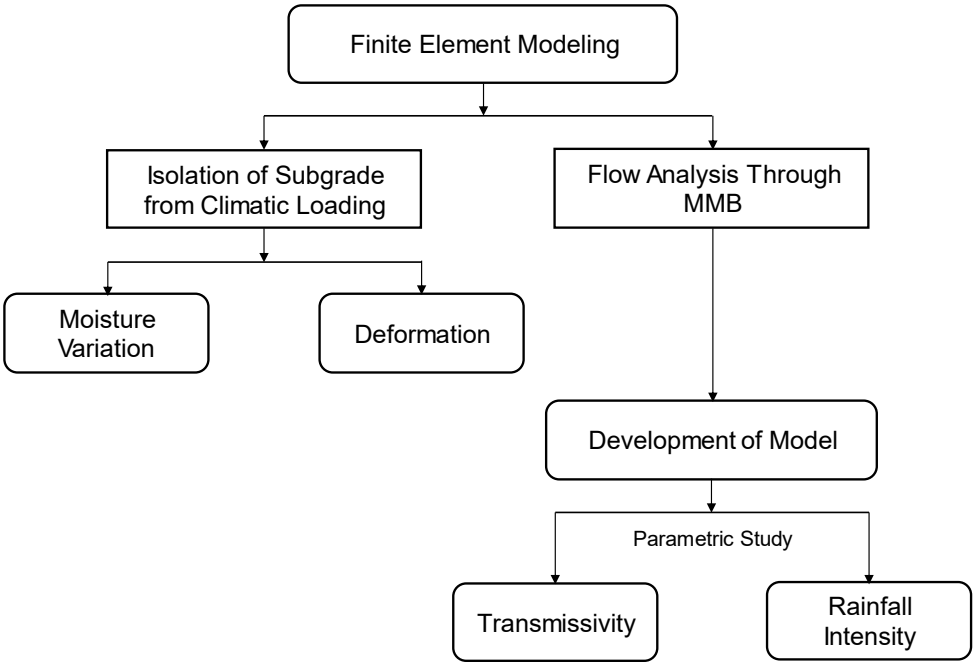

Figure 7–1 Tasks Performed under Numerical Study

7.2 Finite Element Based Numerical Model

GeoStudio software provides a single platform for solving complex coupled and uncoupled physical processes in geotechnical and geosciences using combination of different packages (GeoStudio, 2020). The software can be efficiently used to model slope stability, ground deformation, heat and mass transfer in soil and rock etc. The model provides numerical solution by discretizing the model domain into numerous elements and solving governing equations for each element nodes. Mesh configuration and time steps play a major role for converged solution, especially in transient analyses where soil response is governed by rainwater infiltration. Since the main objective of this study is to evaluate the hydro mechanical behavior of subgrade soil and flow through MMB in response to climatic loading, several trials were done for each cases with different mesh configurations and time step to establish a suitable numerical scheme and converged solution.

The hydro-mechanical behavior of expansive soil was evaluated using coupled stress-strain and moisture flow modeling under SIGMA/W. Wong et al. (1998) verifies the capability of SIGMA/W in performing coupled saturated and unsaturated hydro-mechanical analysis of soil. A flow through drainage layer of MMB i.e., geo composite, on the other hand was studied using transient seepage analysis under SEEP/W. For the study, model geometry was drawn based on field measurements with the material definition as per laboratory investigation of subgrade soil and other relevant literatures. The section below discusses in detail the modelling procedure and analysis performed under both the studies.

7.3 Hydro-Mechanical Behavior of Expansive Subgrade Soil

This section of the numerical study primarily focuses on the behavior of expansive subgrade soil in response to rainfall and evaporation. Although laboratory and field determined parameters were used to define materials, few adjustments on the parameter were required to bring the homogeneous soil model close to field condition where number of external factors alters the soil response. The calibrated model was further used to evaluate soil response at different dry and wet initial condition. It should be noted that steady state and in-situ analyses type was performed prior to coupled analysis to establish initial hydraulic and stress conditions. The governing equations for numerical calculation, model geometry, boundary conditions, soil input parameters, initial conditions, and FEM simulation approach are discussed in detail in the subsequent sections.

7.3.1 Coupled Stress-Strain and Moisture Flow

The soil response in terms of seepage and deformation was evaluated using coupled stress-strain and moisture flow modeling where both stress-deformation and seepage dissipation equations are solved simultaneously. Two equilibrium equations and one continuity equation are developed under this analysis for displacement and moisture flow.

As the equations are solved simultaneously by the software, pore pressure changes and displacements are obtained. This analysis type is capable of providing time dependent change in pore-water pressure and effective stresses.

The finite element equilibrium equations are formulated using the principle of virtual work, which states that for a system in equilibrium, the total internal virtual work is equal to the external virtual work. The virtual work equation can be written as follows (Geo-slope International Ltd, 2013)

$$\sum [B]^T\,[D]\,[B]\,\{\Delta\delta\} + \sum [B]^T\,[D]\,\{m_h\}\,\langle N\rangle\,\{\Delta u_w\} = \sum F$$

$$[K] = [B]^T[D][B]$$

$$[L_d] = [B]^T[D]\{m_h\}\,N$$

$$\{m_H\}^T = \langle \frac{1}{H}\ \frac{1}{H}\ \frac{1}{H}\ 0\rangle$$

Where [B] = gradient matrix, (also called the strain matrix); [D] = drained constitutive matrix; [K] = stiffness matrix; $[L_d]$ = coupling matrix; {Δδ} = incremental displacement vector; and $\{\Delta u_w\}$ = incremental pore-water pressure vector.

Input parameters such as initial stress and pore-water conditions, time duration and number of time steps, hydraulic and stress-strain boundary conditions and material properties are needed to be defined for the analysis (GeoStudio, 2020).

7.3.2 Model Geometry and Boundary Conditions

Figure 7–2 shows the pavement modeled in two-dimensional space. Due to symmetrical road geometry, half of the pavement cross-section including a lane, shoulder, a side slope along with some portion of toe was modeled. The geometry of the model was drawn as per

field measurements. Since shallow soil layers are significantly affected by climatic loading, the topsoil layer was provided with finer mesh for more converged solution.

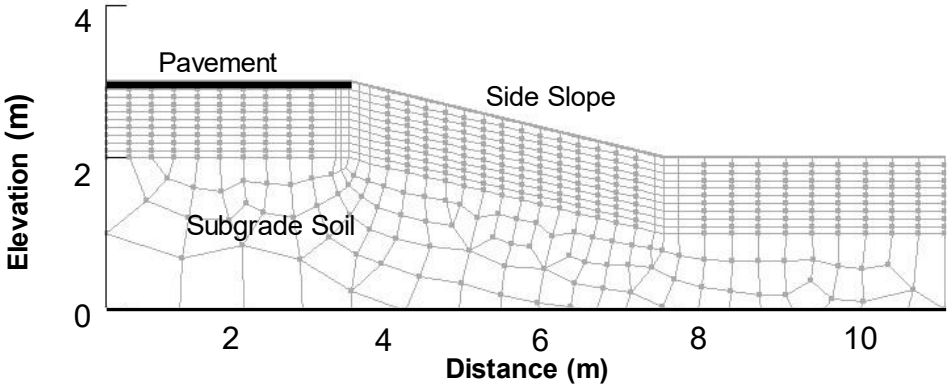

Figure 7–2 Geometry for Finite Element Analysis

The response of the soil model largely depends on the defined boundary condition. For the current analysis, the model needed to be defined for both flow and displacement. As such, model was fixed at the bottom to restrict the movement in all directions. The lateral boundaries were allowed to move vertically and restrained in horizontal direction. The top boundary was not fixed in any direction in order to capture the free movement of subgrade soil with the applied boundary flux.

As for the seepage analysis, hydraulic boundary conditions can be defined in terms of head (pressure head or total head) or flow. The initial pore pressure distribution in the model domain can be defined by assigning a pressure head at boundary or by defining water table. These assignments allow the pore pressure to vary linearly along the model height. It should be noted that the water table in the actual field scenario was well below to cause any strain in the expansive soil at shallow depth. The initial pore pressure distribution in the model may vary based on the initial dry or wet conditions in the field prior to application

of boundary flux. Therefore, care must be taken while assigning initial pressure head boundary conditions. The model computes the moisture content corresponding to the pore pressure distribution from defined SWCC in material definition.

7.3.3 Material Properties

The hydraulic and stress-strain material properties were assigned for the subgrade soil under material definition. A single layer of subgrade soil was considered which was modeled as an isotropic elastic material with the assumption that repeated cycles of swelling and shrinkage generally results in over consolidation of soil increasing the elastic portion of stress strain curve (Hedayati, 2014). In addition to that, void ratio, poison's ratio, and soil modulus as a function of effective stresses were defined in order to capture the deformation of soil. Table 7–1 summarizes the stress-strain material properties assigned in the model.

Under hydraulic properties, unsaturated flow parameters were defined in terms of Soil Water Characteristics Curve (SWCC) and hydraulic conductivity functions. The hydraulic properties were initialized as per the field determined SWCC which was adjusted for model calibration. Table 7–2 summarizes the hydraulic properties of soil which was obtained after several trials during model calibration. The air entry value and permeability were primarily considered as calibration parameter.

Table 7–1 Stress-Strain Material Properties Used in the Model

Parameters	Values
Void Ratio	0.8

Unit weight (KN/m^3)	17
Poisson's Ratio	0.334

Table 7–2 Hydraulic Material Properties Used in the Model

Soil type	Field SWCC of soil					Saturated permeability
	α	m	n	θ_s	θ_r	K_s (m/s)
High plastic clay	44 kPa	0.30	1.43	0.5	0.05	3.53 X 10^{-7}

7.3.4 Climatic Boundary Flux

Climatic boundary flux in terms of rainfall and evapotranspiration was applied in the model to numerically evaluate the hydromechanical response of the soil with and without moisture control mechanism. The real time rainfall data was collected from the nearest weather station while evapotranspiration was determined from theoretically estimated potential evapotranspiration and available soil moisture in the field. The potential evapotranspiration for the site was determined using Thornthwaite method which is the simplest approach that uses monthly average temperature to estimate the parameter (McKenney and Rosenberg, 1993). The method uses the following equation to calculate maximum possible evaporation i.e., potential evapotranspiration when the soil is at its full saturation level,

$$PET = 16\,X\left(\frac{10\,T_i}{I}\right)^a X\left(\frac{N}{12}\right) X\left(\frac{L}{30}\right)$$

where, PET is the potential evapotranspiration (mm/months), L is the monthly mean daytime duration (hours), N is the number of days in a month, Ti is the mean monthly temperature, and I is the heat index expressed as

$$I = \sum_{i=1}^{12} \left(\frac{T_i}{5}\right)^{1.514}$$

$$\alpha = (492390 + 17920I - 771I^2 + 0.675I^3)\, X\, 10^{-6}$$

Site specific conditions were utilized to estimate potential evapotranspiration. Figure 7–3 (a) shows the estimated PET for the site at different time of year. However, it may be noted that soil is rarely at its full capacity at all times and the real time rate of evaporation may vary spatially and temporally based on available soil moisture. As such, actual evapotranspiration from the soil may vary largely than the potential evapotranspiration which can be computed by modifying the potential evapotranspiration based on soil properties including available soil moisture content, field capacity, and wilting point. The equation that can be used to determine actual evapotranspiration is shown below:

$$AET = \frac{\theta - \theta_{WP}}{\theta_{FC} - \theta_{WP}}\, X\, PET$$

where θ = Soil moisture content from sensors

θ_{WP} = Moisture content at wilting point of soil corresponding to 1500 kPa

θ_{FC} = Moisture content at field capacity of soil corresponding to 10- 33 kPa

Figure 7–3 (b) shows the curve of AET/PET ratio as a function of field suction which was provided as a modifier function in the numerical model for modifying potential evapotranspiration. As the figure suggests, AET becomes equal to PET when suction is zero which is when the soil is at its full saturation, however with the increase in suction actual evapotranspiration becomes less than potential evapotranspiration.

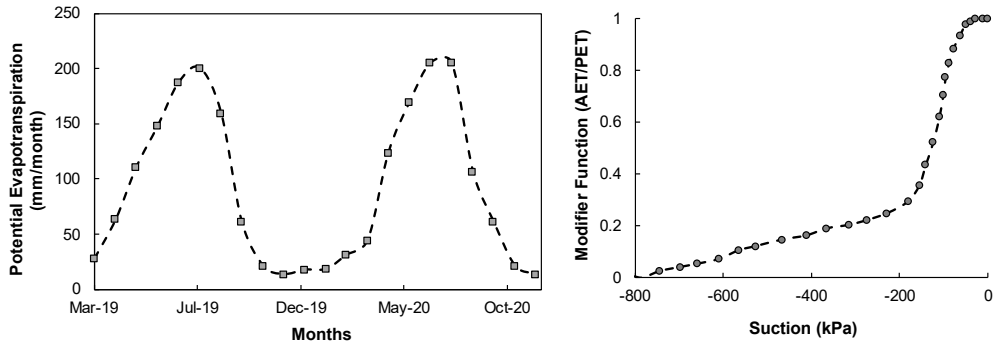

Figure 7–3 (a) Estimated PET from Thornthwaite Method (b) AET/PET as a function of Suction.

7.3.5 Model Calibration

Model calibration is an important aspect of numerical modeling as the developed model should be able to simulate the real field response with acceptable agreement. The model was calibrated using field results from control section in order to simulate the soil behavior in its natural condition. In the current study, one month of rainfall and evapotranspiration data from May 2020 was used for seepage calibration. The impact of climatic loading was observed to be significant during this time period with 17% increase in VMC and therefore was used for model calibration. Prior to the application of boundary flux in terms of rainfall and evapotranspiration, initial conditions were set up by defining pore pressure distribution corresponding to the field recorded moisture values. Figure 7–4 illustrates the pore pressure distribution contour before applying boundary flux. After the establishment of initial condition, rainfall and potential evapotranspiration along with modifier function to account for actual evapotranspiration was applied.

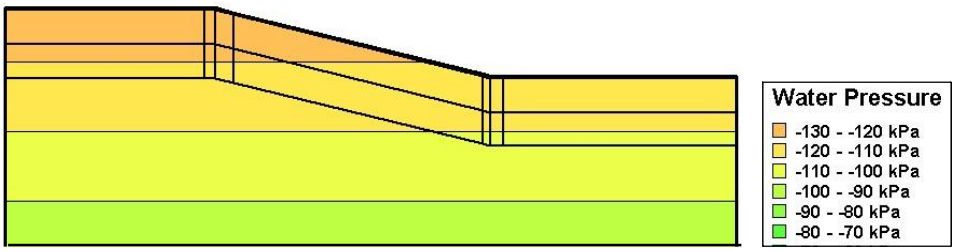

Figure 7–4 Initial Pore Pressure Distribution Contour

Figure 7–5 shows the selected boundary flux from the overall data that was utilized to calibrate the seepage model. Several trials with saturated permeability and SWCC was performed to calibrate the model to actual field conditions. The in-situ permeability of soil may vary largely due to various external factors one of which is the formation of cracks. Aubeny and Lytton (2003) states 10 times increase in in-situ permeability as a result of cracks. Another research by Zhang (2003) states that cracks may allow the infiltration rate to increase by three order of magnitude. Therefore, permeability and unsaturated flow parameters were varied until the results from the model became close to field measurements. When the results obtained were within acceptable accuracy, the model was considered calibrated. Figure 7–6 show the measured and modeled volumetric water content due to one month of real time climatic flux.

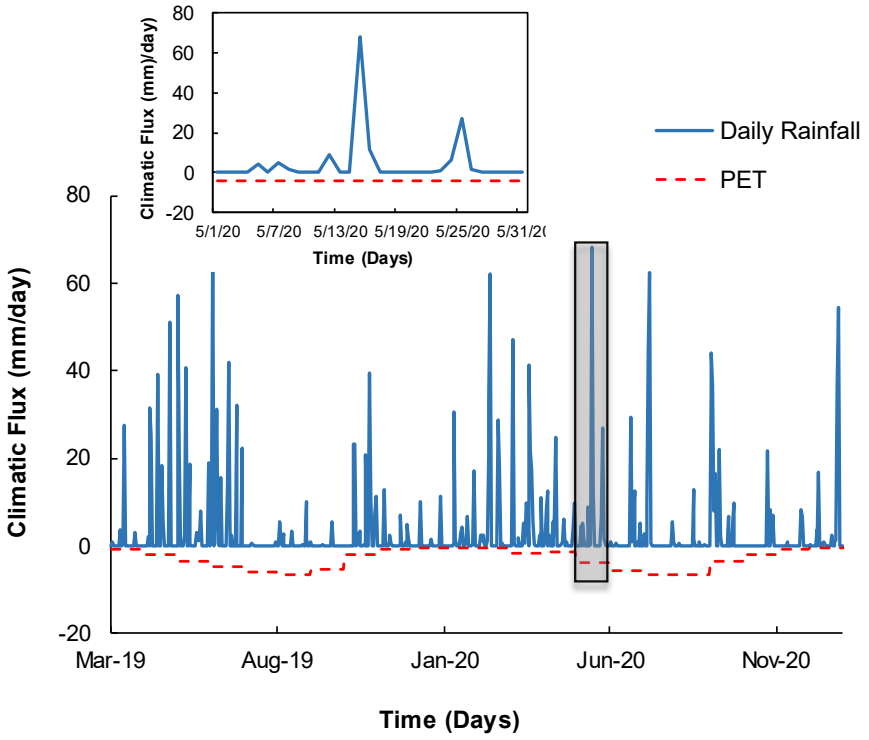

Figure 7–5 Boundary flux for Seepage Calibration

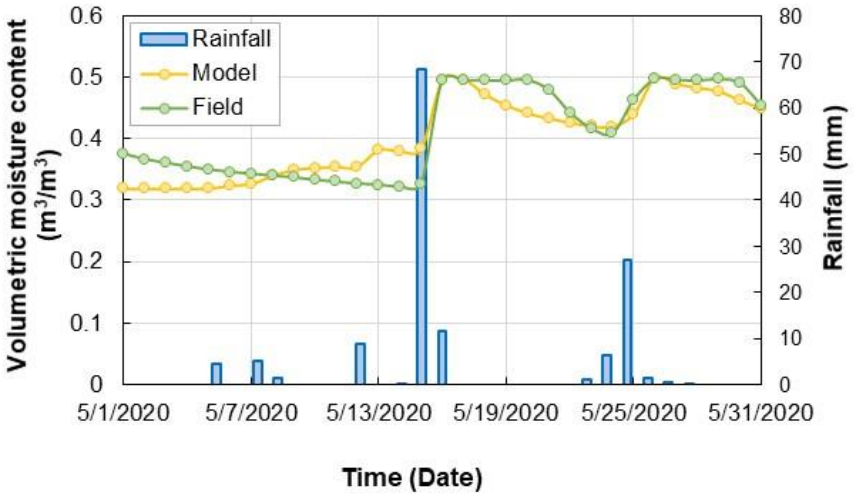

Figure 7–6 Measured and Modeled Volumetric Moisture Content

The model was also calibrated for deformation. As the inclinometer readings were taken in a monthly basis, one year of deformation results were considered for the calibration (Figure 7–8). The initial condition was set prior to the application of climatic flux as the response of transient analysis depends on the initial wet or dry condition of the soil. Here, the initial condition represented the wet period with minimum suction value since the base reading was taken when the soil was at its maximum saturated water content as presented in Chapter 5. Once the initial pore pressure distribution was initialized in steady state analysis, in-situ analysis was run with gravity activation to establish initial stress state. Figure 7–7 illustrates the initial stress contour in the model domain which was subjected to one year of climatic flux. Several trails were done with soil modulus function. Finally, the model was considered calibrated when the range of deformation was close to field observed inclinometer readings (Figure 7–9)

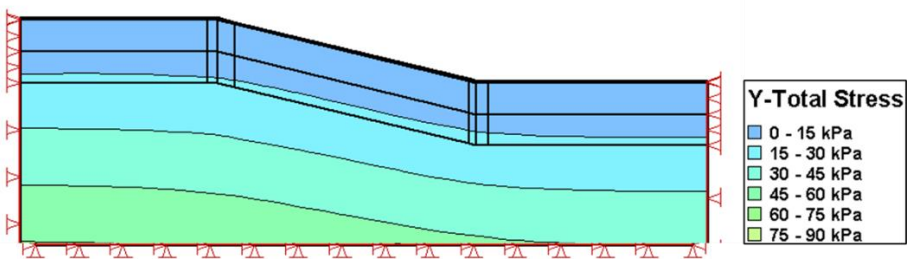

Figure 7–7 Initial Stress Contour

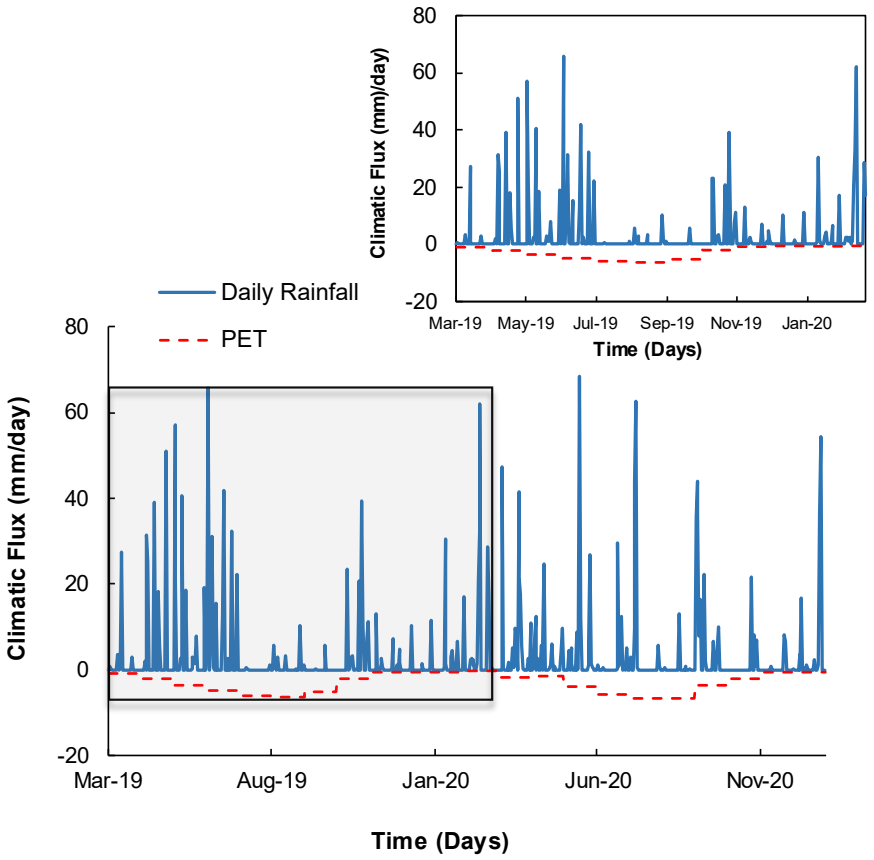

Figure 7–8 Boundary flux for Deformation Calibration

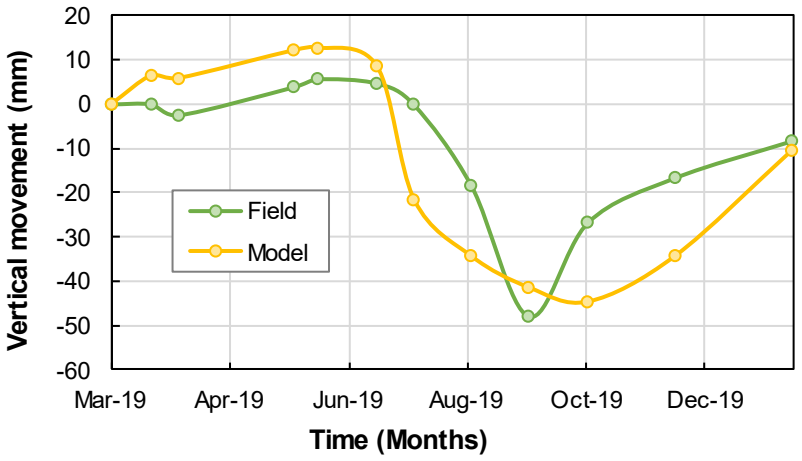

Figure 7–9 Measured and Modeled Deformation of Subgrade Soil

7.3.6 Effect of Modified Moisture Barrier in Generated FE Model

Once the model was calibrated, an impermeable moisture barrier system was introduced to compare and evaluate soil behavior in presence of moisture control mechanism. A default impermeable layer was assigned over the subgrade soil and the infiltrated water was allowed to flow down the slope. Detail analysis on the flow characteristics of modified moisture barrier have been conducted and presented in another section of this chapter. Figure 7–10 and Figure 7–11 show the moisture variation and deformation of the subgrade soil, respectively from the field and model in presence of moisture barrier system from May 2019 till December 2019 covering both dry and wet periods.

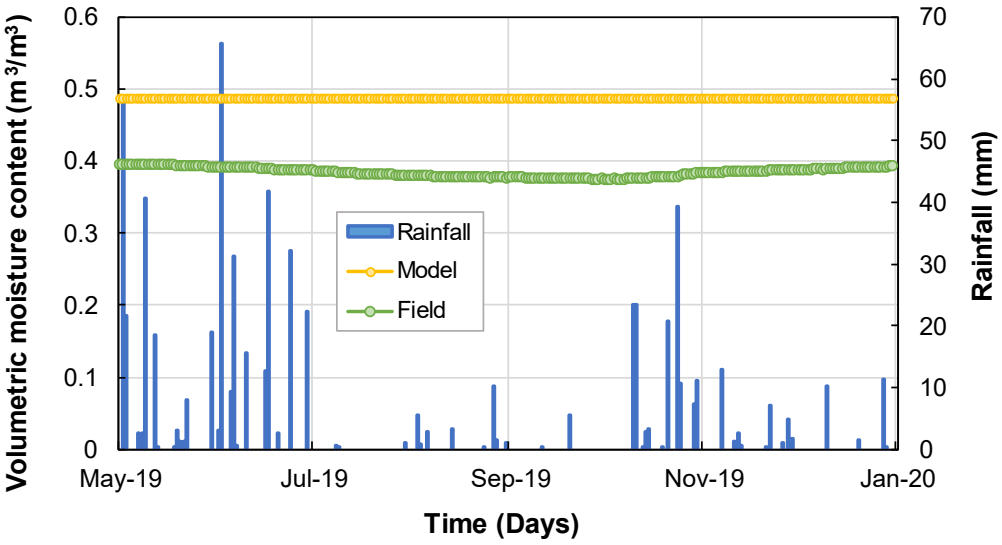

Figure 7–10 Measured and Modeled Volumetric Moisture Content in Presence of Impermeable MMB

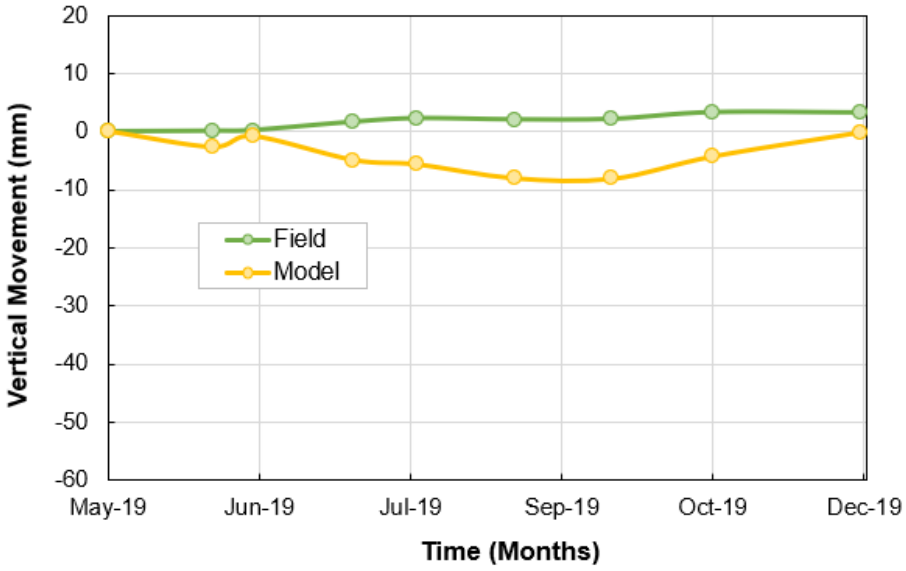

Figure 7–11 Measured and Modeled Deformation of Subgrade Soil in Presence of Impermeable MMB

7.3.7 Moisture Infiltration and PWP Variations

Figure 7–12 compares the numerical modeling result of rainwater infiltration in the presence and absence of impermeable barrier system. In absence of moisture control mechanism, the rainwater was found to largely infiltrate into the subgrade soil. The system allowed maximum infiltration of 25 mm/day without moisture barrier in response to applied boundary flux. The infiltration may be even higher in the real field with the presence of surface cracks (Novak et al., 2000). On the contrary, constant infiltration profile was obtained for the barrier section which was zero.

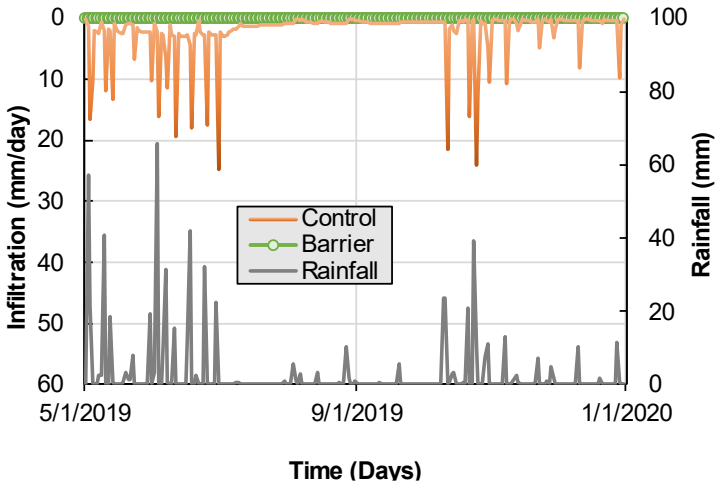

Figure 7–12 Rainwater Infiltration without and with Barrier from the Model

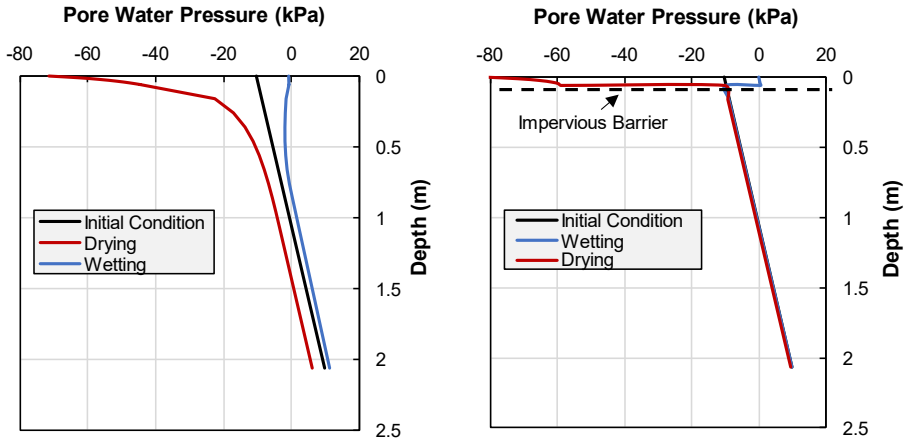

Figure 7–13 Pore Pressure Changes (a) without and (b) with Moisture Barrier During Wetting and Drying

Figure 7–13 presents distribution of pore water pressure along the depth. The pore water pressure in shallow depth was found to be sensitive towards the climatic loading with the value ranging in between 0 to - 70 kPa (Figure 7–13 a) at the surface in case of no moisture

barrier. On the other hand, constant pore pressure profile along the depth was observed in the section with barrier due to no moisture infiltration. The model was also able to capture the excessive pore pressure change in the region above the barrier where the soil was in continuous contact to the climatic loading.

Deformation in expansive soil mainly occurs as a result of change in pore pressure. Since the pore pressure variation was observed to be more in case of soil model with no barrier, excessive deformation can be expected as was observed from the field instrumentations. However, the magnitude of swelling may vary depending on the initial soil moisture conditions. Nayak and Christensen (1970) reports that the swelling potential of expansive clay reduces with increase in initial soil water content. Therefore, parametric evaluation with the range of suction (negative pore pressure) from -10 kPa to -200 kPa was performed to evaluate the swell potential of soil at different initial conditions.

7.3.8 Soil Deformation at Different Initial Drying and Wetting Conditions

The calibrated model was used to study the potential swelling in the subgrade soil in response to moisture change. The soil in its natural state is usually unsaturated (i.e., pore water pressure is negative) within the active zone where the effect of climatic loading is maximum. The FE model was initialized at different suction (negative pore pressure) condition to simulate the dry and wet period observed in the field. As seen in Figure 7–14, maximum swelling was observed in the model initialized at driest suction i.e., initial suction of -200 kPa. The swelling in the subgrade was observed as high as 83 mm when the soil suction changed from initial suction value of -200 kPa to zero suction. Likewise, minimum swelling was observed in the subgrade when initialized at wet condition with initial suction of -10 kPa. Swelling of about 20 mm was observed at this condition.

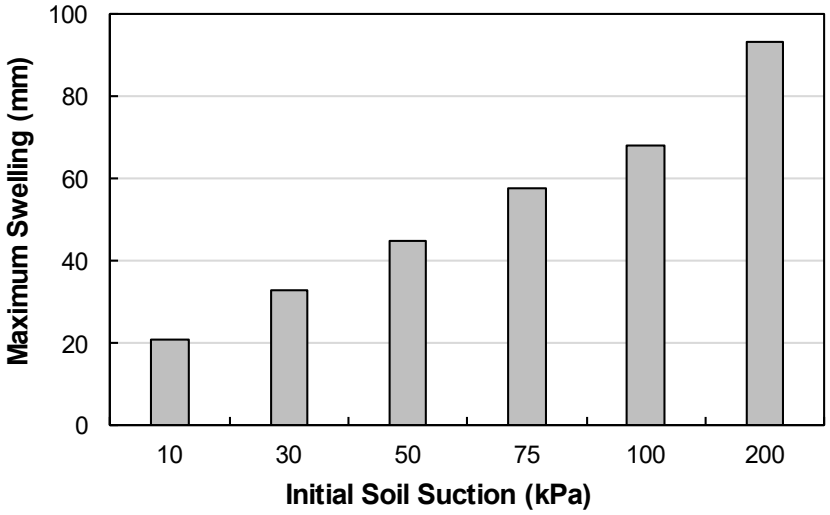

Figure 7–14 Swell Potential at Different Initial Suction

The use of moisture barrier can greatly reduce such swelling of expansive soil by preventing the moisture infiltration and exfiltration that may otherwise result in significant change in soil suction (i.e., negative pore pressure).

7.4 Flow Analysis Along Modified Moisture Barrier

Several research can be found in the literature with the focus on pavement damage due to water infiltration (Birgisson et al., 2003; Wang, 2011; Dan et al., 2017). Also, the importance of adequate drainage for the stability of pavement structure has been highlighted by many studies. Conventionally, free draining aggregates were used for this purpose, however the materials lose their strength over time due to migration of fines. Beside isolation and separation, modified moisture barrier utilized in the current study has great potential in enhancing the drainage of pavement system by laterally draining infiltrated rainwater along geo composite layer. The drainage in geo composite layer occurs due to its highly transmissive nature allowing flow along the material. This can greatly minimize the effect of sustained over-saturation of pavement layers after heavy rainfall which may otherwise

result in significant damage to the pavement structures. Figure 7–15 show the schematic diagram showing water drainage from MMB in pavement system.

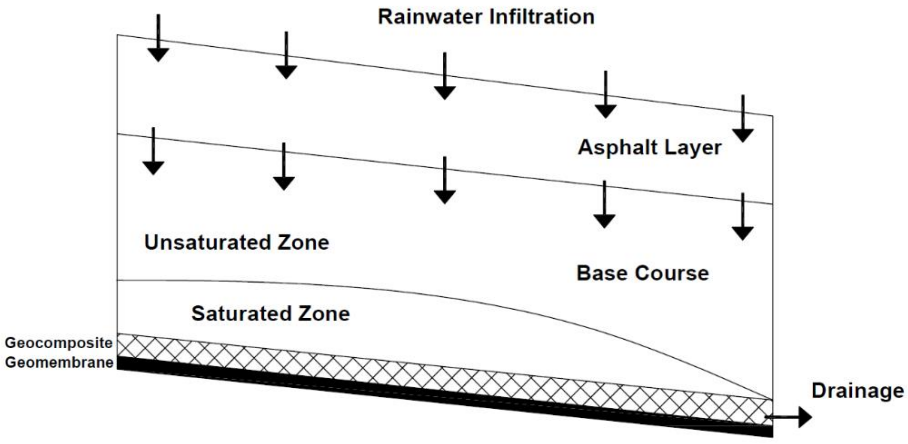

Figure 7–15 Schematic Diagram Showing Water Drainage from MMB in Pavement System (Modified after Dan et al., 2017)

In this part of numerical study, flow characteristics of geosynthetic drainage layer i.e., geo composite was evaluated through seepage analysis. The study was performed by utilizing the calibrated model from previous section. The model geometry was modified with the section only below pavement, however unsaturated flow parameters of subgrade soil remained the same. The width of model was kept as 4 m representing the dimension of pavement lane in one direction. In addition, the asphalt thickness of 0.767 m was used as determined from pavement coring and ground penetrating radar. The thickness of base was taken as 0.305 m for the purpose of modelling. In order to allow flow across the pavement section, the cross slope of the pavement section was set to a typical value of 2.5%.

Asphalt pavements exhibit cracks owing to temperature change, traffic load, wearing and ageing of asphalt surface etc., allowing rainwater to seep into the underlying layers. The current study focuses primarily on the effectiveness of geo composite drainage layer with certain transmissivity in routing this excess infiltrated rainwater away from the pavement cross-section. The study does not intend to capture the individual performance of components of geo composite rather focusses on performance of drainage layer as a whole. Five rainfall intensities were considered for the study and parametric study was performed with varying transmissivity of drainage layer.

7.4.1 Finite Element Modelling

The numerical study of flow through geocomposite with impermeable barrier underneath was conducted using SEEP/W program which is capable of modeling both the steady state and transient flow analyses in saturated and unsaturated condition. Flow in unsaturated porous medium follows Darcy's law. The flow is proportional to the hydraulic gradient and the hydraulic conductivity. For a two-dimensional homogenous anisotropic medium, the governing flow equation can be written as:

$$\frac{\partial y}{\partial x}\left(k_x \frac{\partial y}{\partial x}\right) + \frac{\partial y}{\partial x}\left(k_y \frac{\partial y}{\partial x}\right) + Q = \frac{\partial \theta}{\partial t}$$

where,

k_x = Unsaturated hydraulic conductivity in x- direction

k_y= Unsaturated hydraulic conductivity in y- direction

Q= Applied Boundary Flux

θ= Volumetric Water Content

t = time

7.4.2 Material Definition and Mesh Generation

The model consisted of typical layers of flexible pavement system including asphalt on the top, base-course, and subgrade soil. The modified moisture barrier was modeled as a thin layer of thickness 6 mm at the base-subgrade interface representing geocomposite layer with an impermeable layer underneath. The asphalt layer, base course, and modified moisture barrier were modelled as surface layer in order to avoid possible convergence issue due to thin soil layers. The layer below modified moisture barrier consisted of a homogeneous soil layer of expansive subgrade soil. The asphalt layer was discretized into 2 horizontal layers, base into 5 horizontal layers, and modified moisture barrier into 3 horizontal layers. Number of trials were done to achieve a suitable size of mesh. Finally, the mesh size of 10 cm was deemed suitable for this numerical study.

Asphalt layer was modeled as a saturated layer with properties extracted from Cooley et al. (2002) who performed several tests on twenty-three pavement construction projects. For asphalt layer, saturated water content was taken as 0.13 and saturated permeability was taken as 1.22×10^{-5} m/s. The properties correspond to the permeability of super pave asphalt with aggregate size 25 mm and lift thickness to aggregate size ratio of 4.0 as measured by Cooley et al. (2002). While the asphalt layer was defined as saturated model, the base course was defined as saturated/ unsaturated model to simulate unsaturated flow in response to rainfall. The permeability of base course was taken as 1×10^{-4} m/s. The properties of geocomposite were taken as α = 0.12 kPa, n = 5, θ_s = 0.45 and θ_r = 0.02 (Kuhn et al., 2005).

7.4.3 Boundary Conditions

The boundary condition in SEEP/W can be applied either in terms of flux or head. No flow condition was applied along left boundary. A potential seepage face was defined at the exit of modified moisture barrier system in order to allow flux out of the model. An initial suction was defined such that the base material is almost at its residual moisture condition. Different intensity of rainfall, as a flux boundary was applied at the surface of asphalt layer to evaluate the performance of geo composite layer.

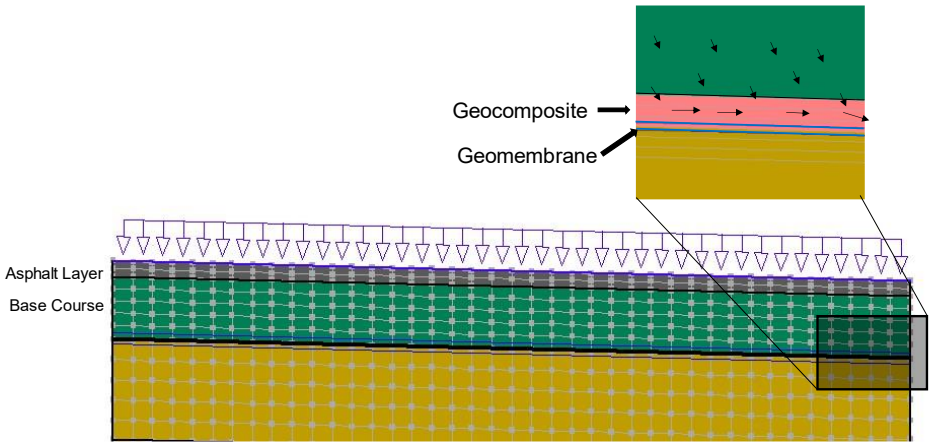

Figure 7–16 Model Geometry for Flow Study

7.4.4 Parametric Study

The main purpose of modified moisture barrier placement at the base-subgrade interface is to isolate highly expansive subgrade from infiltrated rainwater and laterally drain the infiltrated rainwater towards the edge. The performance of drainage layer largely depends on the infiltrated rainwater in the base course and the transmissivity value with which the water can be drained laterally. To study the response of geo composite layer with different transmissivity values, the generated seepage model was evaluated through parametric study. The parameters considered in this study were:

1. Transmissivity: Transmissivity gives the measure of lateral flow capacity of a material. It can be obtained by multiplying in-plane permeability by thickness and gradient of slope. Here, several in-plane permeability corresponding to transmissivity values were considered to determine minimum transmissivity required to drain incoming rainwater. Again, outflow rate for several commercially available geocomposite was evaluated.
2. Rainfall Intensity: Different rainfall intensities were applied for 24 hours duration. The considered intensities were 5 mm/hr., 10 mm/hr., 20 mm/hr., 40 mm/hr., and 60 mm/hr. The considered rainfall intensities were applied uniformly for 24 hours and the movement of wetting front through base layer, entry of water to the geo composite layer and flow rate through geo composite layer at different time were evaluated.

7.4.5 Rainwater Infiltration Analysis

Prior to the application of rainfall on the developed model, the volumetric water content in base layer was maintained to be at residual moisture content of 0.05 m^3/m^3 corresponding to the suction value of -20 kPa. This state represents the driest condition of base course. Figure 7–17 illustrates the movement of wetting front for different cases of rainfall intensities. The profiles indicate increase in volumetric water content along the depth with the advancement of wetting front. For different cases, the wetting front advanced at different rate. It was observed that the higher intensity rainfall moved to deeper soils much faster than the low intensity rainfall attaining saturated moisture content of 0.38 m^3/m^3 at the bottom of base. For instance, 10 mm/hour rain reached base-geo composite layer within 2 to 4 hours of constant rainfall while 20 mm/hour reached within 1 to 2 hours. Therefore, the high intensity rain for short duration can have more impact on the transient

moisture change within the soil as compared to low intensity rainfall that may occur for longer period.

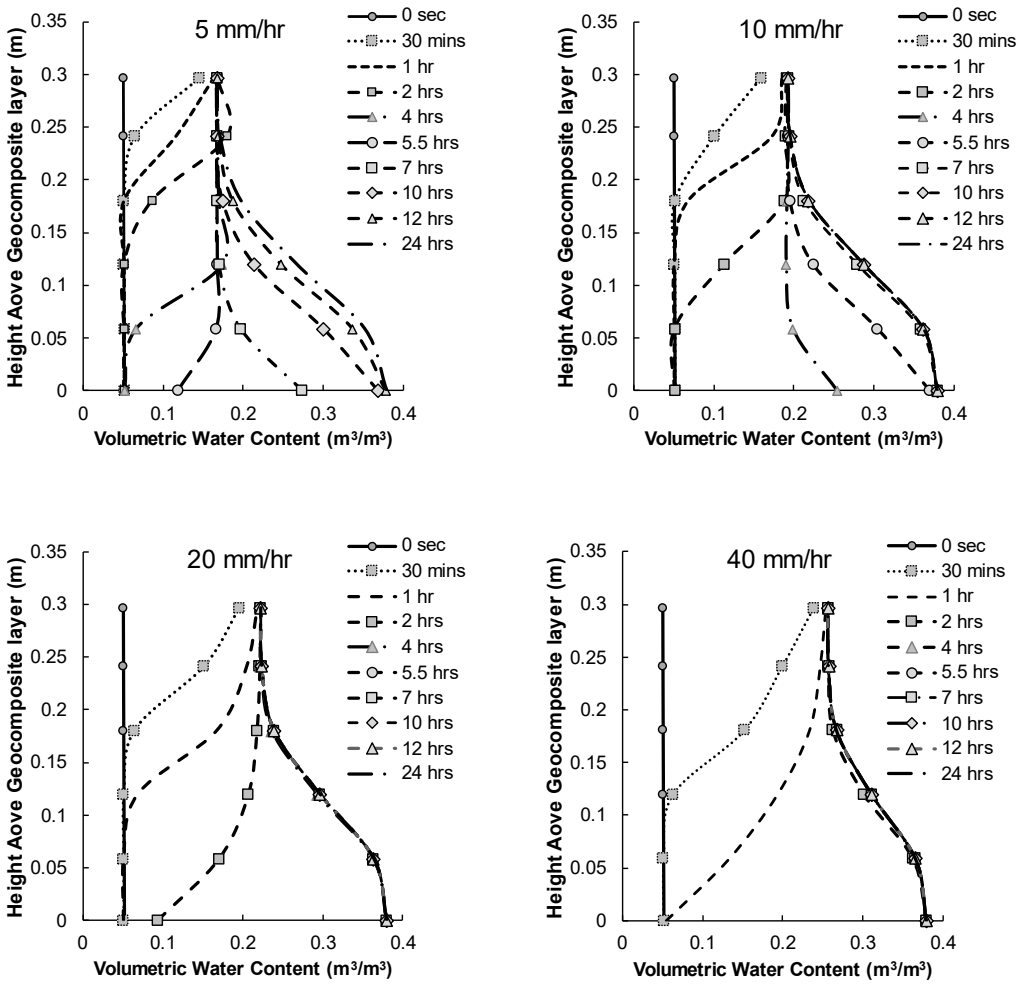

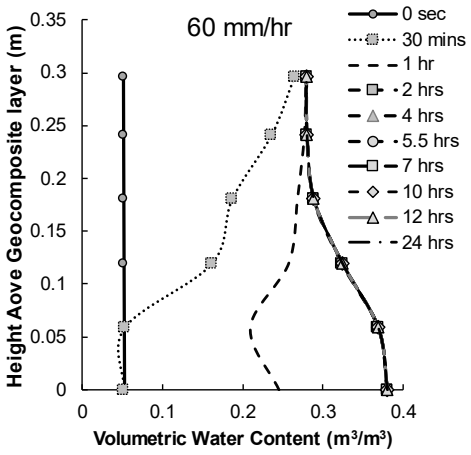

Figure 7–17 Wetting Front Movement in Base

7.4.6 Moisture Infiltration into Geocomposite Layer

The flow within the geo composite did not start as soon as the wetting front reached the bottom of the base. As the wetting front reaches the interface between base and geo composite, the wetting front travels along the interface until the air entry value of geo composite is reached. Once the pore pressure right at the interface reaches air entry value of geo composite, capillary barrier breaks at the interface between base and geo composite and flow begins in the geo composite layer. When the flow enters the geo composite, the base course is nearly saturated towards the bottom.

The time required for the flow to start in the geo composite layer depends on the intensity of rainfall. Higher intensity of rainfall can break the capillary barrier in less time and enter the geo composite layer. Hence, flow in the geo composite layers starts much faster. Once the flow starts in the geo composite layer, the flow gradually increases till it reaches a steady state with flow capacity equal to the assigned transmissivity of geo composite layer. Figure 7–18 illustrates the time required for different intensities of rainfall to reach the bottom of the base (base-geo composite interface) i.e., T_b, time at which water enters the

geo composite, which is also the time at which drainage starts in geo composite i.e., T_g and the time at which the flow reaches steady state i.e., T_s. T_b, T_g and T_s are calculated from the start of rainfall events.

For 5 mm/ hour rain, flow entered geo composite three hours after the wetting front reached the bottom of base course. As discussed earlier this time is utilized for attaining the air entry value of geo composite and breaking the capillary barrier which usually forms due to difference in hydraulic characteristics of two different materials. The breakthrough time i.e., duration in between T_b and T_g was found to be decreasing with the increase in rain intensity (Figure 7–19).

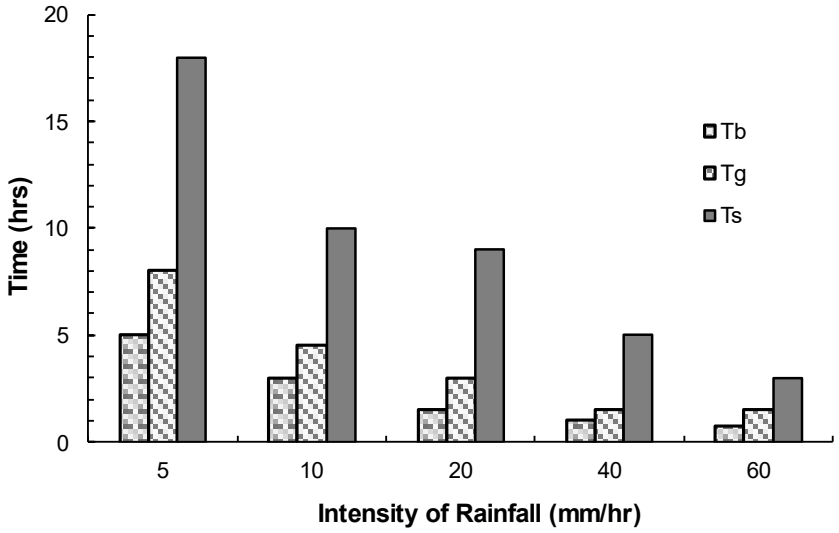

Figure 7–18 Time vs. Rainfall Intensity

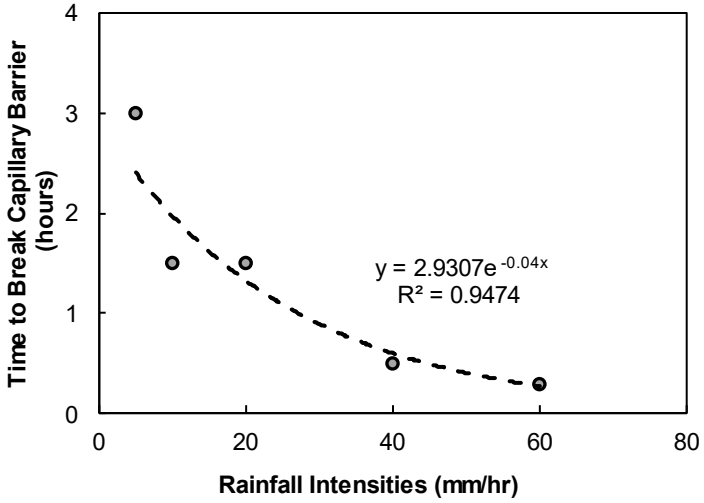

Figure 7–19 Time to Break Capillary Barrier at Base-Geocomposite Interface

7.4.7 Flow Through Geocomposite

Kamon et al. (2001) studied performance of geo composites in embankments and concluded that geo composites were able to effectively drain the water expelled from the soil. Similarly, geo composite in the current study was found to be effectively draining the water expelled from the base course, however the time at which the flow reached steady state varied for different intensities of rainfall. With the increase in rainfall intensity, the flow in geo composite was found to attain steady state quicker as can be seen in Figure 7–20.

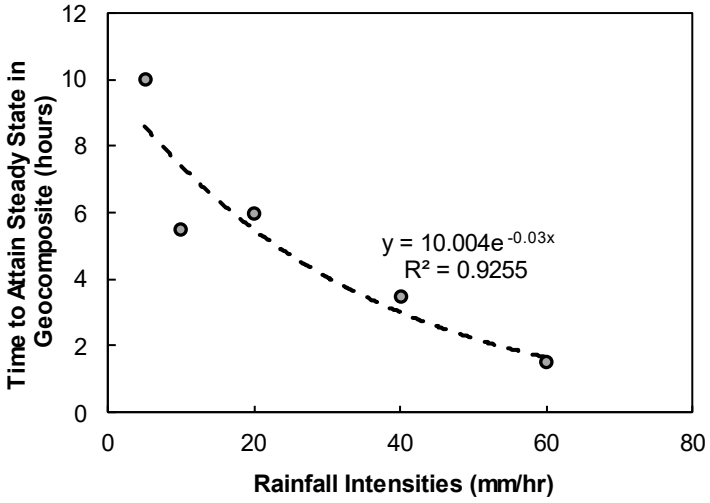

Figure 7–20 Time to Attain Steady State Flow in Geocomposite

Figure 7–21 shows the observed flow pattern along the length of geo composite with transmissivity of 3 X 10^{-6} m^3/sec/m for different rainfall intensities. The maximum flow in geo composites corresponded its transmissivity value. Similar observations were made by Iryo and Rowe (2005) who performed a numerical study to evaluate the hydraulic behavior of soil-geo composite layers in slopes and studied the influence of several parameters such as soil type, slopes, and infiltration rate on the flow characteristics geocomposite. It should be noted that the in-plane permeability multiplied by the thickness and gradient gives transmissivity. The mobilization of full capacity along the length of geo composite varied for different intensities. As the rainfall intensity increased, the length over which the water was drained at its full capacity increased. For instance, water flows with the full capacity along 2-meter length of geo composite for 5 mm/hour rain i.e., covering 50% of length, while for 10 mm/hour of rain, full flow occurs along 3-meter length covering 75% of geo composite. For 60 mm/hour rain, full flow occurs almost along the entire length indicating critical flow where infiltration exceeded the capacity of geocomposite to transmit flow.

Therefore, more transmissivity is required to effectively drain such huge intensity of rain. The results showed that the mobilized transmissivity length depends on intensity of rainfall and at certain transmissivity value, the mobilized transmissivity length becomes maximum.

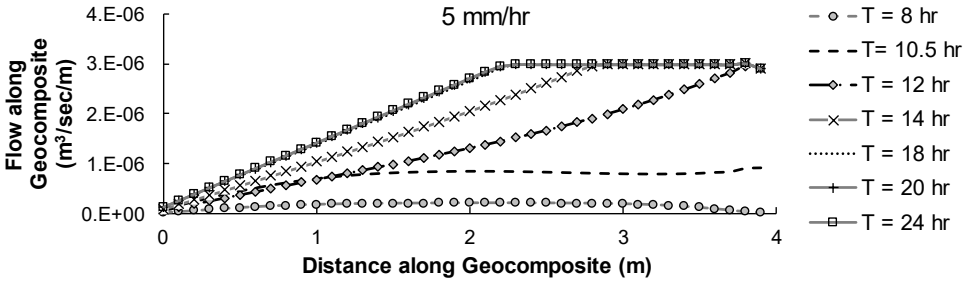

(a)

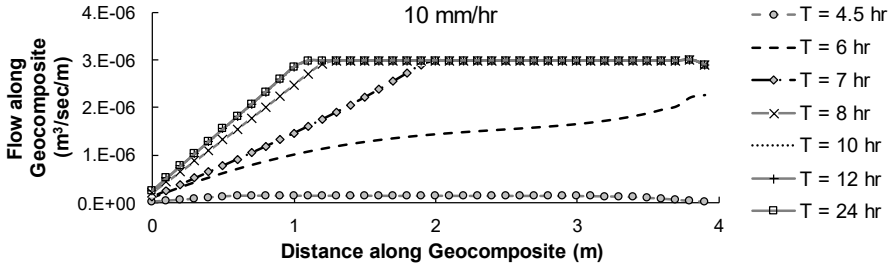

(b)

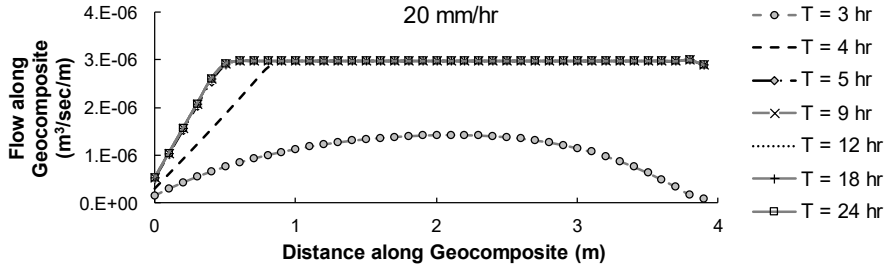

(c)

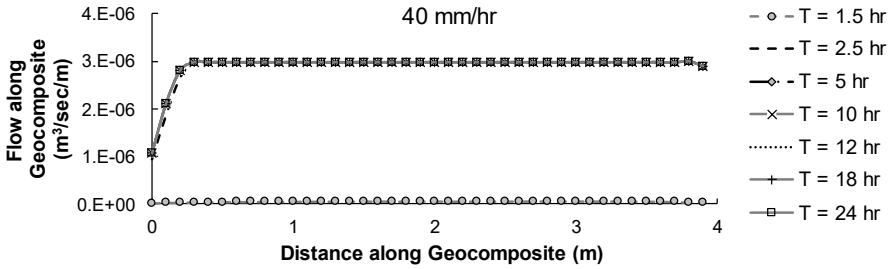

(d)

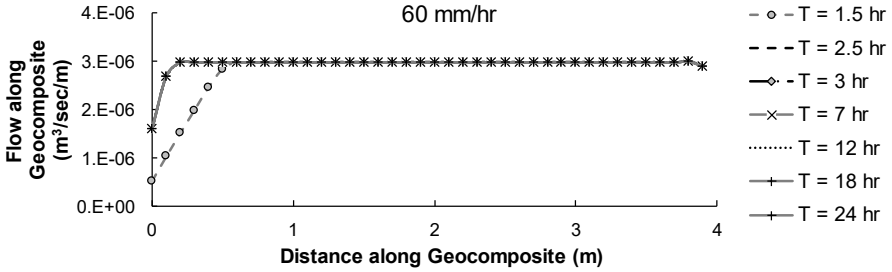

(e)

Figure 7–21 Flow Along Geocomposite for (a) 5 mm/hour (b) 10 mm/hour (c) 20 mm/hour (d) 40 mm/hour (e) 60 mm/hour

Again, flow along drainage layer with different transmissivities were analyzed for several rainfall intensities. Figure 7–22 shows observed flow along geo composite with varying transmissivities for 10 mm/hour rainfall intensity while others are presented in the appendix.

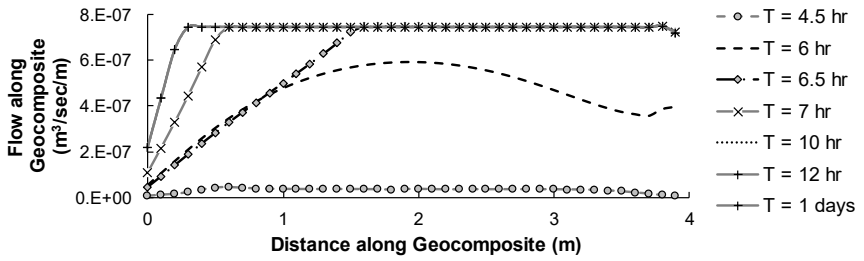

(a)

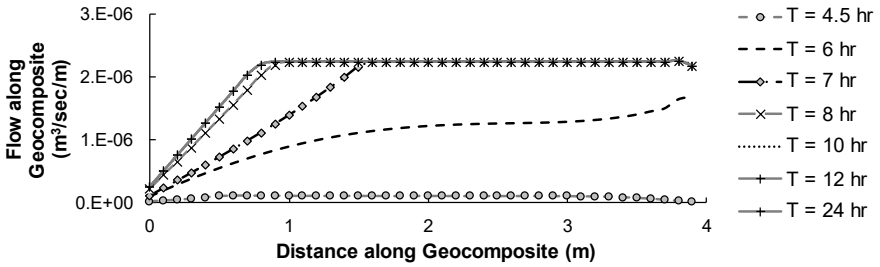

(b)

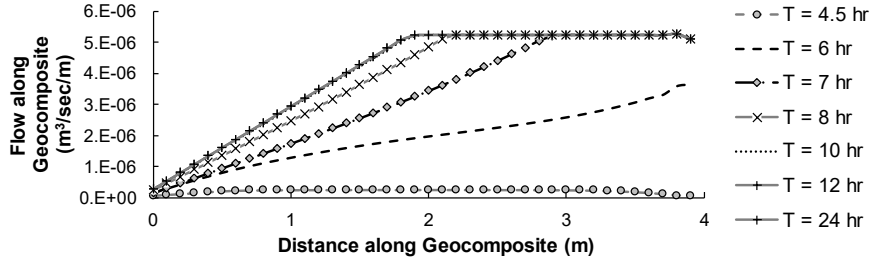

(c)

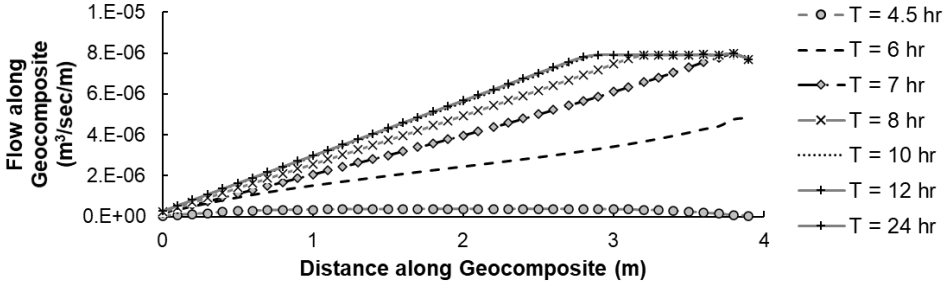

(d)

Figure 7–22 Flow Along Geocomposite for 10 mm/hour of Rainfall with (a) 7.2 X 10^{-7} m^3/sec/m (b) 2.16 X 10^{-6} m^3/sec/m (c) 5.06 X 10^{-6} m^3/sec/m and (d) 7.7 X 10^{-6} m^3/sec/m of Transmissivity

The transmissivity value of 7.212 X 10^{-7} m^3/sec/m was found to be critical for 10mm/hour intensity of rainfall where almost entire length drained the water with maximum capacity. Therefore, for 10 mm/hour of rainfall intensity, transmissivity values greater than 7.212 X 10^{-7} m^3/sec/m should be considered. With the increasing transmissivity values, the mobilized transmissivity length was found to be decreasing. For instance, full transmissivity

was mobilized along 75%, 50% and 25% length of geo composite when transmissivity of 2.17 X 10^{-6} m^3/sec/m, 5.08 X 10^{-6} m^3/sec/m and 7.7 X 10^{-6} m^3/sec/m respectively were used. Table 7–3 summarizes the transmissivity values for which the mobilized transmissivity length was 25%, 50%, 75% along with critical transmissivity for analyzed rainfall intensities.

Table 7–3 Transmissivities for Different Rainfall Intensities

Rainfall Intensities	Transmissivity for Optimum Flow Capacity along				Design Transmissivity
	25% Length of Geo composite	50% Length of Geo composite	75% Length of Geo composite	90% Length of Geo Composite (Minimum)	
5 mm/hour	3.92 X 10^{-6}	2.47 X 10^{-6}	1.16 X 10^{-6}	2.13 X 10^{-7}	> 2.13 X 10^{-7}
10 mm/hour	7.7 X 10^{-6}	5.08 X 10^{-6}	2.17 X 10^{-6}	7.2 X 10^{-7}	> 7.2 X 10^{-7}
20 mm/hour	1.59 X 10^{-5}	1.017 X 10^{-5}	4.79 X 10^{-6}	1.446 X 10^{-6}	> 1.45X 10^{-6}
40 mm/hour	3.2 X 10^{-5}	2.108 X 10^{-5}	1.02 X 10^{-5}	2.89 X 10^{-6}	> 2.89 X 10^{-6}
60 mm/hour	4.79 X 10^{-5}	3.19 X 10^{-5}	1.55 X 10^{-5}	4.78 X 10^{-6}	> 4.78 X 10^{-6}

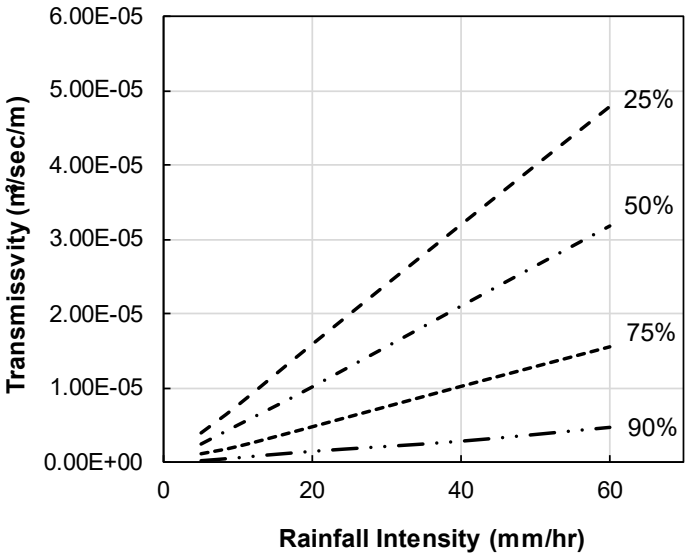

Figure 7–23 Transmissivity with Different Mobilized Length for Varying Rainfall Intensities

The average outflow rate for each of the minimum transmissivities were extracted from numerical model and are shown in Figure 7–24.

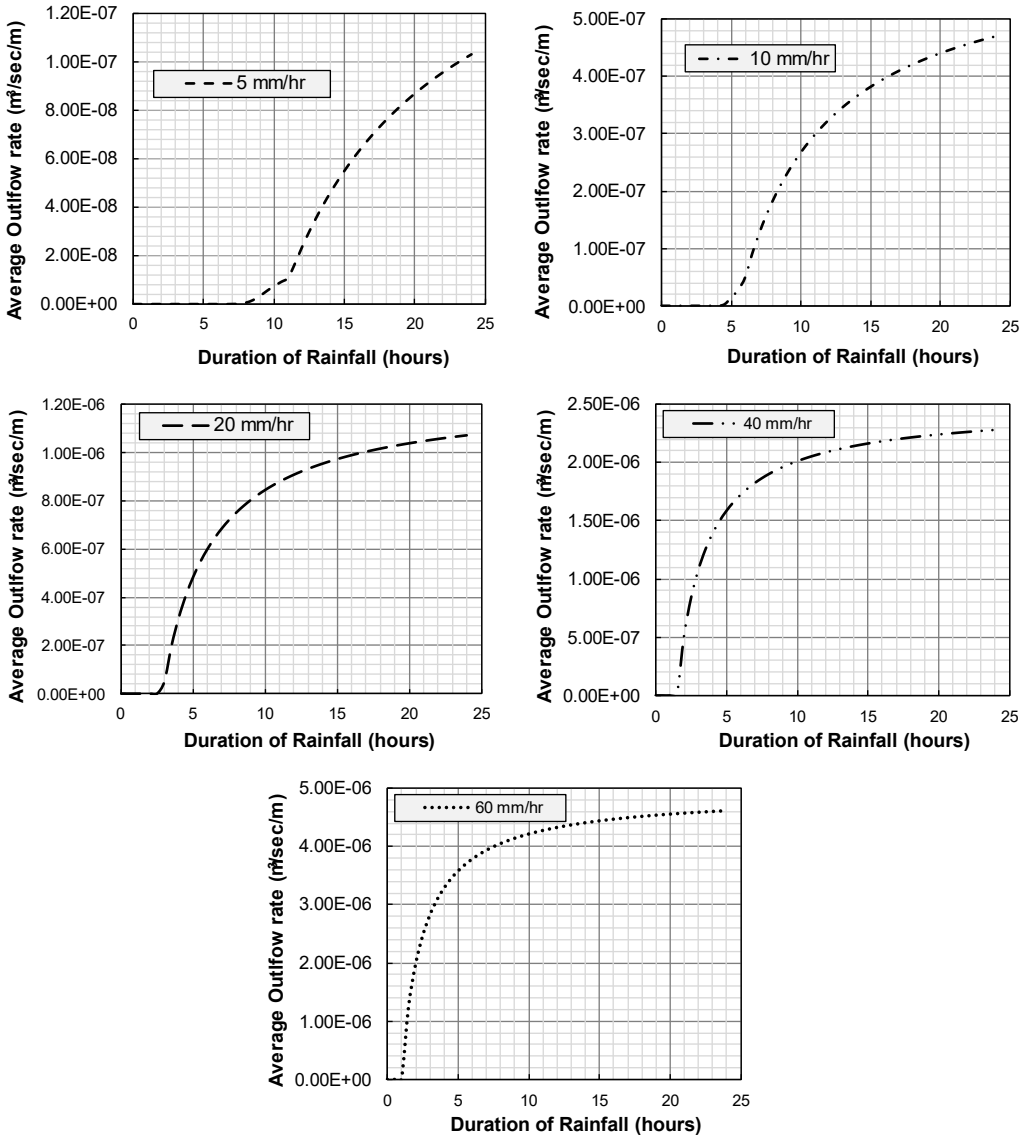

Figure 7–24 Average Outflow Rate from Minimum Required Transmissivities

It should be noted that the in-plane flow capacity of a geocomposite may be affected by several factors over the years and may result in reduced performance of the material.

Reduction in the thickness of geocomposite and intrusion of geotextile surface into the core of geocomposite due to high confining pressure have been stated as the cause of reduced inflow capacity of the geocomposite (Bamforth, 2009). Several reduction factors are usually considered to determine the allowable flow capacity of geocomposite. Care must be taken such that the transmissivity of geocomposite does not drop below the minimum required transmissivity as determined from the previous section.

7.4.8 Drainage Along Commercially Available Geocomposites

Figure 7–25 to Figure 7–29 show the outflow rate for different rainfall intensities through commercially available geocomposites. Iryo and Rowe (2005) stated geocomposites can drain more water with an increase in infiltration rate. Similar observations were made in the current study where increased outflow rates were observed for higher rainfall intensities. The rate of outflow from the geocomposites was found to be higher for greater rainfall intensities when compared at the same duration.

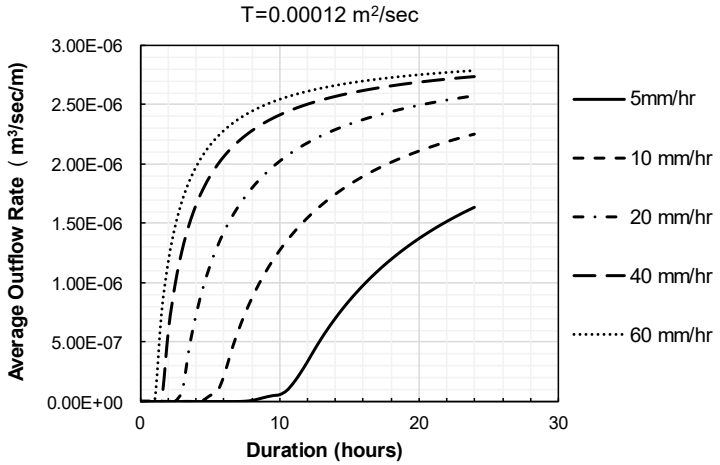

Figure 7–25 Average Outflow Rate for Different Rainfall Intensities using Geocomposite with T = 0.00012 m^2/s

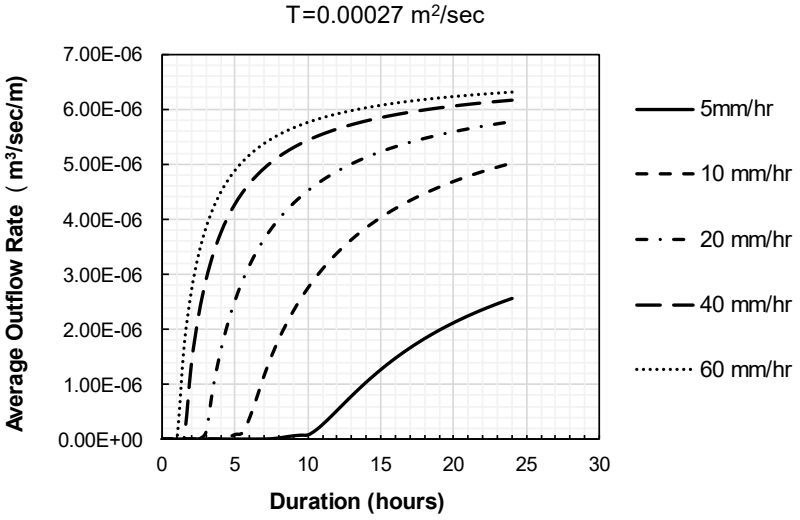

Figure 7–26 Average Outflow Rate for Different Rainfall Intensities using Geocomposite with T = 0.00027 m^2/s

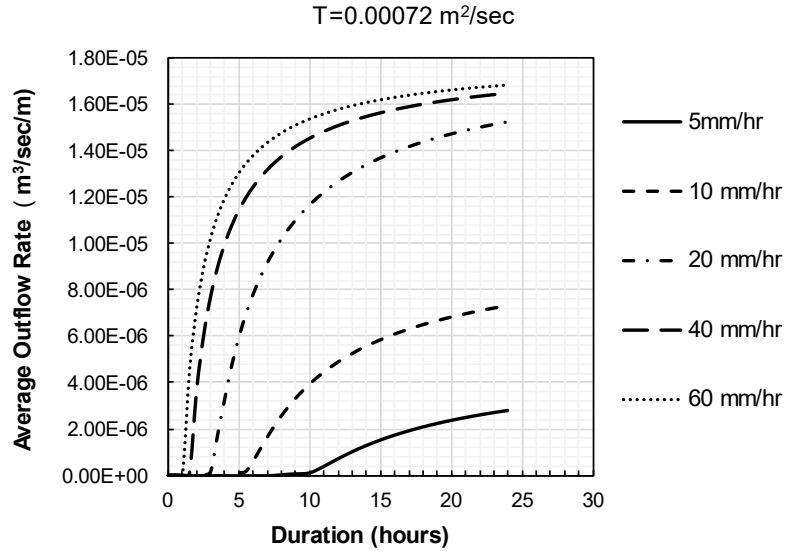

Figure 7–27 Average Outflow Rate for Different Rainfall Intensities using Geocomposite with T = 0.00072 m^2/s

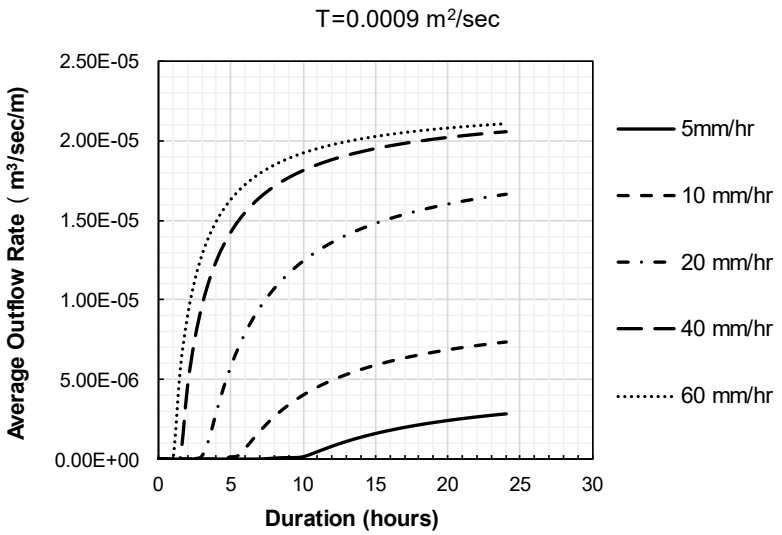

Figure 7–28 Average Outflow Rate for Different Rainfall Intensities using Geocomposite with T = 0.0009 m^2/s

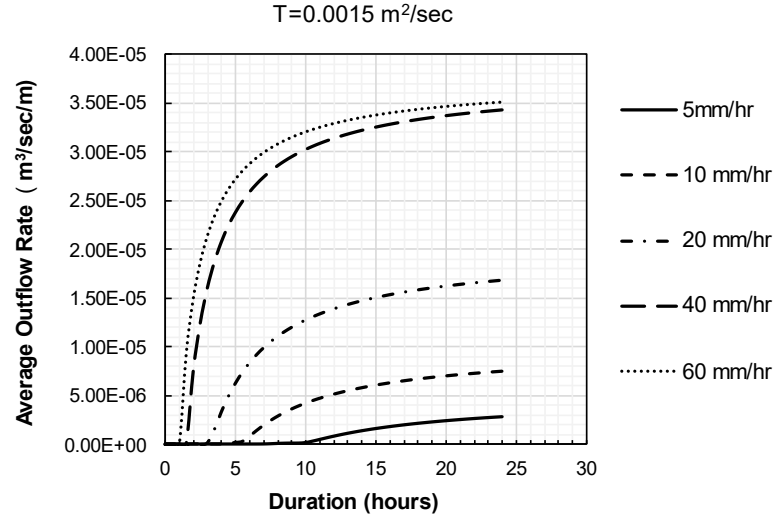

Figure 7–29 Average Outflow Rate for Different Rainfall Intensities using Geocomposite with T = 0.0015 m^2/s

7.4.9 Time to Desaturate Geocomposite after Rainfall Event

Figure 7–30 shows the time required by the geocomposite of varying transmissivity to drain the excess water out of the system once the rainfall stops. The time required was independent of rainfall intensities. Since the outflow rate increased with increasing rainfall intensity, the final time to desaturate was same for each rainfall intensity.

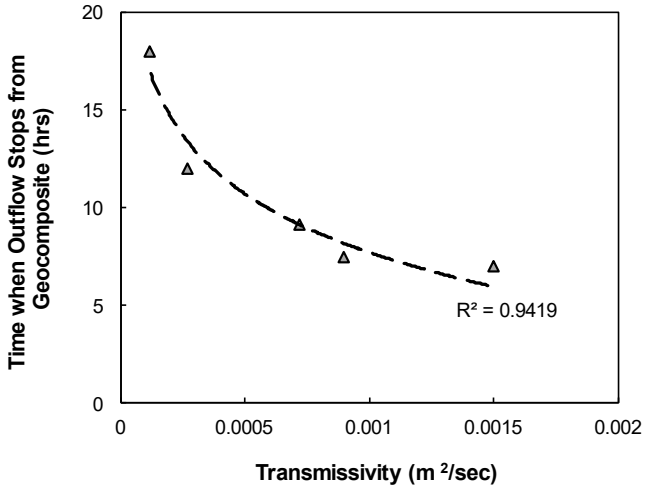

Figure 7–30 Desaturation after Rainfall Event

7.4.10 Factor of Safety

Average outflow rate was considered to calculate the factor of safety. Based on the study, average outflow rate gradually increases with rainfall duration. From Figure 7–24, minimum required outflow rate for given rainfall duration can be determined. Similarly, average outflow rate for commercially available geocomposite can be obtained from Figure 7–25 and Figure 7–29 for same duration of rainfall. Comparing these two values, factor of safety can be computed. The section below demonstrates an example calculation of factor of safety for a rainfall duration of 15 hours.

Example calculation:

Table 7–4 Calculation Example

Rainfall Intensity (mm/hr)	Duration (hours)	Average outflow from Min. Required Transmissivity (m^3/sec/m)	Avg outflow rate when T= 0.00012 m^3/s/m	FS	Avg outflow rate when T= 0.00027 m^3/s/m	FS	Avg outflow rate when T= 0.00072 m^3/s/m	FS	Avg outflow rate when T= 0.0009 m^3/s/m	FS	Avg outflow rate when T= 0.0015 m^3/s/m	FS
5	15	5.60 E-08	8.50 E-07	15.2	1.3 E-06	23.2	1.60 E-06	28.6	1.60 E-06	28.6	1.60 E-06	28.6
10	15	3.80 E-07	1.80 E-06	4.7	4.00 E-06	10.5	5.80 E-06	15.3	6.00 E-06	15.8	6.00 E-06	15.8
20	15	9.60 E-07	2.30 E-06	2.4	5.20 E-06	5.4	1.36 E-05	14.2	1.50 E-05	15.6	1.50 E-05	15.6
40	15	2.17 E-06	2.7 E-06	1.2	5.80 E-06	2.7	1.56 E-05	7.2	1.96 E-05	9.0	3.2 E-05	14.7
60	15	4.50 E-06	2.7 E-06	0.6	6.00 E-06	1.3	1.62 E-05	3.6	2.00 E-05	4.4	3.4 E-05	7.6

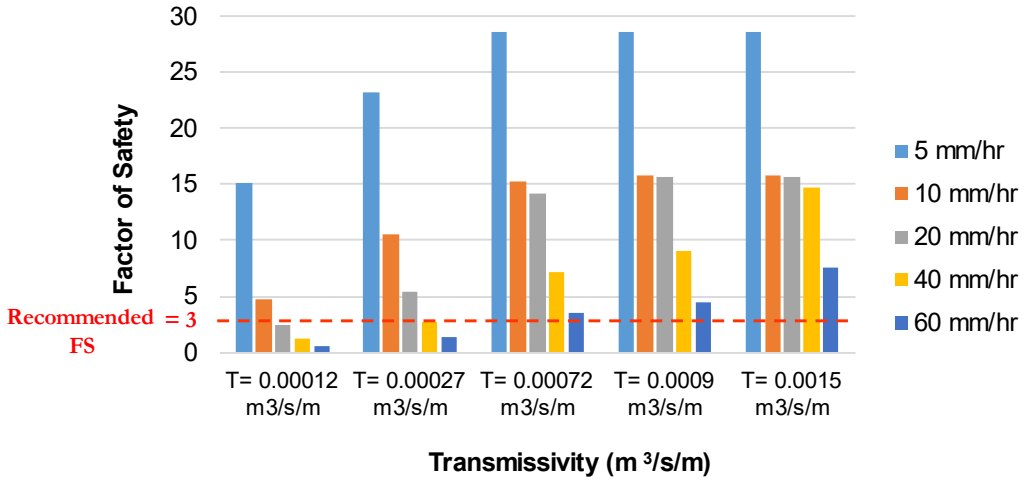

Figure 7–31 Factor Safety for 15 hours of Uniform Rainfall

Typically factor of safety of 3 is recommended for such applications, which is also marked in Figure 7–31. In real field scenario, the flow capacity of geocomposite decreases with time. The average flow rate obtained in Figure 7-25 to 7-29 can be further reduced by considering reduction factors as reported in Koerner (2012).

Chapter 8

SUMMARY AND CONCLUSIONS

8.1 Introduction

The current study is mainly focused on mitigating frequently occurring surficial distresses in pavement constructed over highly expansive subgrade soil. High plasticity expansive soil tends to exhibit swelling and shrinkage behavior due to seasonal changes in climatic condition. Moisture intrusion may occur from the pavement surface, cracks or side slope causing increased moisture variation in the subgrade soil. Inadequate drainage of infiltrated rainwater is another critical factor for failure of pavements over expansive soil. Among several types of available moisture barrier system, modified moisture barrier offers great potential in maintaining equilibrium moisture content through the combined performance of geomembrane and geo-composite materials serving as an impermeable layer and a drainage layer, respectively. Although past studies have used modified moisture barrier in controlling edge moisture intrusion, no studies have been conducted with the barrier placed across the full width of pavement. As rainwater infiltration up to 33 to 50% can occur through pavement surface and along fine cracks formed by the wearing and ageing of asphalt layer over the years, such a study was much needed.

The main objective of the study is to evaluate the behavior of expansive subgrade soil with and without modified moisture barrier when placed across the full width of pavement. To fulfil this objective, an actual compromised pavement section was selected for the study after thorough site investigations. Modified moisture barrier (MMB) was placed across the full width of 91 m long distressed pavement section while an adjacent 30.48 m section was considered as a control section with no MMB. Both the barrier and control sections were instrumented with integrated moisture and temperature sensors, suction sensors, and

inclinometers to monitor real time moisture and temperature variations, suction variation, and deformation of the subgrade soil, respectively. The field monitoring results showed that both the moisture and deformation in the control section varied throughout the year while the barrier section showed nearly constant profile. The variations observed in the control section were analyzed in MATLAB and prediction models were developed which can predict the moisture content and deformation of subgrade soil in response to climatic loading. The developed models were validated against several field studies. The behavior of subgrade soil was further evaluated through numerical analysis and flow along geocomposite was assessed for different transmissivities and rainfall intensities.

8.2 Summary of Conclusions

The results and conclusions from the current study can be summarized as below:

8.2.1 Site Investigation

- Detailed site investigation using ground penetrating radar survey and pavement coring were performed to evaluate the subsurface condition, and the severity and extent of observed surface distresses beneath the pavement. In addition, subgrade soil assessment was conducted by performing laboratory tests on both disturbed and undisturbed samples collected from the site. The borings for soil sampling extended to a depth of 3 m under the centerline and edges of roadway.
- Pavement coring was performed at four locations on the failed portion of the roadway to evaluate the existing pavement thicknesses and the integrity of underlying pavement layers. The extracted samples revealed the pavement thickness to be in the range of 30-38 cm (12-15 in.).
- GPR scanning, performed along five lines in the distressed section estimated the layer thickness consistent with the results obtained from pavement coring. The

survey was able to capture surficial distresses along with the soil movement to a depth of 114.3 cm (45 in.) due to highly expansive nature of underlying subgrade soil.

- The laboratory tests on the collected soil samples classified subgrade soil as highly plastic fat clay (as per USCS classification) with liquid limit and plasticity index ranging from 70% to 85%, and 39% to 53%, respectively. At all depths, soil samples consisted of 89% to 94% fines. The free swell potential for the soil sample at 2 ft and 5 ft under existing overburden pressure was observed to be 6.5% and 0.55%, respectively. The in-situ moisture content was found to be ranging in between 21% to 35% at the time of soil sampling probably due to excessive wetting from rainwater infiltrated through cracks.

8.2.2 Moisture and Suction Variation in Subgrade Soil

- The installation of modified moisture barrier under the entire pavement section at the base-subgrade interface provided a barrier and isolated the pavement from changing environmental conditions.
- The soil moisture in the control section depicted seasonal variation along with instantaneous response to rainfall events while equilibrium moisture content was observed within the section stabilized with modified moisture barrier.
- The average soil moisture content was found to be higher in wet period than in dry period in control section while no variation in initial in-situ moisture content was observed in barrier section throughout the monitoring period. Maximum of 17% change in volumetric moisture content occurred in the control section at a depth of 0.9 m. The variation decreased with depth.

- The suction variation in control was measured to be in the range of -10 kPa to -733.73 kPa while no change was observed in the barrier section.
- No rainfall dependent behavior in barrier section indicates no moisture intrusion into the subgrade soil from pavement's surface, thus verifying the potential of moisture barrier in preventing the moisture to reach the subgrade and mitigate the probability of pavement failure.

8.2.3 Subgrade Soil Deformation

- Seasonal movement of subgrade soil was observed in the control section while nearly constant profile was observed in the barrier section. The movement corresponded to the observed moisture profile in both the sections, such that higher moisture content resulted in swelling and vice versa.
- Maximum movement of -61.7 mm and +7.36 mm was observed in the control and barrier sections, respectively during the monitoring period. This value was recorded at certain distance from pavement edge.
- The incremental movement in control was observed to follow seasonal pattern with positive displacement (indicating swelling) in wet period and negative displacement (indicating shrinkage) in dry period.
- Modified moisture barrier installed throughout the pavement was able to reduce swelling and shrinkage of highly expansive subgrade soil by 89% based on the performance monitoring results.
- Based on the results of the study, it can be summarized that the overall performance of the section stabilized with modified moisture barrier at the base-subgrade interface was better than that of the control section. The combination of geocomposite (geotextile + geonet + geotextile) and geomembrane material could

in fact provide an effective solution to the frequently observed failure of pavements built over expansive subgrade soil in semi-arid regions.

8.2.4 Moisture and Deformation Modeling

- The field results of control section were used to develop prediction models for predicting moisture and deformation in response to climatic loading.
- Non-parametric analyses were performed on the field observed moisture and deformation in control section. The temporary effects of both rainfall and temperature were incorporated in the final models.
- The final moisture model took the forms as follows:

  M.C = Seasonal M.C. + Increase in M.C (Due to Rainfall) – Decrease in M.C. (Due to Soil Temperature)

  $M.C = [35.29 + 1.974 * \cos (x * 0.01717) + 3.41 * \sin (x * 0.01717)] + [0.2407 * x_R + 0.9639] – [0.3912 * x_t + 1.9757]$

  where, x = Day number (February 09, 2020 regarded as Day 1)

  x_R = Rainfall in mm

  x_t = Increase in soil temperature form the seasonal value in ^oC.
- The final deformation model took the form as follows:

  Subgrade Deformation = Seasonal Deformation + Swelling (Due to Rainfall) – Shrinkage (Due to Soil Temperature)

  $Subgrade\ Deformation = [-17.6 + 12.55 * \cos (x * 0.01751) + 22.04 * \sin (x * 0.01751)] + [0.0537 * x_R + 1.6262] – [1.6192 * x_t + 30.935]$

  where, x = Day number (March 21, 2019 regarded as Day 1)

  x_R = Rainfall in mm

  x_t = Air Temperature in ^oC.

- The moisture model was validated with field results from different parts of North Texas and for different years. The deformation model was validated with the readings from the same pavement at different locations. Both the prediction models satisfied the statistical tests conducted to verify the model's applicability.

8.2.5 Numerical Study

- The behavior of expansive subgrade soil with and without moisture barrier system was studied numerically along with the flow evaluation along geocomposite drainage layer of modified moisture barrier system.
- The incorporation of modified moisture barrier was able to control the moisture intrusion into the pavement system causing reduced deformation.
- The movement of wetting front was observed to vary for different rainfall intensities. The wetting front advanced much faster in case of higher intensity rainfall than lower intensity rainfall.
- Capillary barrier was formed at the base-geocomposite interface making the bottom of the base nearly saturated. Once the capillary barrier broke, the flow gradually increased in the geocomposite until it reached a steady state condition. The maximum flow capacity of the geocomposite corresponded to its transmissivity value.
- The mobilization of full capacity along the length of geo composite varied for different intensities. Greater transmissivity was required to effectively drain high rainfall intensity.
- Minimum transmissivity for different rainfall intensities were determined based on the transmissivity mobilization length.
- Geocomposites could drain more water with increased infiltration rate.

- The time to desaturate geocomposite layer after the rainfall events decreased with the increased transmissivity.
- Factor of safety for specific rainfall intensity and duration can be calculated based on average flow rate for minimum required transmissivity and commercial transmissivity.

8.3 Recommendations for Future Study

Based on the field monitoring and analyses, following recommendations are suggested for future studies:

- More field studies with the application of modified moisture barrier are needed to evaluate its effectiveness in different site conditions.
- The current study provides the field performance of modified moisture barrier for two years, however long- term performance monitoring is recommended to evaluate the performance of MMB in the long run.
- The inclinometer readings are recommended to be taken more frequently to avoid missing swelling and shrinkage in between long measurement intervals (particularly during peak wet and dry periods).
- Future studies should consider instrumentation within base course to quantify rainwater infiltration and evaluate the performance of geocomposite layer in reducing base saturation.
- It is recommended to extend the modified moisture barrier installed underneath the pavement towards the side slope to prevent potential lateral moisture intrusion.
- Different types of geocomposite and geomembrane materials should be considered and investigated for the enhanced performance of modified moisture barrier.

- Numerical study of moisture movement through individual components of modified moisture barrier can develop greater insights upon the working mechanism of MMB.
- Numerical flow evaluation with different types of base course can provide better understanding of flow interaction at the interface of base and geocomposite and establish better opting criteria with suitable combination of base and geocomposite material.

REFERENCES

Abbaszadeh, M. (2011). *The effect of cracks on unsaturated flow and volume change properties of expansive clays and impacts on foundation performance,* Doctoral Dissertation, Arizona State University.

Ahmed, A. (2017). *Effects of Climatic Loading in Flexible Pavement Subgrades in Texas*. Doctoral Dissertation, University of Texas at Arlington.

Ahmed, A., & Islam, M. A. (2020). Effect of Using Geosynthetics in Mitigation of Freeze-Thaw through Numerical Analysis. In *Geo-Congress 2020: Geotechnical Earthquake Engineering and Special Topics* (pp. 436-445). Reston, VA.

Ahmed, A., Alam, M. J. B., Pandey, P., & Hossain, M. S. (2021). Estimation of unsaturated flow parameters and hysteresis curve from field instrumentation. In *MATEC Web of Conferences* (Vol. 337, p. 01008). EDP Sciences.

Ahmed, A., Hossain, M. S., Khan, M. S., & Greenwood, K. (2018). Use of Modified Moisture Barrier to Reduce Subsurface Moisture in Flexible Pavement in North Texas (No. 18-04256). *97th Annual Meeting of Transportation Research Board,* Transportation Research Board, Washington D.C.

Ahmed, A., Islam, M. A., & Imtiaz, T. (2020). Effectiveness of Geosynthetics as Insulation to Freeze-Thaw: Field Instrumentation and Numerical Modeling. *Transportation Research Board 99th Annual Meeting*, Washington DC, USA.

Ahmed, A., Khan, S., Hossain, S., Sadigov, T., & Bhandari, P. (2020). Safety prediction model for reinforced highway slope using a machine learning method. *Transportation Research Record, 2674*(8), 761-773.

Al-Qadi, I. L., Lahouar, S., Loulizi, A., Elseifi, M. A., & Wilkes, J. A. (2004). Effective approach to improve pavement drainage layers. *Journal of Transportation Engineering*, *130*(5), 658-664.

Armstrong, C. P., & Zornberg, J. G. (2018). Monitoring of Moisture Fluctuations in a Roadway over an Expansive Clay Subgrade. In *IFCEE 2018* (pp. 415-424).

ASCE (2021). America's Infrastructure Scores a C-. 2021 Infrastructure Report Card, <https://www.infrastructurereportcard.org/> (April 02, 2021).

Aubeny, C., & Long, X. (2007). Moisture diffusion in shallow clay masses. *Journal of Geotechnical and Geo-environmental engineering*, *133*(10), 1241-1248.

Aubeny, C., & Lytton, R. (2003). *Long-term strength of compacted high-PI clays* (No. FHWA/TX-03/2100-1,). Texas Transportation Institute, Texas A & M University System.

Badhon, F. F., Zaman, M. N. B., Bhandari, P., Islam, M. A., & Hossain, M. S. (2021). Performance of Recycled Plastic Pins (RPP) for Improving the Bearing Capacity of MSE Wall Foundation. *International Foundations Congress & Equipment Expo*, Dallas, Texas.

Bamforth, A. (2009). Interpretation of In-plane Flow Capacity of Geocomposite Drainage by Tests to ISO 12958 with Soft Foam and ASTM D4716 with Various Natural Backfill Materials. *GIGSA GeoAfrica, Cape Town*.

Barksdale, R. D., Brown, S. F., & Chan, F. (1989). Potential benefits of geosynthetics in flexible pavement systems. *National Cooperative Highway Research Program (NCHRP) Report No. 315. Washington, DC: Transportation Research Board.*

Bayomy, F and Salem, H. (2004). Monitoring and Modeling Subgrade Soil Moisture for Pavement Design and Rehabilitation in Idaho Phase III: Data Collection and Analysis.

Bhandari, P., Rauss, C., Sapkota, A., & Hossain, M. S. (2020). Long Term Performance of Shallow Slopes Stabilized with Recycled Plastic Pins. In *Geo-Congress 2020: Engineering, Monitoring, and Management of Geotechnical Infrastructure* (pp. 163-172). Reston, VA: American Society of Civil Engineers.

Bhandari, P., Timsina, S., Ahmed, A., Hossain, M. S., & Thian, B. (2019). Development of a Strength Prediction Model for Recycled Base Materials with Soil Intrusion. In *Geo-Congress 2019: Geotechnical Materials, Modeling, and Testing* (pp. 204-213). Reston, VA: American Society of Civil Engineers.

Bhandari, P., Zaman, M. N. B., Islam, M. A., Badhon, F. F., & Hossain, M. S. (2021). Increasing Shearing Resistance of MSE Wall Base Using Recycled Plastic Pins. *International Foundations Congress & Equipment Expo*, Dallas, Texas.

Birgisson, B., Roque, R., & Page, G. C. (2003). Evaluation of water damage using hot mix asphalt fracture mechanics (with discussion). *Journal of the association of asphalt paving technologists*, *72*.

Buhler, R. L., & Cerato, A. B. (2007). Stabilization of Oklahoma expansive soils using lime and class C fly ash. In *Problematic soils and rocks and in situ characterization* (pp. 1-10).

Cedergren, H. R. (1974). *Drainage of highway and airfield pavements*.

Cedergren, H. R., O'Brien, K. H., Arman, J. A., & Cedergren, K. O. B. (1972). *Guidelines for the design of subsurface drainage systems for highway structural sections* (No. FHWA-RD-72-30; NTIS-PB220116). United States. Federal Highway Administration. Office of Research.

Chen, D. H., & Wimsatt, A. (2010). Inspection and condition assessment using ground penetrating radar. *Journal of geotechnical and geo environmental engineering*, *136*(1), 207-214.

Chen, F. H. (1988). *Foundation on Expansive Soils*. Amsterdam. Elseveier Scientific Publication Company, New York, USA, 463.

Chen, L., & Bulut, R. (2015). Numerical analysis of vertical moisture barriers in controlling expansive soils in presence of soil cracks. In *IFCEE 2015* (pp. 2102-2111).

Chen, L., & Bulut, R. (2016). Numerical Analysis of Horizontal Moisture Barriers in Pavements Constructed on Expansive Soils. *Procedia engineering*, *143*, 229-236.

Christopher, B. R., Hayden, S. A., & Zhao, A. (2000). Roadway base and subgrade geocomposite drainage layers. In *Testing and performance of geosynthetics in subsurface drainage*. ASTM International.

Clarke, C. R. (2006). Monitoring long-term subgrade moisture changes with electrical resistivity tomography. In *Unsaturated Soils 2006* (pp. 258-268).

Clothier, B. E., & White, I. (1981). Measurement of sorptivity and soil water diffusivity in the field. *Soil Science Society of America Journal*, *45*(2), 241-245.

Cooley, L. A., Prowell, B. D., & Brown, E. (2002). Issues pertaining to the permeability characteristics of coarse-graded super pave mixes. *Journal of the Association of Asphalt Paving Technologists,* 71, 1-29.

Dan, H. C., Tan, J. W., Zhang, Z., & He, L. H. (2017). Modelling and estimation of water infiltration into cracked asphalt pavement. *Road Materials and Pavement Design*, *18*(3), 590-611.

De Bruyn, C. M. A. (1974). *Moisture redistribution in southern African soils*. National Building Research Institute.

Dempsey, B. J., & Robnett, Q. L. (1979). Influence of precipitation, joints, and sealing on pavement drainage. *Transportation Research Record*, (705).

Dessouky, S. H., Oh, J., Ilias, M., Lee, S. I., & Park, D. (2015). Investigation of various pavement repairs in low-volume roads over expansive soil. *Journal of Performance of Constructed Facilities*, *29*(6), 04014146.

Dondi, G. (1994, September). Three-dimensional finite element analysis of a reinforced paved road. In *Proceedings of the Fifth International Conference on Geotextiles, Geomembranes and Related Products* (Vol. 1, pp. 95-100).

Elseifi, M. A., Al-Qadi, I. L., Loulizi, A., & Wilkes, J. (2001). Performance of geocomposite membrane as pavement moisture barrier. *Transportation Research Record*, *1772*(1), 168-173.

Evans, R. P., & Holden, J. C. (1997, April). Use of geomembranes to control pavement movements from expansive soils. In *Management of Moisture in Expansive Soils, Seminar, 1997, Melbourne, Victoria, Australia*.

Evans, R. P., & McManus, K. J. (1999). Construction of vertical moisture barriers to reduce expansive soil subgrade movement. *Transportation Research Record*, *1652*(1), 108-112.

Fredlund, D. G., & Hung, V. Q. (2001). Prediction of volume change in an expansive soil as a result of vegetation and environmental changes. In *Expansive Clay Soils and Vegetative Influence on Shallow Foundations* (pp. 24-43).

Fredlund, D. G., & Vu, H. Q. (2003, May). Numerical modelling of swelling and shrinking soils around slabs-on-ground. In *Proceeding, Post-Tensioning Institute Annual Technical Conference, Huntington Beach, CA, USA*.

Fredlund, D. G., Rahardjo, H., & Fredlund, M. D. (2012). *Unsaturated soil mechanics in engineering practice*. Hoboken, NJ: John Wiley & Sons.

Fredlund, M. D., Stianson, J. R., Fredlund, D. G., Vu, H., & Thode, R. C. (2006). Numerical modeling of slab-on-grade foundations. In *Unsaturated Soils 2006* (pp. 2121-2132).

Gautam, S., Hoyos, L. R., He, S., Prabakar, S., & Yu, X. (2020). Chemical Treatment of a Highly Expansive Clay Using a Liquid Ionic Soil Stabilizer. *Geotechnical and Geological Engineering*, *38*, 4981-4993.

Gay, D. (1994). *Development of a predictive model for pavement roughness on expansive soils*, Doctoral Dissertation, Texas A&M University.

Geo Studio (2020). *Stress Strain Modeling with GeoStudio.* Geoslope, Calgary, AB, Canda

GEO-SLOPE International. Ltd, (2013). *Stress- Deformation Modeling with SIGMA/W*. Calgary, Canada.

Hansson, K., Lundin, L. C., & Šimůnek, J. (2005). Modeling water flow patterns in flexible pavements. *Transportation Research Record*, *1936*(1), 132-141.

Harris, P. (2008). *Evaluation of stabilization of sulfate soils in Texas* (No. FHWA/TX-08/5-4240-01-1). Texas Transportation Institute, Texas A & M University System.

Hedayati, M. (2014). *Rainfall induced distress in low volume pavements*. Doctoral Dissertation, University of Texas at Arlington.

Henry, K. S., & Stormont, J. C. (2000). *U.S. Patent No. 6,152,653*. Washington, DC: U.S. Patent and Trademark Office.

Henry, K. S., Stormont, J. C., Barna, L. A., & Ramos, R. D. (2002, September). Geocomposite capillary barrier drain for unsaturated drainage of pavements. In *Geosynthetics: State of The Art-Recent Developments. Proceedings of the Seventh International Conference on Geosynthetics, 7-Icg, Held 22-27 September 2002, Nice, France.* (Vol. 3).

Hensen, E. J., & Smit, B. (2002). Why clays swell. *The Journal of Physical Chemistry B*, *106*(49), 12664-12667.

Heydinger, A. G. (2003). Evaluation of seasonal effects on subgrade soils. *Transportation Research Record*, *1821*(1), 47-55.

Hillel, D. (1982). *Introduction to soil physics.* New York, Academic Press (No. 631.43 H54).

Holden, J. C. (1992, February). Reduction of pavement damage from expansive soils using moisture barriers. In *Proceedings of the 6* Australia-New Zealand Conference on Geomechanics, Christchurch, New Zealand* (pp. 83-89).

Holtz, R. D., Kovacs, W. D., & Sheahan, T. C. (1981). *An introduction to geotechnical engineering* (Vol. 733). Englewood Cliffs: Prentice-Hall.

Holtz, W. G., & Gibbs, H. J. (1956). Engineering properties of expansive clays. *Transactions of the American Society of Civil Engineers*, *121*(1), 641-663.

Hossain, J. (2013). Geohazard potential of rainfall induced slope failure on expansive clay. Doctoral Dissertation. University of Texas at Arlington.

Hossain, S., Ahmed, A., Khan, M. S., Aramoon, A., & Thian, B. (2016). Expansive subgrade behavior on a state highway in North Texas. In *Geotechnical and Structural Engineering Congress 2016 Structural Engineering Institute*.

Hudak, P. F. (1998). Geologic controls on foundation damage in north-central Texas. *GeoJournal*, *45*(3), 159-164.

Ikra, B. A., & Wang, J. X. (2017). Numerical Simulation of Moisture Fluctuations in Unsaturated Expansive Clay, Heave/Settlement Predictions, and Validation with Field Measurements. In *PanAm Unsaturated Soils 2017* (pp. 198-208).

Imtiaz, T., Ahmed, A., Hossain, M. D., & Faysal, M. (2020). Microstructure analysis and strength characterization of recycled base and sub-base materials using scanning electron microscope. *Infrastructures, 5*(9), 70.

Iryo, T., & Rowe, R. K. (2005). Hydraulic behaviour of soil–geocomposite layers in slopes. *Geosynthetics International*, *12*(3), 145-155.

Islam, M. A., Hossain, M. S., Badhon, F. F., & Bhandari, P. (2021a). Performance Evaluation of Recycled-Plastic-Pin-Supported Embankment over Soft Soil. *Journal of Geotechnical and Geo environmental Engineering, 147*(6).

Islam, M. A., Zaman, M. N. B., Badhon, F. F., Bhandari, P., & Hossain, M. S. (2021b). Numerical Modeling of Recycled Plastic Pin Reinforced Embankment over Soft Soils. *International Foundations Congress & Equipment Expo*, Dallas, Texas.

Ito, M., Azam, S., & Hu, Y. (2014). A two-stage model for moisture-induced deformations in expansive soils. *Environmental Systems Research*, *3*(1), 19.

Jayatilaka, R., & Lytton, R. L. (1997). *Prediction of expansive clay roughness in pavements with vertical moisture barriers* (No. FHWA/TX-98/187-28F,).

Jayatilaka, R., Gay, D. A., Lytton, R. L., & Wray, W. K. (1992). Effectiveness of controlling pavement roughness due to expansive clays with vertical moisture barriers.

Jones, L. D., & Jefferson, I. (2012). *Expansive soils, ICE manual of geotechnical engineering*. ICE Publishing, London, 413-441.

Kamon, M., Akai, T., Matsumoto, A., Suwa, S., Fukuda, M., Simonodan, T., & Matsushita, M. (2001, November). High embankment of clay reinforced by GHD and its utilities. In *Proceeding of International Symposium on Landmarks in Earth Reinforcement, Fukuoka, Japan* (pp. 14-16).

Katz, L. E., Rauch, A. F., Liljestrand, H. M., Harmon, J. S., Shaw, K. S., & Albers, H. (2001). Mechanisms of soil stabilization with liquid ionic stabilizer. *Transportation Research Record*, *1757*(1), 50-57.

Kodikara, J., Rajeev, P., Chan, D., & Gallage, C. (2014). Soil moisture monitoring at the field scale using neutron probe. *Canadian Geotechnical Journal*, *51*(3), 332-345.

Koerner, R. M. (2012). *Designing with geosynthetics-Vol. 2* (Vol. 2). Xlibris Corporation.

Kuhn, J. A., McCartney, J. S., & Zornberg, J. G. (2005). Impinging Flow Over Drainage Layers Including a Geocomposite. In *Geosynthetics Research and Development in Progress* (pp. 1-7).

Kutilek, M. (1984). Some theoretical and practical aspects of infiltration in clays with D-constant. In *Proceedings of the ISSS Symposium on Water and Solute Movement in Heavy Clay Soils. ILRI Publ* (Vol. 37, pp. 114-128).

Kutner, M. H., Nachtsheim, C. J., Neter, J., & Li, W. (2005). *Applied linear statistical models* (Vol. 5). Boston: McGraw-Hill Irwin.

Lee, C.M (2017). “Seal Coat and Surface Treatment Manual” *Manual Notice 2017-1* < http://onlinemanuals.txdot.gov/txdotmanuals/scm/scm.pdf> (March 20, 2019)

Lei, S., Daniels, J. L., Bian, Z., & Wainaina, N. (2011). Improved soil temperature modeling. *Environmental Earth Sciences*, *62*(6), 1123-1130.

Liu, F., Liu, Z., Yin, F., Zhang, S., & Wang, Y. (2018, October). Effect of GCL on Moisture and Temperature Fields of Highway Subgrade through Numerical Analysis. In *The International Congress on Environmental Geotechnics* (pp. 608-615). Springer, Singapore.

Liu, Z. (2015). Influence of rainfall characteristics on the infiltration moisture field of highway subgrades. *Road Materials and Pavement Design*, *16*(3), 635-652.

Loken, M. C. (2007). *Use of ground penetrating radar to evaluate Minnesota roads* (No. MN/RC-2007-01).

Luo, R., & Prozzi, J. A. (2010). Development of longitudinal cracks on pavement over shrinking expansive subgrade. *Road Materials and Pavement Design*, *11*(4), 807-832.

Manosuthikij, T. (2008). *Studies on volume change movements in high PI clays for better design of low volume pavements*. Doctoral Dissertation, University of Texas at Arlington.

McKeen, R. G., & Johnson, L. D. (1990). Climate-controlled soil design parameters for mat foundations. *Journal of Geotechnical engineering*, *116*(7), 1073-1094.

McKenney, M. S., & Rosenberg, N. J. (1993). Sensitivity of some potential evapotranspiration estimation methods to climate change. *Agricultural and Forest Meteorology*, *64*(1-2), 81-110.

Mitchell, J. K., & Dermatas, D. (1992). Clay soil heave caused by lime-sulfate reactions. In *Innovations and uses for lime*. ASTM International.

Mitchell, P. W. (1979). The structural analysis of footings on expansive soil. In *Expansive Soils* (pp. 438-447). ASCE.

Mitchell, P. W. (2013). Climate change effects on expansive soil movements. *Proceedings of the 18th ICSMGE*.

Nayak, N. V., & Christensen, R. W. (1971). Swelling characteristics of compacted, expansive soils. *Clays and clay minerals*, *19*(4), 251-261.

Nelson, J. D., Thompson, E. G., Schaut, R. W., Chao, K. C., Overton, D. D., & Dunham-Friel, J. S. (2011). Design procedure and considerations for piers in expansive soils. *Journal of Geotechnical and Geo environmental Engineering*, *138*(8), 945-956.

Nelson, J., & Miller, D. J. (1997). *Expansive soils: problems and practice in foundation and pavement engineering*. John Wiley & Sons.

Nguyen, Q., Fredlund, D. G., Samarasekera, L., & Marjerison, B. L. (2010). Seasonal pattern of matric suctions in highway subgrades. *Canadian Geotechnical Journal*, *47*(3), 267-280.

Novak, V., Šimåunek, J., & Genuchten, M. T. V. (2000). Infiltration of water into soil with cracks. *Journal of irrigation and Drainage Engineering*, *126*(1), 41-47.

Pandey, P., Ahmed, A., Sapkota, A., Hossain, M. S., & Thian, B. (2019, March). Performance Evaluation of Pavement Subgrade by In Situ Moisture and Matric Suction Measurements. In *Geo-Congress 2019: Geotechnical Materials, Modeling, and Testing* (pp. 347-356). Reston, VA: American Society of Civil Engineers.

Pardo, L. R., De Marco, S., Holden, J. C., & McManus, K. J. (1998, October). Performance of vertical moisture barriers. In *Proc. of the Int. Symposium on Problematic Soils, Sendai, Japan*.

Petry, T. M., & Little, D. N. (1992). Update on sulfate-induced heave in treated clays; problematic sulfate levels. *Transportation Research Record*, (1362).

Petry, T. M., & Little, D. N. (2002). Review of stabilization of clays and expansive soils in pavements and lightly loaded structures—history, practice, and future. *Journal of materials in civil engineering*, *14*(6), 447-460.

Pham, H. Q., & Fredlund, D. (2005). *A volume-mass constitutive model for unsaturated soils* (pp. 4971-4971). Saskatchewan: University of Saskatchewan.

Picornell, M., & Lytton, R. L. (1987). *Behavior and design of vertical moisture barriers* (No. 1137).

Picornell, M., Lytton, R. L., & Steinberg, M. L. (1984). Assessment of the effectiveness of a vertical moisture barrier. In *Fifth International Conference on Expansive Soils 1984: Preprints of Papers* (p. 354). Institution of Engineers, Australia.

Pudasaini, B., & Shahandashti, M. (2020). Topological surrogates for computationally efficient seismic robustness optimization of water pipe networks. *Computer-Aided Civil and Infrastructure Engineering, 35*(10), 1101-1114.

Pudasaini, B., & Shahandashti, S. M. (2018). Identification of critical pipes for proactive resource-constrained seismic rehabilitation of water pipe networks. *Journal of Infrastructure Systems, 24*(4), 04018024.

Pudasaini, B., Shahandashti, S. M., & Razavi, M. (2017). Identifying critical links in water supply systems subject to various earthquakes to support inspection and renewal decision making. *Computing in Civil Engineering 2017, American Society of Civil Engineers, Reston, VA*, 231–238.

Pufahl, D. E., & Lytton, R. L. (1991). Temperature and suction profiles beneath highway pavements: Computed and measured. *Transportation Research Record*, *1307*, 268-276.

Puppala, A. J., Manosuthikij, T., & Chittoori, B. C. (2014). Swell and shrinkage strain prediction models for expansive clays. *Engineering Geology*, *168*, 1-8.

Qi, S., & Vanapalli, S. K. (2015). Numerical study on expansive soil slope stability considering the cracks and coupling effects. In *Proceedings of the 6th Asia-Pacific Conference on Unsaturated Soils*.

Rahardjo, H., Santoso, V. A., Leong, E. C., Ng, Y. S., & Hua, C. J. (2012). Performance of an instrumented slope covered by a capillary barrier system. *Journal of geotechnical and geo-environmental engineering*, *138*(4), 481-490.

Rahim, M. A. B. A., & Picornell, M. (1989). *Moisture movement under the pavement structure*. Center for Geotechnical & Highway Materials Research, University of Texas at El Paso.

Rajeev, P., Chan, D., & Kodikara, J. (2012). Ground–atmosphere interaction modelling for long-term prediction of soil moisture and temperature. *Canadian Geotechnical Journal*, *49*(9), 1059-1073.

Ridgeway, H. H. (1982). Pavement subsurface drainage systems. *NCHRP synthesis of highway practice*, (96).

Rollins, K. M., & Christie, R. (2002). *Pavement and Subgrade Distress-Remedial Strategies for Construction and Maintenance (I-15 Mileposts 200-217)* (No. UT-02.17).

Sabnis, A. K. (2008). *Impact of moisture variation on strength and deformation of clays*. The University of Texas at El Paso.

Saha, S., Hariharan, N., Gu, F., Luo, X., Little, D. N., & Lytton, R. L. (2019). Development of a mechanistic-empirical model to predict equilibrium suction for subgrade soil. *Journal of Hydrology*, *575*, 221-233.

Sapkota, A. (2019). *Effect of Modified Moisture Barriers on Slopes Stabilized With Recycled Plastic Pins*, Doctoral Dissertation, University of Texas at Arlington.

Sapkota, A., Ahmed, A., Pandey, P., Hossain, M. S., & Lozano, N. (2019, March). Stabilization of Rainfall-Induced Slope Failure and Pavement Distresses Using Recycled Plastic Pins and Modified Moisture Barrier. In *Geo-Congress 2019: Embankments, Dams, and Slopes* (pp. 237-246). Reston, VA: American Society of Civil Engineers.

Sapkota, A., Hossain, M. S., Ahmed, A., & Pandey, P. (2019). Effect of Modified Moisture Barrier on the Slopes Stabilized with Recycled Plastic Pins. *98th Annual Meeting of Transportation Research Board,* Transportation Research Board, Washington D.C.

Sastry, S. S. (2012). *Introductory methods of numerical analysis*. PHI Learning Pvt. Ltd.

Sebesta, S. (2002). *Investigation of maintenance base repairs over expansive soils: Year 1 report* (No. FHWA/TX-03/0-4395-1,). Texas Transportation Institute, Texas A & M University System.

Shahandashti, S. M., & Pudasaini, B. (2019). Proactive seismic rehabilitation decision-making for water pipe networks using simulated annealing. *Natural Hazards Review, 20*(2), 04019003.

Shahidehpour, M., Liu, X., Li, Z., & Cao, Y. (2016). Microgrids for enhancing the power grid resilience in extreme conditions. *IEEE Transactions on Smart Grid, 8*(2), 1–1.

Sherwood, P. T. (1962). Effect of sulfates on cement-and lime-stabilized soils. *Highway Research Board Bulletin*, (353).

Snethen, D. R. (1979). An evaluation of methodology for prediction and minimization of detrimental volume change of expansive soils in highway subgrades.

Stalin, V. K., Ravi, E., & Arun Murugan, R. B. (2010, December). Control of swell: shrink behaviour of expansive clays using geosynthetics. In *Proceedings of Indian Geotechnical Conference-2010, GEOtrendz, December* (pp. 16-18).

Steinberg, M. L. (1980). Deep Vertical Fabric Moisture Seals. In *Expansive Soils* (pp. 383-400). ASCE.

Steinberg, M. L. (1985). *Controlling expansive soil destructiveness by deep vertical geomembranes on four highways* (No. 1032).

Steinberg, M. L. (1989). *Further Monitoring of Twelve Geomembrane Sites in Texas* (No. DHT-18).

Steinberg, M. L. (1992). Controlling expansive soils: twenty Texas highway projects. In *International conference on expansive soils* (pp. 392-397).

Stormont, J. C., & Morris, C. E. (1998). Method to estimate water storage capacity of capillary barriers. *Journal of Geotechnical and Geo environmental Engineering*, *124*(4), 297-302.

Stormont, J. C., Henry, K. S., & Roberson, R. (2009). Geocomposite capillary barrier drain for limiting moisture changes in pavements: Product application. *Transportation Research Board, National Cooperative Highway Research Program, NCHRP-113*.

Tailor, R. M., & Shah, N. C. (2014). Performance Improvement of Flexible Pavement on Swelling Subgrade Using Geotextile. *Journal of Traffic and Logistics Engineering Vol*, *2*(2).

Talluri, N., Puljan, V., Manosuthikij, T., Puppala, A. J., & Saride, S. (2011). Prediction of swell-shrink movements of pavement infrastructure. In *Geo-Frontiers 2011: Advances in Geotechnical Engineering* (pp. 2740-2749).

Tella Firma (2017). Find Out Why Texas Has Some of the Most Expansive Soils. https://www.tellafirma.com/find-texas-expansive-soils/ (March 11, 2019).

Teltayev, B. B., & Suppes, E. A. (2019). Temperature in pavement and subgrade and its effect on moisture. *Case Studies in Thermal Engineering*, *13*, 100363.

Timsina, S., Bhandari, P., Zaman, M. N. B., Ahmed, A., Hossain, M. S., & Thian, B. (2019). Effect of fine clay particles on the strength characterization of cement treated flex-base materials. In *Geo-Congress 2019: Geotechnical Materials, Modeling, and Testing* (pp. 382-390). Reston, VA: American Society of Civil Engineers.

Uzan, J., Livneh, M., & Shklarsky, E. (1972). Cracking mechanism of flexible pavements. *Transportation Engineering Journal of ASCE*, *98*(1), 17-36.

Wang, J. L. (2011). Study of elastic-viscoplastic analysis and water damage mechanism for the asphalt pavement. In *Key Engineering Materials* (Vol. 467, pp. 996-999). Trans Tech Publications Ltd.

Wanyan, Y., Abdallah, I., Nazarian, S., & Puppala, A. J. (2010). Expert system for design of low-volume roads over expansive soils. *Transportation Research Record*, *2154*(1), 81-90.

Wanyan, Y., Abdallah, I., Nazarian, S., & Puppala, A. J. (2014). Moisture content-based longitudinal cracking prediction and evaluation model for low-volume roads over expansive soils. *Journal of Materials in Civil Engineering*, *27*(10), 04014263.

Williams, A. A. B., & Pidgeon, J. T. (1983). Evapo-transpiration and heaving clays in South Africa. *Geotechnique*, *33*(2), 141-150.

Williams, H. F. (2003). Urbanization pressure increases potential for soils-related hazards, Denton County, Texas. *Environmental Geology*, *44*(8), 933-938.

Wong, T. T., Fredlund, D. G., & Krahn, J. (1998). A numerical study of coupled consolidation in unsaturated soils. *Canadian Geotechnical Journal*, *35*(6), 926-937.

Xu, Q., Liu, S., Wan, X., Jiang, C., Song, X., & Wang, J. (2012). Effects of rainfall on soil moisture and water movement in a subalpine dark coniferous forest in southwestern China. *Hydrological Processes*, *26*(25), 3800-3809.

Young, R. (2012). *Soil properties and behaviour* (Vol. 5). Elsevier.

Zhan, T. L., Ng, C. W., & Fredlund, D. G. (2007). Field study of rainfall infiltration into a grassed unsaturated expansive soil slope. *Canadian geotechnical journal*, *44*(4), 392-408.

Zhang, X. (2005). *Consolidation theories for saturated-unsaturated soils and numerical simulation of residential buildings on expansive soils*. Doctoral Dissertation. Texas A&M University.

Zhang, X., & Liu, J. (2008). Numerical Simulation of Influence of Climatic Factors on Concrete Pavements Built on Expansive Soil. In *Geo Congress 2008: Geo sustainability and Geohazard Mitigation* (pp. 554-561).

Zhang, X., Li, L., & Chen, L. (2009). Impact of a Tree on a Residential Building on Expansive Soils: A Numerical Approach. In *Contemporary Topics in Ground Modification, Problem Soils, and Geo-Support* (pp. 614-621).

Zornberg, J. G., & Gupta, R. (2009, October). Reinforcement of pavements over expansive clay subgrades. In *Proceedings of the 17th International Conference on Soil Mechanics and Geotechnical Engineering* (Vol. 1, pp. 765-768).

APPENDIX A

Borelogs

LOGO UT Arlington

BORING NUMBER BC1

CLIENT Texas Department of Transportation
PROJECT NAME FM 639
PROJECT NUMBER
PROJECT LOCATION Frost, TX
DATE STARTED 2/27/19 **COMPLETED** 2/27/19
GROUND ELEVATION **HOLE SIZE** 4 inches
DRILLING CONTRACTOR West Drilling
GROUND WATER LEVELS:
DRILLING METHOD Continuous Flight Auger
AT TIME OF DRILLING ---
LOGGED BY P.P **CHECKED BY**
AT END OF DRILLING ---
NOTES
AFTER DRILLING ---

DEPTH (ft)	SAMPLE TYPE NUMBER	BLOW COUNTS (N VALUE)	U.S.C.S.	GRAPHIC LOG	MATERIAL DESCRIPTION
0					
			CH		(CH) FAT CLAY
5		2-3-6 (9)			
					5.0
			CH		(CH) FAT CLAY
10		3-6-9 (15)			
					10.0

Bottom of borehole at 10.0 feet.

LOGO UT Arlington

BORING NUMBER BC2

CLIENT Texas Department of Transportation
PROJECT NAME FM 639
PROJECT NUMBER
PROJECT LOCATION Frost, TX
DATE STARTED 2/27/19 **COMPLETED** 2/27/19
GROUND ELEVATION **HOLE SIZE** 4 inches
DRILLING CONTRACTOR West Drilling
GROUND WATER LEVELS:
DRILLING METHOD Continuous Flight Auger
AT TIME OF DRILLING ---
LOGGED BY P.P **CHECKED BY**
AT END OF DRILLING ---
NOTES
AFTER DRILLING ---

DEPTH (ft)	SAMPLE TYPE NUMBER	TESTS	U.S.C.S.	GRAPHIC LOG	MATERIAL DESCRIPTION
0		MC = 21% MC = 26%	CH		(CH) FAT CLAY, Gray, moist with some traces of sandy particles
4.0		MC = 23%	CH		(CH) FAT CLAY, moist with some aggregates
6.0		MC = 21%	CH		(CH) FAT CLAY, Yellow
8.0		MC = 25%	CH		(CH) FAT CLAY, moist with some aggregates
10.0					Bottom of borehole at 10.0 feet.

LOGO UT Arlington

BORING NUMBER BC3

CLIENT Texas Department of Transportation
PROJECT NAME FM 639
PROJECT NUMBER
PROJECT LOCATION Frost, TX
DATE STARTED 2/27/19 **COMPLETED** 2/27/19
GROUND ELEVATION **HOLE SIZE** 4 inches
DRILLING CONTRACTOR West Drilling
GROUND WATER LEVELS:
DRILLING METHOD Continuous Flight Auger
AT TIME OF DRILLING ---
LOGGED BY P.P **CHECKED BY**
AT END OF DRILLING ---
NOTES
AFTER DRILLING ---

DEPTH (ft)	SAMPLE TYPE NUMBER	TESTS	U.S.C.S.	GRAPHIC LOG	MATERIAL DESCRIPTION
0			CH		(CH) FAT CLAY
5		MC = 32% LL = 77 PL = 41		5.0	
			CH		(CH) FAT CLAY
10		MC = 30% LL = 86 PL = 52		10.0	

Bottom of borehole at 10.0 feet.

LOGO UT Arlington

BORING NUMBER BH1

CLIENT Texas Department of Transportation
PROJECT NAME FM 639
PROJECT NUMBER
PROJECT LOCATION Frost, TX
DATE STARTED 2/27/19 **COMPLETED** 2/27/19
GROUND ELEVATION **HOLE SIZE** 4 inches
DRILLING CONTRACTOR West Drilling
GROUND WATER LEVELS:
DRILLING METHOD Continuous Flight Auger
AT TIME OF DRILLING ---
LOGGED BY P.P **CHECKED BY**
AT END OF DRILLING ---
NOTES
AFTER DRILLING ---

DEPTH (ft)	SAMPLE TYPE NUMBER	TESTS	U.S.C.S.	GRAPHIC LOG	MATERIAL DESCRIPTION
0		MC = 35% MC = 35%	CH		(CH) FAT CLAY, Gray, moist with some traces of stones and sand particles in the top layer
4.0					(CH) FAT CLAY, Brown in color, moist
5		MC = 36% DD = 95 pcf MC = 30% LL = 77 PL = 40	CH		
8.0					(CH) FAT CLAY, Yellow, moist
10		MC = 30% LL = 78 PL = 48	CH		
10.0					Bottom of borehole at 10.0 feet.

LOGO

UT Arlington

BORING NUMBER BH2

CLIENT Texas Department of Transportation
PROJECT NAME FM 639
PROJECT NUMBER
PROJECT LOCATION Frost, TX
DATE STARTED 2/27/19 **COMPLETED** 2/27/19
GROUND ELEVATION **HOLE SIZE** 4 inches
DRILLING CONTRACTOR West Drilling
GROUND WATER LEVELS:
DRILLING METHOD Continuous Flight Auger
AT TIME OF DRILLING ---
LOGGED BY P.P **CHECKED BY**
AT END OF DRILLING ---
NOTES
AFTER DRILLING ---

DEPTH (ft)	SAMPLE TYPE NUMBER	TESTS	U.S.C.S.	GRAPHIC LOG	MATERIAL DESCRIPTION
0					
			CH		(CH) FAT CLAY
5		MC = 30%		5.0	
			CH		(CH) FAT CLAY
10		MC = 31%		10.0	

Bottom of borehole at 10.0 feet.

LOGO UT Arlington

BORING NUMBER BH3

CLIENT Texas Department of Transportation
PROJECT NAME FM 639
PROJECT NUMBER
PROJECT LOCATION Frost, TX
DATE STARTED 2/27/19 **COMPLETED** 2/27/19
GROUND ELEVATION **HOLE SIZE** 4 inches
DRILLING CONTRACTOR West Drilling
GROUND WATER LEVELS:
DRILLING METHOD Continuous Flight Auger
AT TIME OF DRILLING ---
LOGGED BY P.P **CHECKED BY**
AT END OF DRILLING ---
NOTES
AFTER DRILLING ---

DEPTH (ft)	SAMPLE TYPE NUMBER	TESTS	U.S.C.S.	GRAPHIC LOG	MATERIAL DESCRIPTION
0					(CH) FAT CLAY
5		MC = 33% LL = 70 PL = 48	CH	5.0	(CH) FAT CLAY
10		MC = 31% LL = 83 PL = 52	CH	10.0	Bottom of borehole at 10.0 feet.

APPENDIX B

Transmissivity with Different Mobilized Length for Varying Rainfall Intensities

Transmissivity with Different Mobilized Length for Varying Rainfall Intensities

Rainfall: 5mm/hr; Transmissivity: 2.13 X 10^{-7} m^2/s

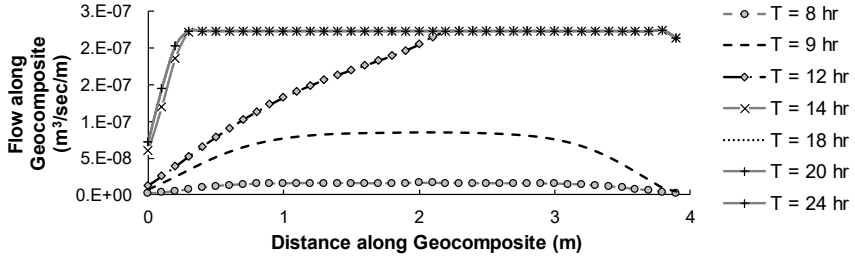

Rainfall: 5mm/hr; Transmissivity: 1.15 X 10^{-6} m^2/s

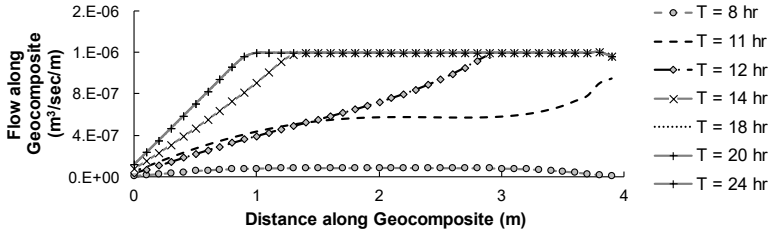

Rainfall: 5mm/hr; Transmissivity: 2.46 X 10^{-6} m^2/s

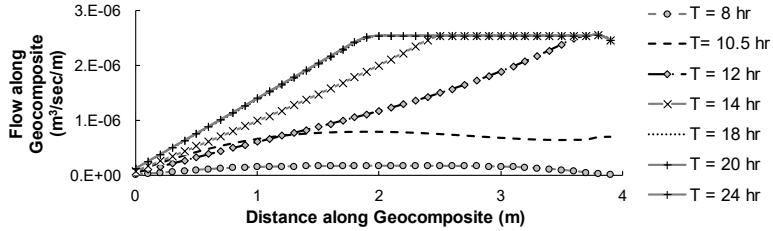

Rainfall: 5mm/hr; Transmissivity: 3.92 X 10^{-6} m^2/s

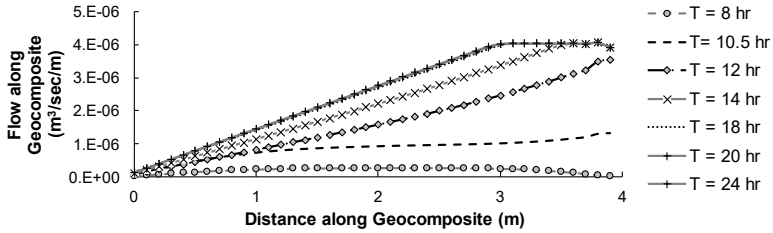

Rainfall: 20 mm/hr; Transmissivity: 1.44 X 10^{-6} m^2/s

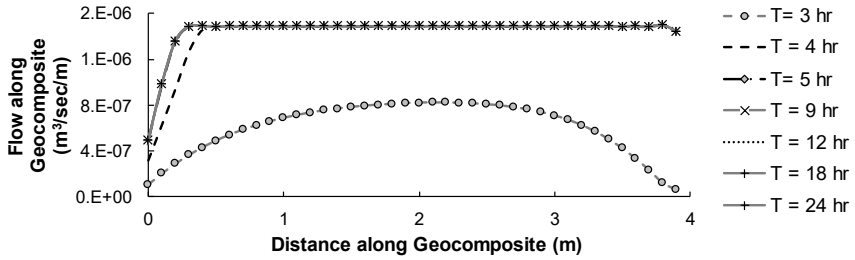

Rainfall: 20 mm/hr; Transmissivity: 4.79 X 10^{-6} m^2/s

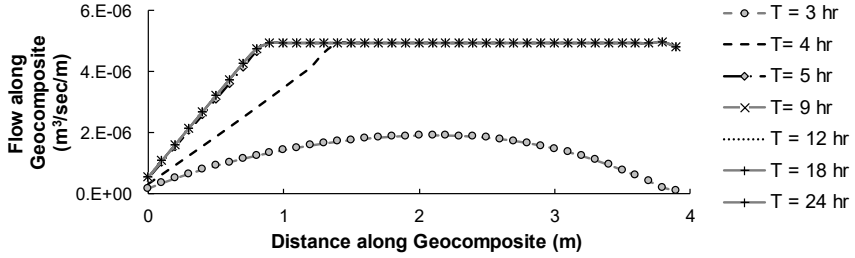

Rainfall: 20 mm/hr; Transmissivity: 1.02 X 10^{-5} m^2/s

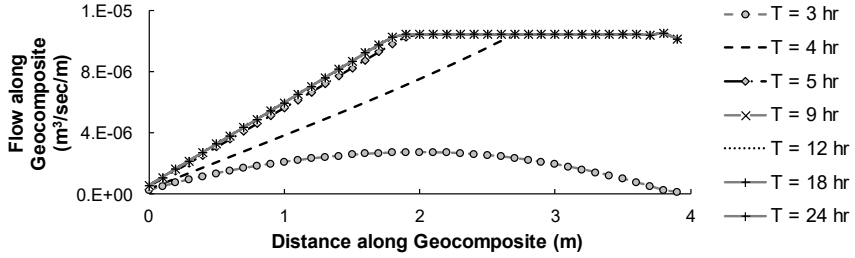

Rainfall: 20 mm/hr; Transmissivity: 1.59 X 10^{-5} m^2/s

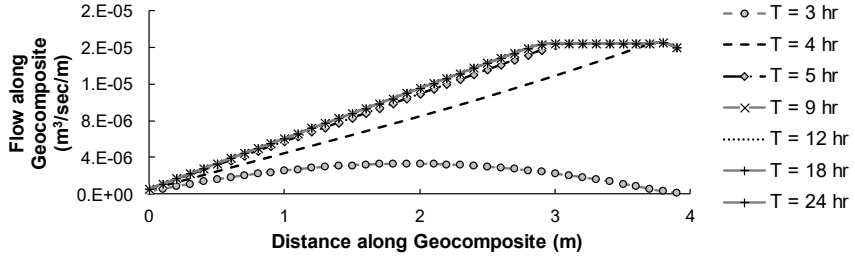

Rainfall: 40 mm/hr; Transmissivity: 2.89 X 10^{-6} m^2/s

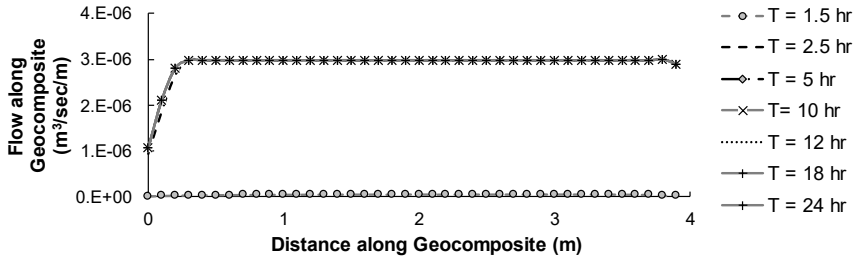

Rainfall: 40 mm/hr; Transmissivity: 1.02 X 10^{-5} m^2/s

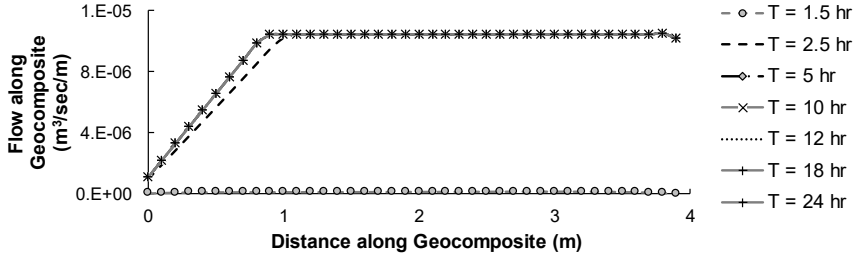

Rainfall: 40 mm/hr; Transmissivity: 2.1 X 10^{-5} m^2/s

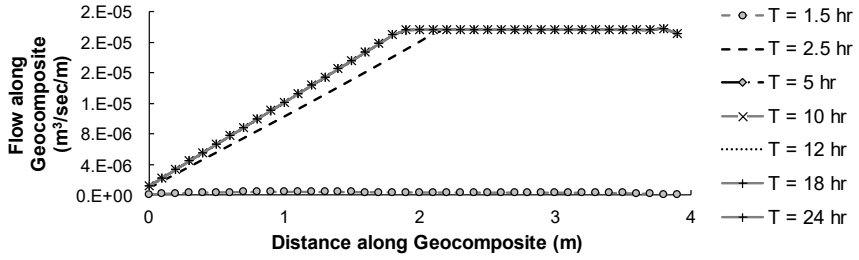

Rainfall: 40 mm/hr; Transmissivity: 3.2 X 10^{-5} m^2/s

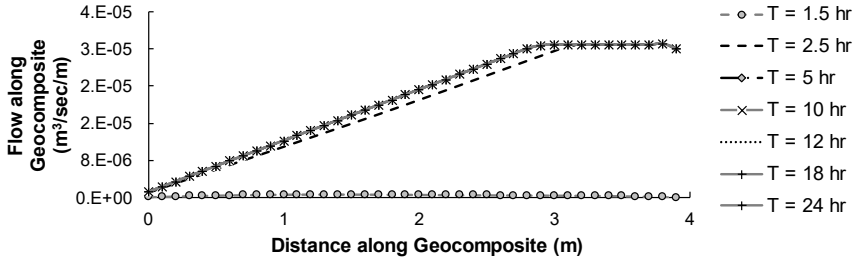

Rainfall: 60 mm/hr; Transmissivity: 4.78 X 10^{-6} m^2/s

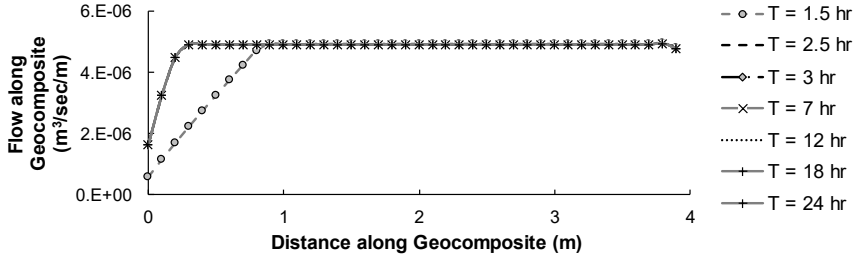

Rainfall: 60 mm/hr; Transmissivity: 1.55 X 10^{-5} m^2/s

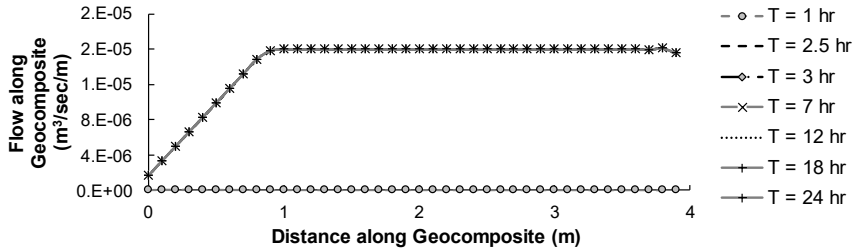

Rainfall: 60 mm/hr; Transmissivity: 3.19 X 10^{-5} m^2/s

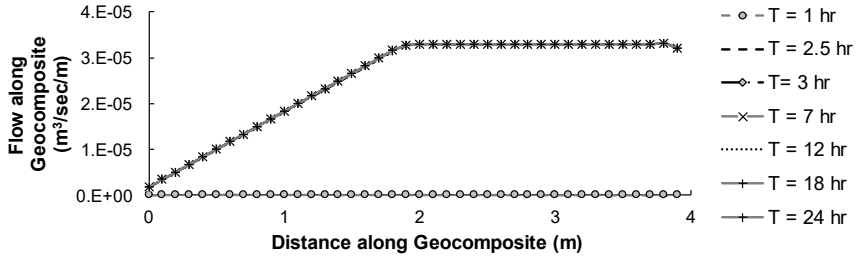

Rainfall: 60 mm/hr; Transmissivity: 4.79 X 10^{-5} m^2/s

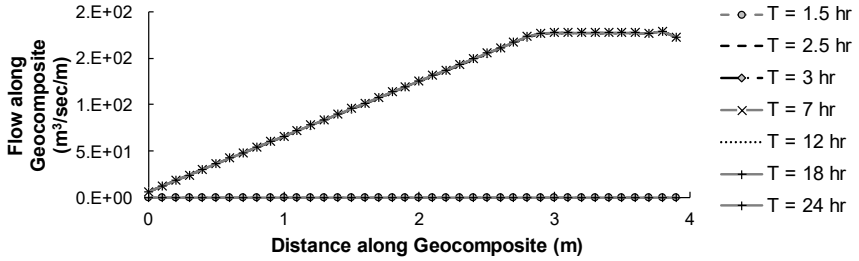

BIOGRAPHY

Pratibha Pandey graduated with bachelor's degree in Civil Engineering from Pulchowk Campus, Tribhuvan University in Kathmandu, Nepal in 2015. She then joined National Reconstruction Authority under Nepal government and worked as a civil engineer for the reconstruction of the infrastructures damaged by the earthquake that occurred in 2015. Pratibha started her graduate studies at The University of Texas at Arlington in Fall 2017. She worked as a graduate research assistant during her graduate studies under Dr. MD Sahadat Hossain. The author's research interest includes expansive soil, pavement maintenance, slope stability, foundation system, application of geosynthetics, unsaturated soil mechanics, geophysical investigation, and numerical modeling.